Chapter 4

Results from Single-Degree-of-Freedom Focused Analytical Studies

This chapter summarizes the results of focused analytical studies on single-spring and multi-spring systems, compares results to recommendations contained in FEMA 440, and explains the development of a new equation measuring the potential for lateral dynamic instability.

4.1 Summary of Analytical Results

There were 160 single-spring systems (eight basic spring types, “a” and “b” versions of each, with and without cyclic degradation, tuned to five different periods of vibration). Each system was subjected to incremental dynamic analysis using 56 ground motion records scaled to multiple levels of increasing intensity. This resulted in over 600,000 nonlinear response history analyses on single-spring systems.

There were 600 multi-spring systems (six lateral-force-resisting springs, “a” and “b” versions of each, five relative strength multipliers, five different gravity spring combinations, tuned with two different story masses). Each system was subjected to incremental dynamic analysis using 56 ground motion records scaled to multiple levels of increasing intensity. This resulted in over 2,000,000 nonlinear response history analyses on multi-spring systems.

In total, results from over 2.6 million nonlinear response history analyses were available for review. Given the large volume of analytical data, customized algorithms were developed for post-processing, statistical analysis, and visualization of results. Results are summarized in the sections that follow. More complete sets of data are presented in the appendices. A customized visualization tool that was developed to view results of multi-spring studies, along with all available data, is included on the CD accompanying this report. Use of the visualization tool is described in Appendix C and Appendix D.

4.2 Observations from Single-Spring Studies

This section summarizes the results from nonlinear dynamic analyses of single-spring systems. Results from these studies were used to:

- identify predominant characteristics of median incremental dynamic analysis (IDA) curves for these systems,
- demonstrate a relationship between IDA curves and features of the force-displacement capacity boundaries, and
- qualitatively determine the effects of different degrading behaviors on the dynamic stability of structural systems.

Only selected results are presented here. Quantile (16th, 50th and 84th percentile) IDA curves for each of the single-spring systems are provided in Appendix B. The horizontal axis for all single-spring IDA results is the maximum story drift ratio, θ_{max}, in radians.

4.3 Characteristics of Median IDA Curves

Individual incremental dynamic analysis (IDA) curves for single ground motion records are very sensitive to dynamic interaction between the properties of the system and the characteristics of the ground motion. Quantile (16th, 50th and 84th percentile) IDA curves, however, are much more stable and provide better information on the central tendency (median) and variability (dispersion) in system response. In general, median IDA curves exhibit the following characteristics (Figure 4-1):

- An initial linear segment corresponding to linear-elastic behavior in which in lateral deformation demand is proportional to ground motion intensity, regardless of the characteristics of the system or the ground motion. This segment extends from the origin to the onset of yielding.
- A second curvilinear segment corresponding to inelastic behavior in which lateral deformation demand is no longer proportional to ground motion intensity. As intensity increases, lateral deformation demands increase at a faster rate. This segment corresponds to softening of the system, or reduction in stiffness (reduction in the slope of the IDA curve). In this segment, the system "transitions" from linear behavior to eventual dynamic instability. Although a curvilinear segment is always present, in some cases the transition can be relatively long and gradual, while in other cases it can be very short and abrupt.
- A final linear segment that is horizontal, or nearly horizontal, in which infinitely large lateral deformation demands occur at small increments in ground motion intensity. This segment corresponds to the point at which a system becomes unstable (lateral dynamic instability). For SDOF systems, this point corresponds to the ultimate deformation capacity at which the system loses all lateral-force-resisting capacity.

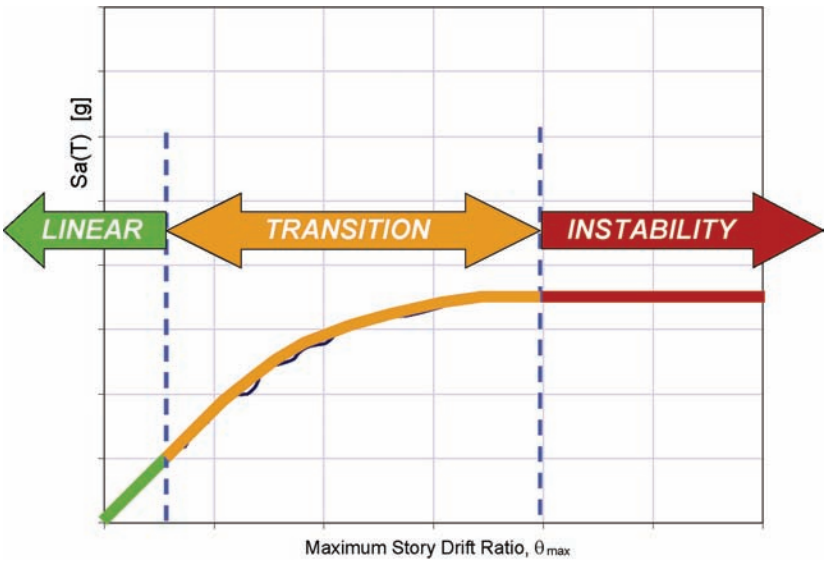

Figure 4-1 Characteristic segments of a median IDA curve.

In some systems, the initial linear segment can be extended beyond yield into the inelastic range (Figure 4-2). In this segment lateral deformation demand is approximately proportional to ground motion intensity, which is consistent with the familiar equal-displacement approximation for estimating inelastic displacements. The range of lateral deformation demands over which the equal-displacement approximation is applicable depends on the characteristics of the force-displacement capacity boundary of the system and the period of vibration.

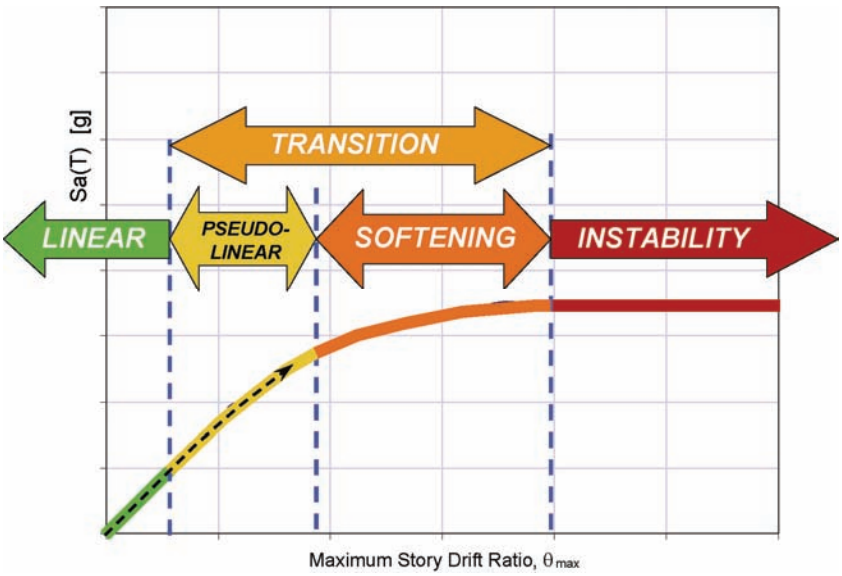

Figure 4-2 Characteristic segments of a median IDA curve with a pseudo-linear segment.

4.3.1 Dependence on Period of Vibration

Figure 4-3 shows the force-displacement capacity boundary and resulting IDA curves for Spring 3a with different periods of vibration. Each system is tuned to a different lateral strength and stiffness so results are compared using the normalized intensity measure $R = S_a(T,5\%)/S_{ay}(T,5\%)$. Intensities larger than $R = 1.0$ mean the system is behaving inelastically.

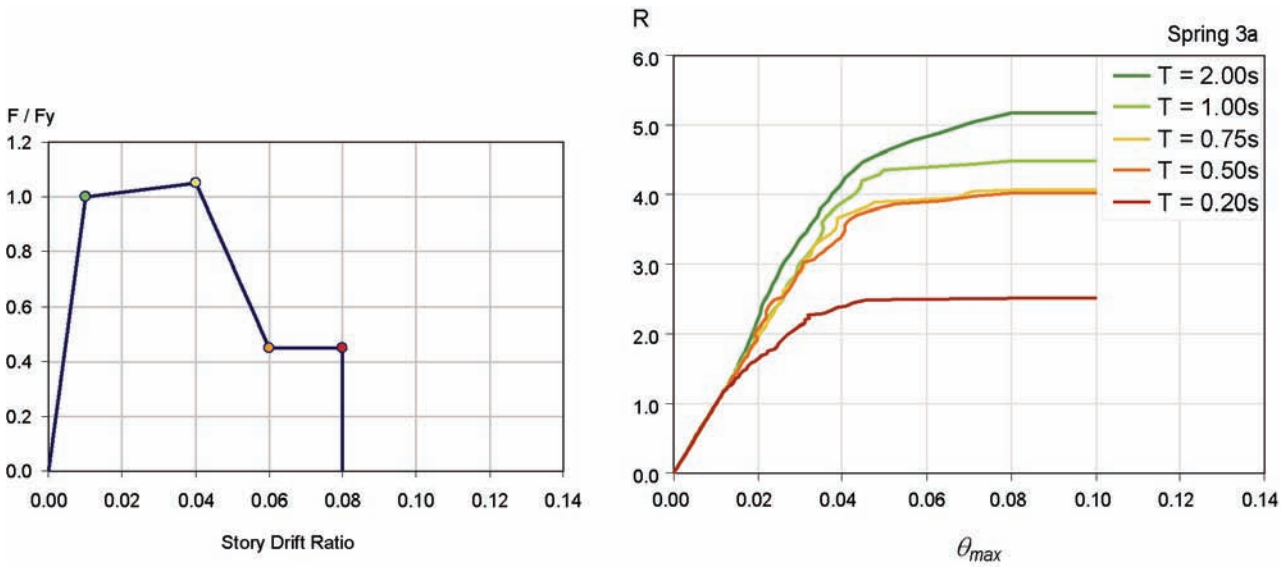

Figure 4-3 Force-displacement capacity boundary and median IDA curves for Spring 3a with various periods of vibration.

In general, moderate and long period systems with zero or positive post-yield stiffness in the force-displacement capacity boundary follow the equal displacement trend well into the nonlinear range. For systems with periods longer than 0.5s, Spring 3a exhibits an extension of the initial linear segment well beyond the yield drift of 0.01. In contrast, the short period system (T=0.2s) diverges from the initial linear segment just after yielding, even at deformations within the strength-hardening segment of the force-displacement capacity boundary (drifts between 0.01 and 0.04).

4.3.2 Dispersion in Response

Nonlinear response is sensitive to the characteristics of the ground motion record, and will vary from one ground motion to the next, even when scaled to the same intensity. For a given level of ground motion intensity, the lateral deformation demand can be significantly smaller or significantly larger than the value shown on median IDA curves. As the level of ground motion intensity increases, the dispersion in response tends to increase.

Figure 4-4 shows three quantile IDA curves for Spring 3b with period of vibration of 2.0s. The 50% (median) IDA curve indicates that, for a given level of ground motion intensity (S_a), half of all deformation demands are smaller and half are larger than values along this curve. Because the distribution of demands is lognormally distributed, the dispersion about the median is not symmetric. The upper (16%) curve in the figure indicates that, for a given level of ground motion intensity, 16% of all lateral deformation demands are to the left of this curve while 84% are to the right. This means that lateral deformation demands along this curve have an 84% chance of being exceeded. Similarly the lower (84%) curve corresponds to lateral deformation demands with a 16% chance of being exceeded.

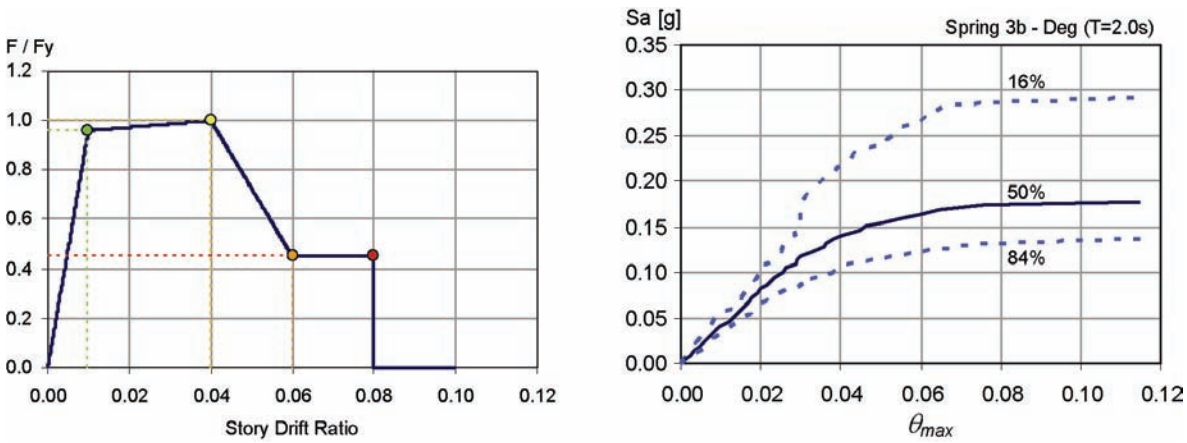

Figure 4-4 Force-displacement capacity boundary and 16th, 50th and 84th percentile IDA curves for Spring 3b with a period of vibration T=2.0s.

4.4 Influence of the Force-Displacement Capacity Boundary

Comparisons between force-displacement capacity boundaries and median IDA curves show a strong correlation between the shape of the resulting curves and key features of the force-displacement capacity boundary, such as post-yield behavior and onset of degradation, slope of degradation, ultimate deformation capacity, and presence of cyclic degradation.

Figure 4-5 shows the force-displacement capacity boundary and resulting median IDA curve for Spring 3b with a period of 2.0s. With a positive post-yield slope, delayed onset of degradation, and robust residual strength plateau with an extended maximum deformation capacity, the resulting IDA curve includes both linear and pseudo-linear segments and a gradual transition to lateral dynamic instability.

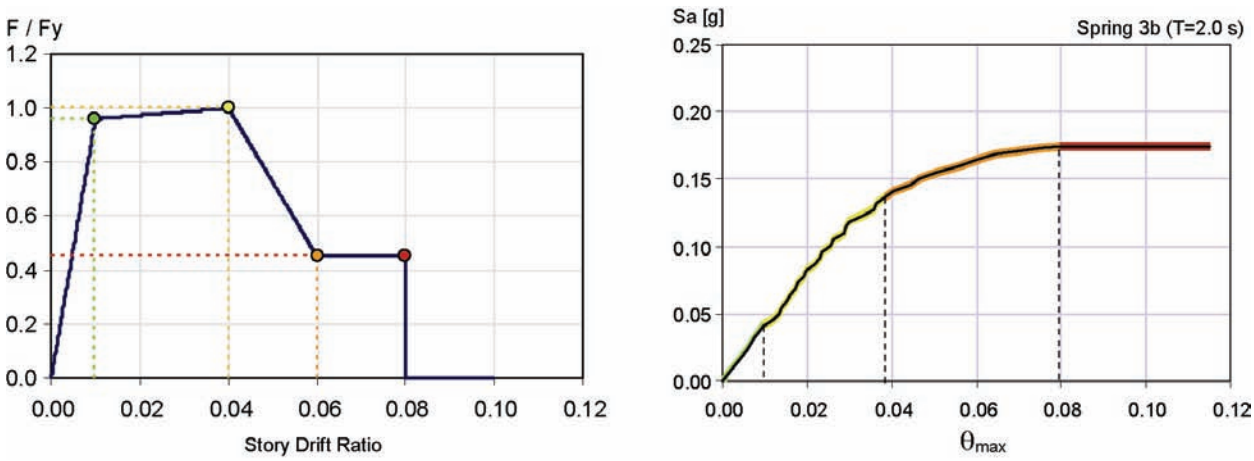

Figure 4-5 Force-displacement capacity boundary and median IDA curve for Spring 3b with a period of vibration T=2.0s.

Figure 4-6 shows the force-displacement capacity boundary and resulting median IDA curve for Spring 2a with a period of 2.0s. With the onset of degradation occurring immediately after yielding, the shape of the resulting IDA curve changes. The pseudo-linear segment disappears, but with the presence of a residual strength plateau, the transition segment remains somewhat gradual until lateral dynamic instability.

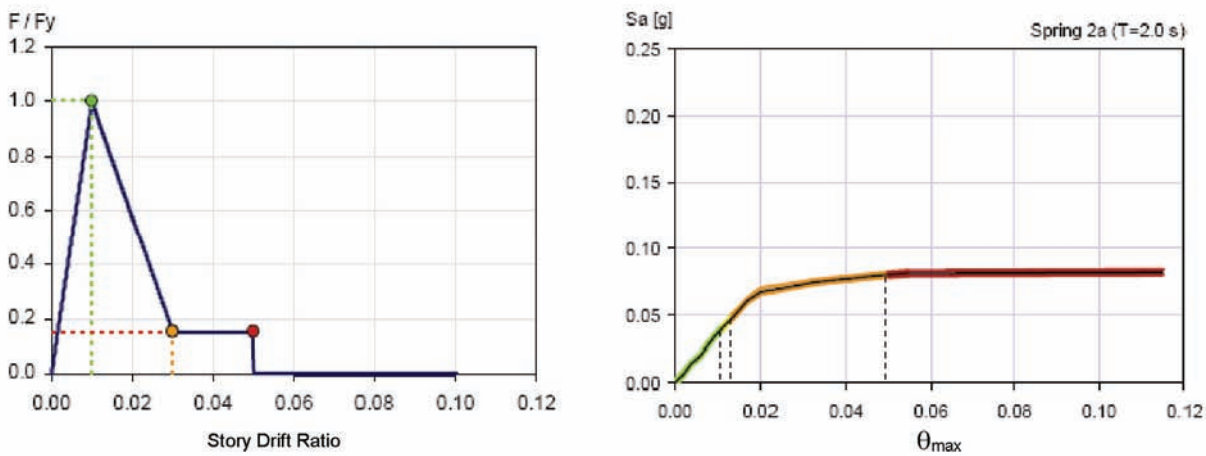

Figure 4-6 Force-displacement capacity boundary and median IDA curve for Spring 2a with a period of vibration T=2.0s.

Figure 4-7 shows the force-displacement capacity boundary and resulting median IDA curve for Spring 6a with a period of 2.0s. With a broad yielding plateau, the pseudo-linear segment extends well into the inelastic range. Without a residual strength plateau, however, the system abruptly transitions into lateral dynamic instability.

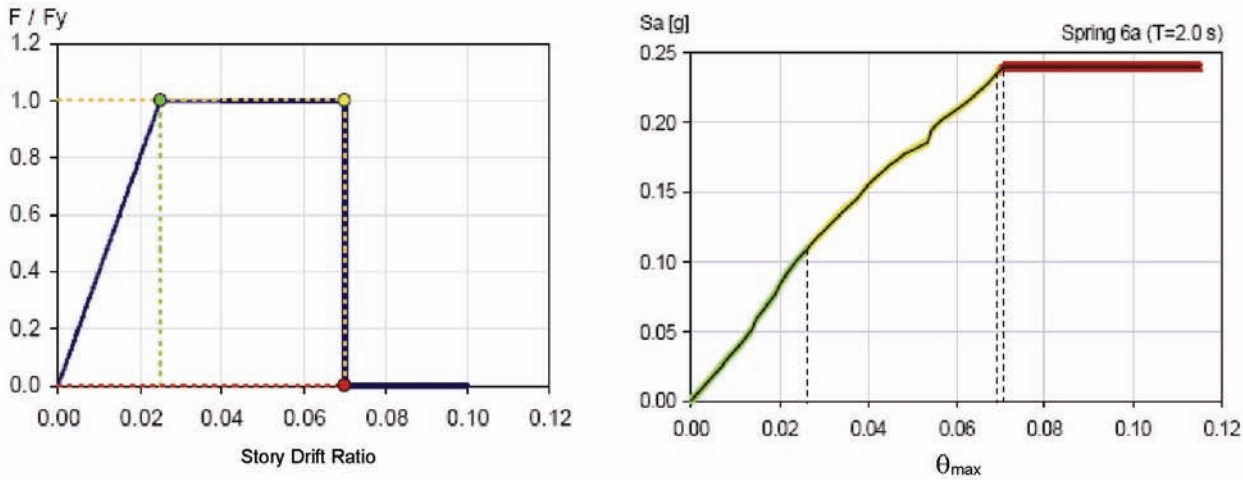

Figure 4-7 Force-displacement capacity boundary and median IDA curve for Spring 6a with a period of vibration T=2.0s.

Figure 4-8 shows the force-displacement capacity boundary and resulting median IDA curve for Spring 8a with a period of 2.0s. With severe strength degradation occurring immediately after yielding, and the absence of a residual strength plateau, the system abruptly transitions from linear elastic behavior directly into lateral dynamic instability with little or no transition.

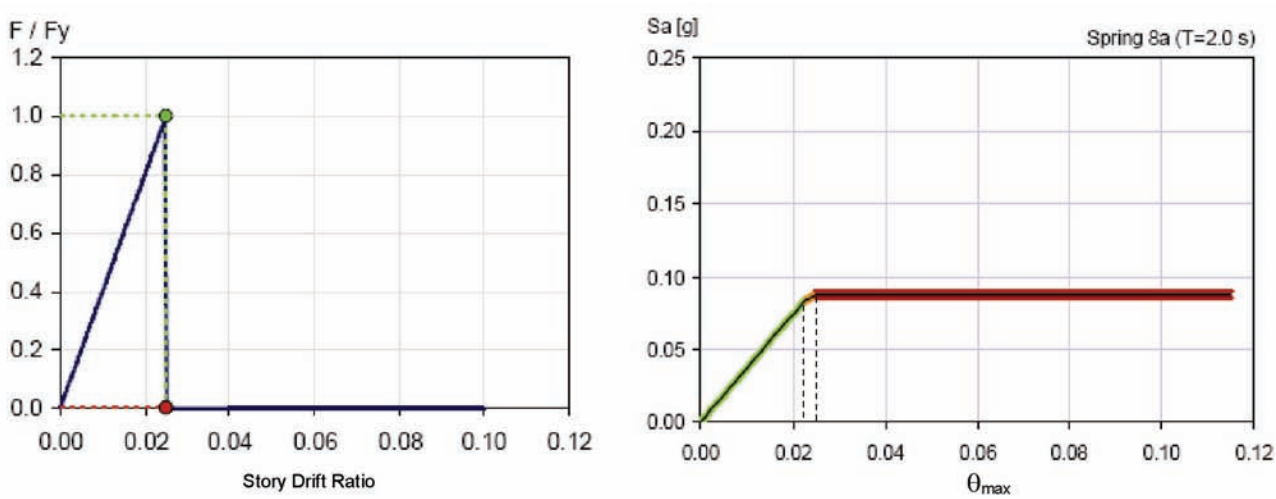

Figure 4-8 Force-displacement capacity boundary and median IDA curve for Spring 8a with a period of vibration T=2.0s.

These observed relationships suggest that dynamic response is directly influenced by the features of a force-displacement capacity boundary. Figure 4-9 shows how the characteristic segments of a median IDA curve relate to these features. Note that the relationship depicted in this idealized graphical representation is dependent upon the period of the system, as described in Section 4.3.1.

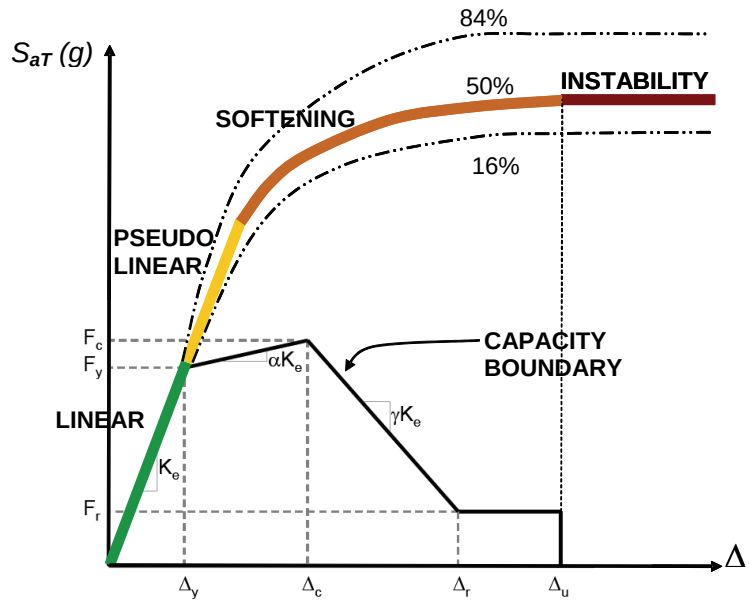

Figure 4-9 Relationship between IDA curves and the features of a typical force-displacement capacity boundary

For low levels of ground motion intensity, the initial linear segment of the IDA curve is controlled by the effective stiffness of the system, K_e. Since the response is linear there is no dispersion evident in this segment. As the intensity increases the system reaches its yield point, F_y, Δ_y. Systems with a non-negative post-elastic stiffness, αK_e, will likely exhibit a pseudo-linear segment. Beyond yield, dispersion appears in the nonlinear response due to ground motion variability, and the 16th and 84th percentile IDA curves begin to diverge from the median curve.

The extent of the pseudo-linear segment depends on the initial post elastic stiffness, αK_e, and ends prior to reaching the strength hardening limit, F_c, Δ_c (also known as the capping point). For systems that exhibit negative stiffness, γK_e, immediately after yielding, the pseudo-linear segment may be very short or non-existent. Also, for short-period systems, the pseudo-linear segment can be very short, even if the system has positive post-yield stiffness.

As the ground motion intensity increases further, deformation demands increase at a faster rate, the IDA curve begins to flatten, and the curvilinear softening segment emerges. Dispersion between the quantile curves also increases. Beyond the strength hardening limit, F_c, Δ_c, degradation occurs, and the softening increases at a faster rate. The presence of a residual

strength plateau, F_r, Δ_r, can extend the softening segment and delay the eventual transition into lateral dynamic instability. The point at which instability occurs corresponds to the ultimate deformation capacity, Δ_u, at which the system loses all lateral force resistance.

This relationship suggests that it is possible to estimate the nonlinear dynamic behavior of a system based on knowledge of the characteristics of the force-displacement capacity boundary of the system. The influence that important features of the force-displacement capacity boundary have on nonlinear response is explained in more detail in the sections that follow.

4.4.1 Post-Yield Behavior and Onset of Degradation

The three systems shown in Figure 4-10 have the same elastic stiffness, same yield strength, but different post-yield characteristics. The force-displacement capacity boundary of Spring 2a experiences strength degradation immediately after yielding. In contrast, Spring 3a has a moderate yielding plateau before the onset of similar strength degradation, while Spring 6a has elastic-perfectly-plastic behavior up to the ultimate deformation capacity.

These three systems have the same elastic behavior, but at drift ratios larger than 0.02, their relative potential for in-cycle strength degradation, and their resulting collapse behaviors, are all very different. Key parameters related to the observed change in response are the post-yield slope and the strength hardening limit (capping point). The presence of a non-negative post-yield slope and any delay before the onset of degradation reduces potential in-cycle strength degradation and improves the collapse capacity of a system.

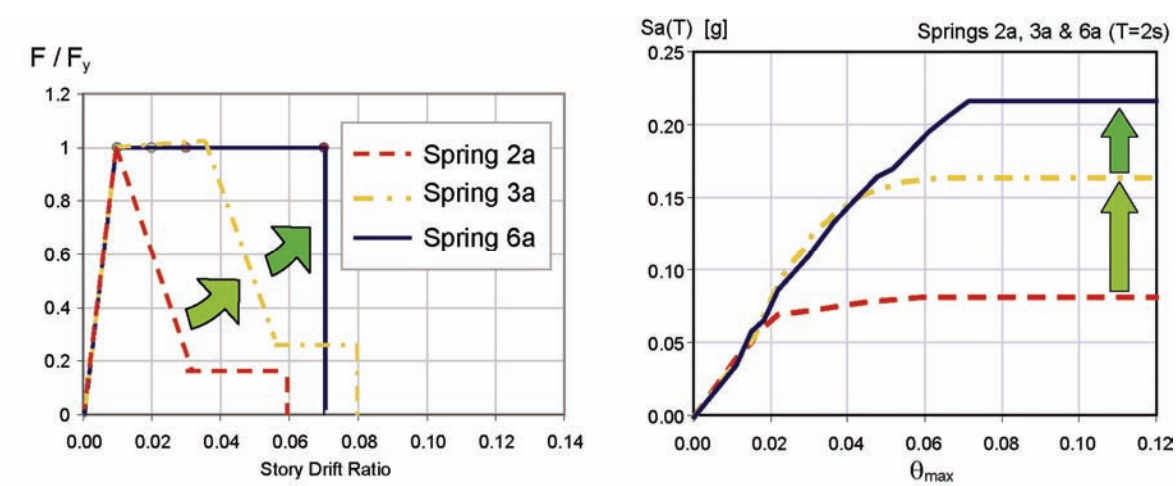

Figure 4-10 Effect of post-yield behavior on the collapse capacity of a system (Springs 2a, 3a and 6a with T=2.0s).

4.4.2 Slope of Degradation

Figure 4-11 shows the force-displacement capacity boundaries of Spring 2a and Spring 2b along with the corresponding IDA curves. These two systems have the same elastic stiffness, same yield strength, but differ in the negative slope of the strength-degrading segment and, therefore, in their potential for in-cycle strength degradation. They also have the same ultimate deformation capacity, but Spring 2b has a shorter residual strength plateau than Spring 2a because of the different slope.

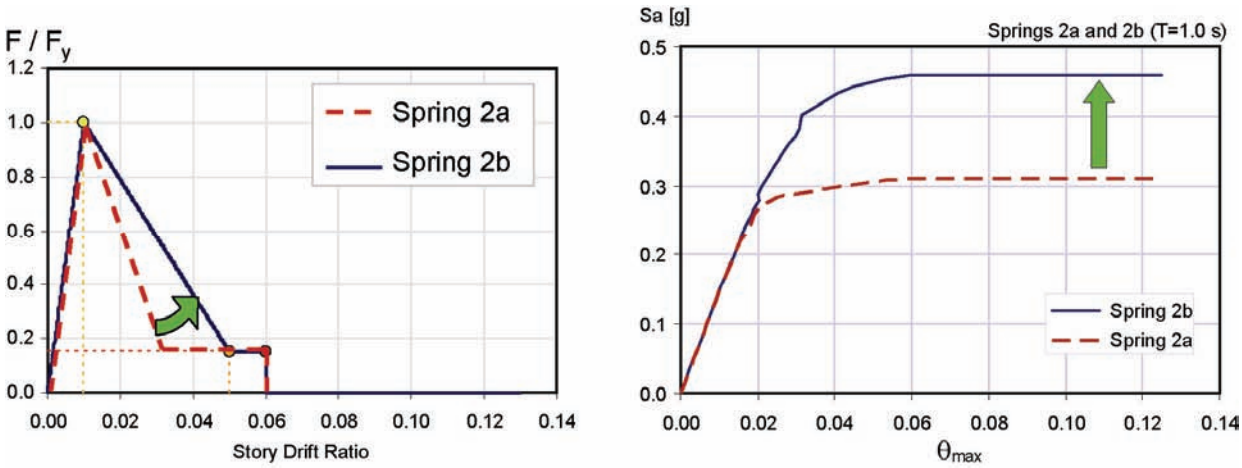

Figure 4-11 Effect of slope of degradation on the collapse capacity of a system (Springs 2a and 2b with T=1.0s).

The two systems have the same elastic behavior, but their response at drift demands larger than 0.01 is very different. Spring 2a, with a steeper degrading slope, likely experiences in-cycle strength degradation and reaches its collapse capacity relatively early, while Spring 2b, with a more shallow degrading slope, reaches a collapse capacity that is approximately 50% larger.

Figure 4-12 shows the force-displacement capacity boundaries of Spring 5a and Spring 5b along with the corresponding IDA curves. As in the case of Springs 2a and 2b, these two systems differ in the negative slope of the strength-degrading segments. They also differ in the presence of a residual strength plateau, which exists in Spring 5a, but not in Spring 5b.

As shown in the figure, the median IDA curves are similar up to 0.005 drift, at which both systems reach their peak strength. Beyond this point, the curves diverge as a result of the change in negative slope. Spring 5a, with steeper degrading slopes, reaches its collapse capacity sooner, while Spring 5b, with more shallow degrading slopes, reaches a higher collapse capacity.

The key parameter related to the observed change in response is the negative slope of the strength-degrading segment. In both examples, the change in negative slope changed the magnitude of potential in-cycle strength degradation, and overshadowed any changes in the residual strength plateau, as long as the ultimate deformation capacity remained the same.

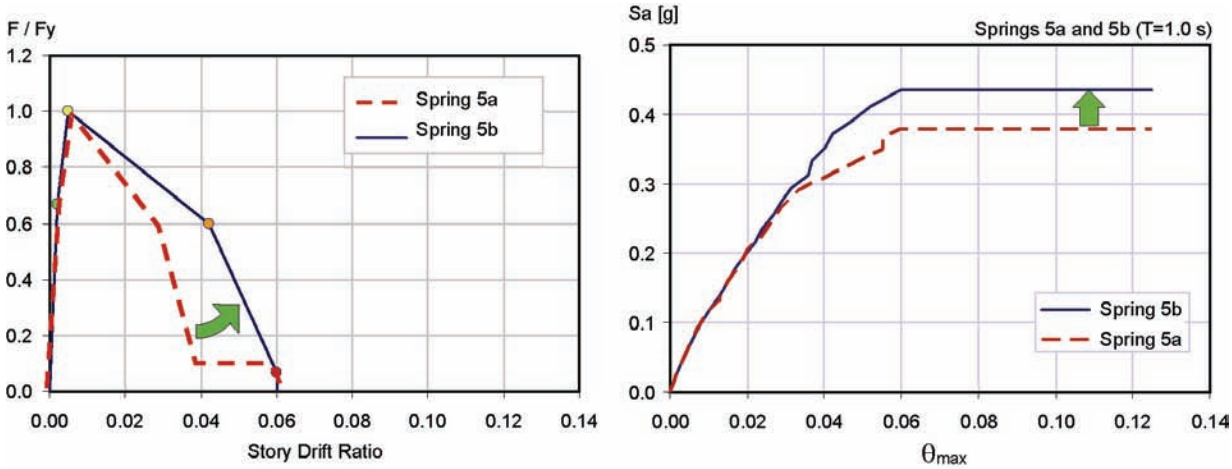

Figure 4-12 Effect of slope of degradation on the collapse capacity of a system (Springs 5a and 5b with T=1.0s).

4.4.3 Ultimate Deformation Capacity

Figure 4-13 shows the force-displacement capacity boundaries and corresponding IDA curves for Springs 1a and 1b. Figure 4-14 shows the force-displacement capacity boundaries and corresponding IDA curves for Springs 6a and 6b. These spring systems have very different post-yield behaviors, one with strength degradation (Springs 1a and 1b) and the other with elasto-plastic behavior (Springs 6a and 6b). In both cases, the "b" versions of each spring have higher ultimate deformation capacities.

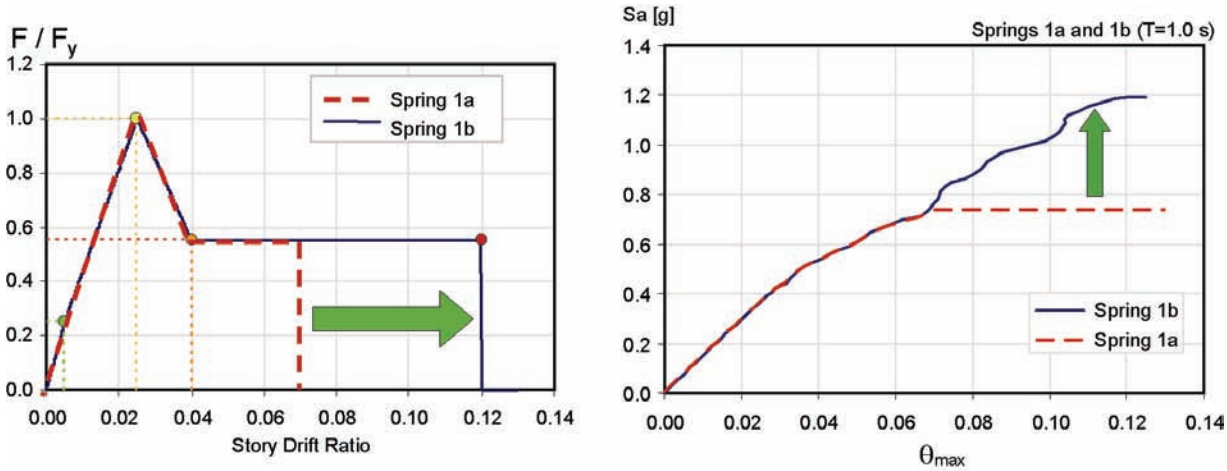

Figure 4-13 Effect of ultimate deformation capacity on the collapse capacity of a system (Springs 1a and 1b with T=1.0s).

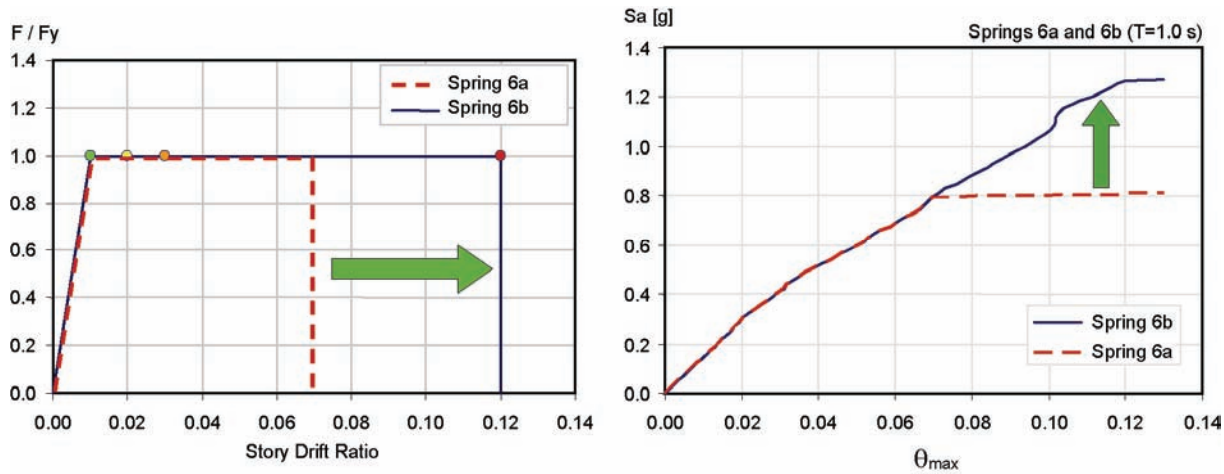

Figure 4-14 Effect of ultimate deformation capacity on the collapse capacity of a system (Springs 6a and 6b with T=1.0s).

In both examples, increasing the ultimate deformation capacity resulted in more than a 50% increase in collapse capacity. The key parameter related to the observed change in response is the increment in the ultimate deformation capacity. Observed changes in collapse capacity resulting from increases in the ultimate deformation capacity were insensitive to the other characteristics of the post-yield behavior of the springs.

4.4.4 Degradation of the Force-Displacement Capacity Boundary (Cyclic Degradation)

In general, most components will exhibit some level of cyclic degradation. To investigate the effects of cyclic degradation, the "a" and "b" versions of each spring (except Spring 6) were analyzed with both a constant force-displacement capacity boundary and a degrading force-displacement capacity boundary.

Consistent with observations from past studies, comparison of results between springs both with and without cyclic degradation show that the effects of cyclic degradation (as measured by gradual movement of the capacity boundary) are relatively unimportant in comparison with in-cycle degradation (as measured by the extent and steepness of negative slopes in the capacity boundary). This trend is illustrated for Spring 3b in Figure 4-15, but can be observed in the results for many spring systems. Although the system without cyclic degradation has a higher median collapse capacity, the difference is not very large. For the single-spring systems studied, the difference between median collapse capacity with and without cyclic degradation is shown in Appendix B. In general, this difference was typically less than 10%.

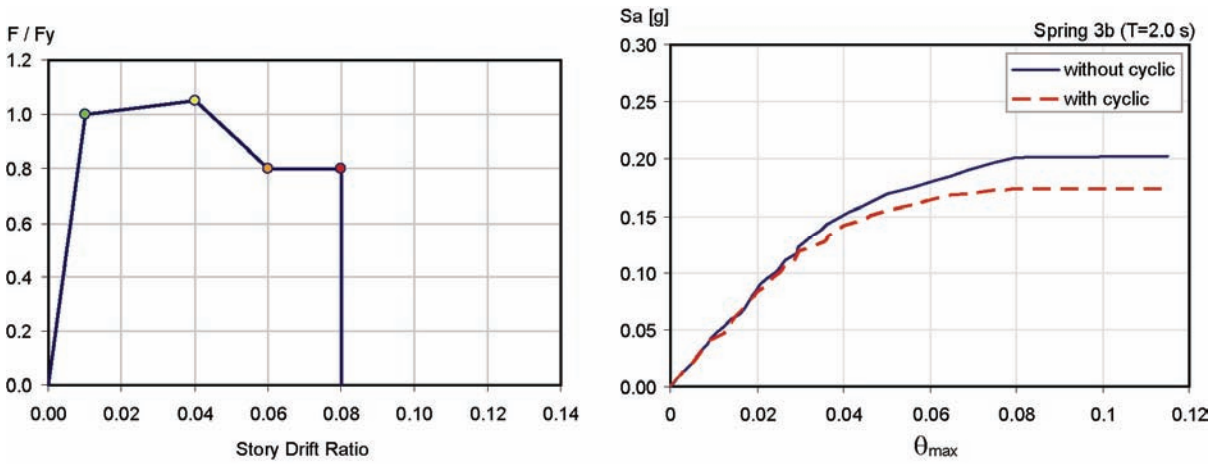

Figure 4-15 Effect of degradation of the force-displacement capacity boundary on the collapse capacity of a system (Spring 3b, T=2.0s, with and without cyclic degradation).

This observation has two important exceptions. First, the effect of cyclic degradation increases as the level of in-cycle degradation increases. Systems such as Spring 2b with a steep negative slope in the capacity boundary, indicating a strong potential for severe in-cycle strength degradation, showed as much as 30% difference in median collapse capacity between systems with and without cyclic degradation (Figure 4-16). Second, the effect of cyclic degradation increases as the period of vibration decreases. The short period (*T*=0.5s) versions of each spring showed more influence from cyclic degradation than the corresponding longer period (*T*=1.0s or *T*=2.0s) versions. This can be seen in the plots in Appendix B.

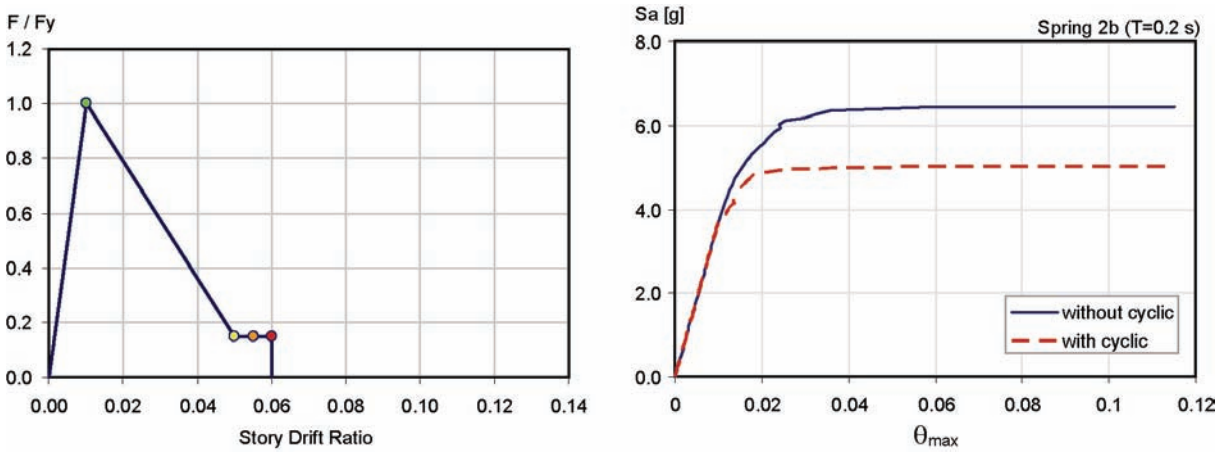

Figure 4-16 Effect of degradation of the force-displacement capacity boundary on the collapse capacity of a system (Spring 2b, T=0.2s, with and without cyclic degradation).

4.5 Observations from Multi-Spring Studies

This section summarizes the results from nonlinear dynamic analyses of multi-spring systems. Results from these studies were used to qualitatively:

- understand the influence of key features of the combined force-displacement capacity boundary on the nonlinear response of multi-spring systems,
- determine the effects of lateral strength on the dynamic stability of multi-spring systems, and
- determine the effects of secondary systems on the dynamic stability of multi-spring systems.

Only selected results are presented here. Combinations Nx2a+1a and Nx3a+1a, for N = 1, 2, 3, 5, or 9, are used to highlight trends observed to be generally applicable for the set of multi-spring combinations studied in this investigation. Results for each combination, plotted versus normalized and non-normalized intensity measures, are provided in Appendix C and Appendix D.

4.5.1 Normalized versus Non-Normalized Results

Two intensity measures were used in conducting incremental dynamic analyses. One was the 5% damped spectral acceleration at the fundamental period of vibration of the oscillator, $S_a(T,5\%)$. While generally appropriate for single-degree-of-freedom systems, this measure does not allow comparison between systems having different periods of vibration. For this reason, a normalized intensity measure, $R = S_a(T,5\%)/S_{ay}(T,5\%)$ was also used, where $S_{ay}(T,5\%)$ is the intensity that causes first yield to occur in the system.

In order to compare the response of different spring systems, it is necessary to plot the IDA curves from several springs in a single figure using a common intensity measure. This can be done in two ways. One way is to plot them using the normalized intensity measure, $R = S_a(T,5\%)/S_{ay}(T,5\%)$. First yield occurs at a normalized intensity of one, and increasing values of $S_a(T,5\%)/S_{ay}(T,5\%)$ represent increasing values of ground motion intensity with respect to the intensity required to initiate yielding in the system. Normalized plots provide a measure of system capacity relative to the yield intensity, and are useful for comparing results across different spring types when evaluating the influence of the key features of the force-displacement capacity boundary on the response of the system.

A second way to compare results is to plot them using an absolute (non-normalized) intensity measure that is somewhere in the middle of the range that would be suitable for the systems being plotted (e.g., T=1.0s). When evaluating the effects of increasing or decreasing the relative contribution of one subsystem with respect to another, use of a single absolute intensity measure allows comparison of results based on the relative strengths of different systems.

Since each method has advantages for viewing results and drawing comparisons, results for multi-spring systems were plotted using both the normalized intensity measure, $S_a(T,5\%)/S_{ay}(T,5\%)$, and non-normalized intensity measures, S_a(1s,5%) for stiff systems and S_a(2s,5%) for flexible systems. Results for normalized intensity measures, IM = $S_a(T,5\%)/S_{ay}(T,5\%)$, are provided in Appendix C, and results for non-normalized intensity measures, IM = S_a(1s,5%) or S_a(2s,5%), are provided in Appendix D. The horizontal axis in all cases is the maximum story drift ratio, θ_{max}, in radians.

4.5.2 Comparison of Multi-Spring Force-Displacement Capacity Boundaries

Figure 4-17 shows the force-displacement capacity boundaries for multi-spring systems Nx2a+1a and Nx3a+1a, normalized by the yield strength, F_y, of the combined system. Figure 4-18 shows the force-displacement capacity boundaries for the same two systems, normalized by the strength of the weakest system. Depending on the normalizing parameter used along the vertical axis, the resulting curves look very different.

In Figure 4-17, the use of a normalized base shear, F/F_y or S_a/S_{ay}, along the vertical axis allows for a better qualitative comparison of the relative shapes of the force-displacement capacity boundaries, without the added complexity caused by the different yield strengths of the systems. In this figure, it is easier to see how increasing the multiplier "N" on the lateral-force-resisting spring causes the combined system to more closely resemble the lateral spring itself (i.e., as "N" increases from 1 to 9, the combination Nx2a+1a begins to look more like Spring 2a).

Figure 4-17, however, is misleading with regard to the relative strengths of the combined systems. In normalizing to the yield strength of the combined system, higher values of yield strength will reduce the plotted values by a larger ratio, so curves for higher strength systems will plot below curves for lower strength systems in F/F_y coordinates.

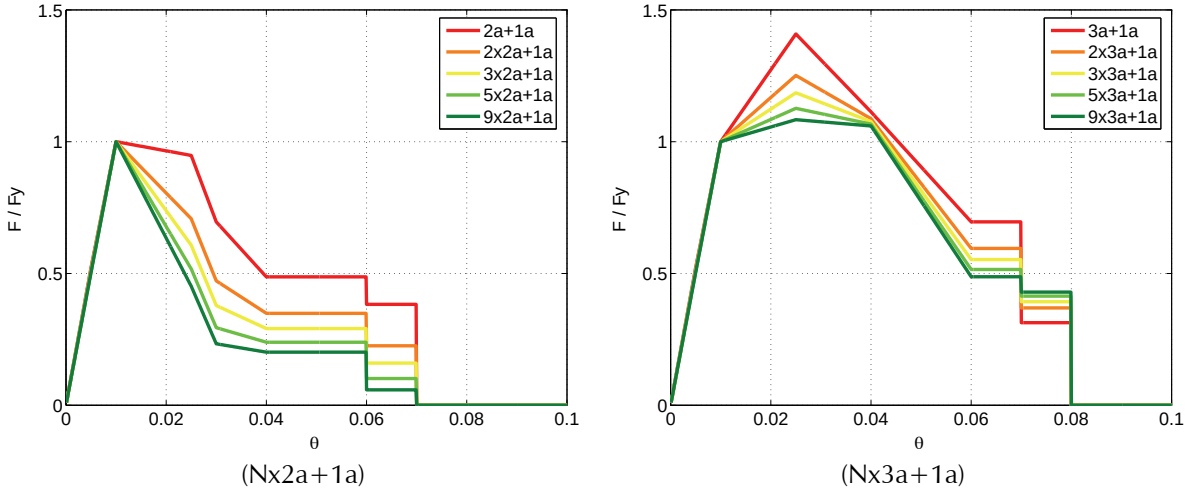

Figure 4-17 Force-displacement capacity boundaries for multi-spring systems Nx2a+1a and Nx3a+1a, normalized by the yield strength, Fy, of the combined system.

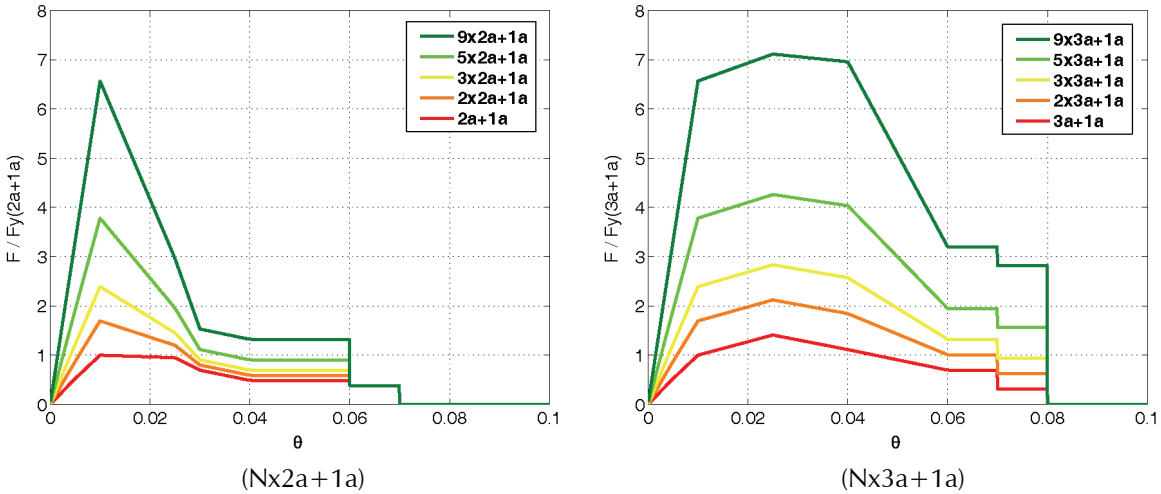

Figure 4-18 Force-displacement capacity boundaries for multi-spring systems Nx2a+1a and Nx3a+1a, normalized by the yield strength of the weakest system

In Figure 4-18, normalizing to the strength of the weakest system allows for a better comparison of the relative strength between the systems. In this figure it is easier to see how increasing the multiplier "N" on the lateral-force-resisting spring increases the strength of the combined system.

4.5.3 Influence of the Combined Force-Displacement Capacity Boundary in Multi-Spring Systems

Regardless of the normalizing parameter, Figure 4-17 and Figure 4-18 show how the combined force-displacement capacity boundaries change as the relative contributions of the springs vary. Results from single-spring studies demonstrated the influence of key features of the force-displacement capacity

boundary on the nonlinear dynamic response of a single-spring system. Results from multi-spring studies followed the same relationships. Multi-spring systems in which the combined force-displacement capacity boundary had more favorable features (e.g., delayed onset of degradation, more gradual slope of degradation, higher residual strength, and higher ultimate deformation capacity) performed better.

Figure 4-19 shows median IDA curves plotted versus the normalized intensity measure $R = S_a(T,5\%)/S_{ay}(T,5\%)$ for multi-spring systems Nx2a+1a and Nx3a+1a with a mass of 8.87 tons, representing a series of relatively stiff systems. As "N" increases, the yield strength of the combined system increases, and each system has a correspondingly shorter period of vibration.

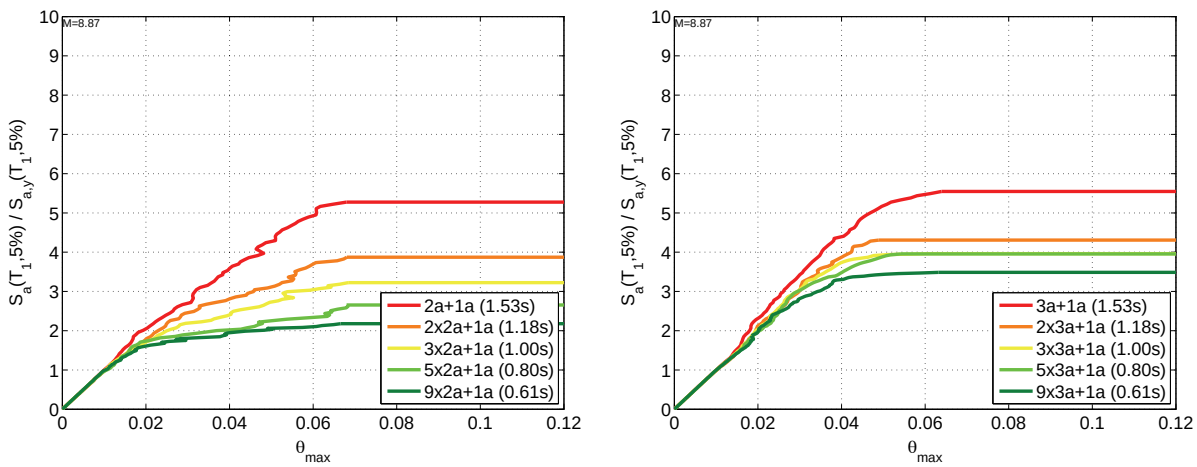

Figure 4-19 Median IDA curves plotted versus the normalized intensity measure Sa(T,5%)/Say(T,5%) for systems Nx2a+1a and Nx3a+1a with a mass of 8.87 tons.

Figure 4-20 shows median IDA curves for the same two systems with a mass of 35.46 tons, representing a series of relatively flexible systems. Because each system has a different period of vibration, normalized plots are used to qualitatively compare IDA curves between systems. Normalized curves, however, can be somewhat misleading with regard to the effect of changing "N" in the different spring combinations. The plotting positions in Figure 4-19, for example, are not an indication of the absolute collapse capacity of each system. Rather, they are a measure of collapse capacity relative to the intensity required to initiate yielding. Systems with high yield strengths may actually collapse at higher absolute intensities than systems with lower yield strengths, but because of the normalization to yield intensity, they plot out at lower ratios.

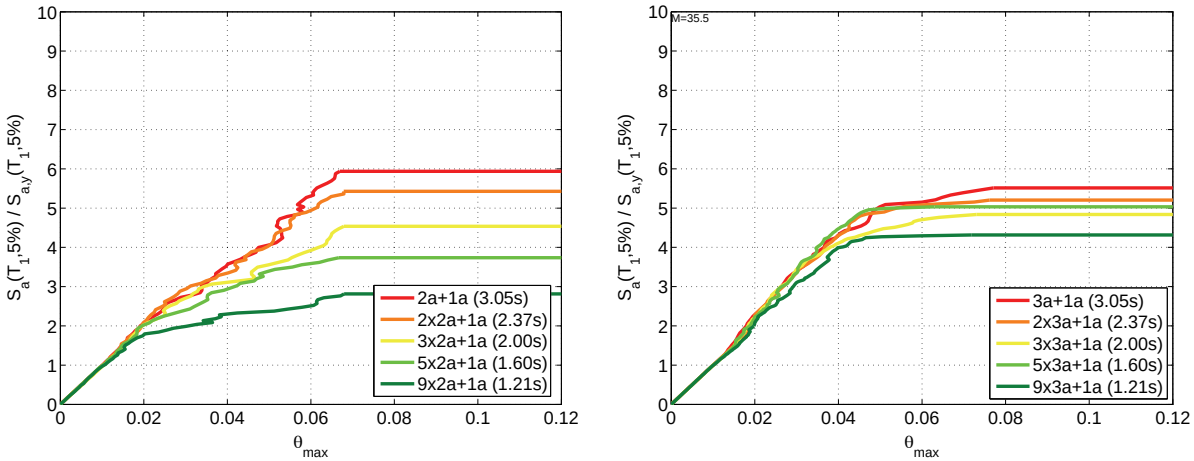

Figure 4-20 Median IDA curves plotted versus the normalized intensity measure $S_a(T,5\%)/S_{ay}(T,5\%)$ for systems Nx2a+1a and Nx3a+1a with a mass of 35.46 tons.

For system Nx2a+1a, Figure 4-19 and Figure 4-20 show that as "N" increases, collapse capacity decreases. The reason for this can be seen in the combined force-displacement capacity boundaries for system Nx2a+1a shown in Figure 4-17. Because of the characteristics of Spring 2a, combinations with higher multiples of "N" have steeper negative slopes. As was the case with single-spring systems, steeper slopes in the strength-degrading segment of the force-displacement capacity boundary result in lower collapse capacities.

For system Nx3a+1a, the results are the same, but less pronounced. Similar to system Nx2a+1a, the force-displacement capacity boundaries shown in Figure 4-17 for system Nx3a+1a with higher multiples of "N" have steeper negative slopes, but the differences are less significant.

Figure 4-19 and Figure 4-20 also show that, in general, combinations with systems that have more favorable characteristics result in higher median collapse capacities relative to yield intensity. For example, in Figure 4-19, system 9x2a+1a exhibits a median collapse capacity that is approximately 2.3 times the yield intensity while system 9x3a+1a exhibits a median collapse capacity that is approximately 3.5 times the yield intensity. The reason for this can be seen by comparing the combined force-displacement capacity boundaries for systems Nx2a+1a and Nx3a+1a shown in Figure 4-17. The post-yield characteristics of system Nx3a+1a are more favorable in terms of the post-yield slope, onset of degradation, and slope of degradation, resulting in better performance.

A more direct illustration of this behavior can be seen by comparing combinations using the "a" and "b" versions of primary spring components. Figure 4-21 shows the median IDA curves for systems Nx3a+1a and

Nx3b+1a. By definition, the "b" version of each spring was created to have more favorable characteristics than the "a" version of the same spring, with all other parameters being equal. As shown in the figure, the curves for system Nx3b+1a outperform all corresponding combinations of Nx3a+1a in terms of collapse capacity relative to yield intensity, for all values of "N" from 1 to 9.

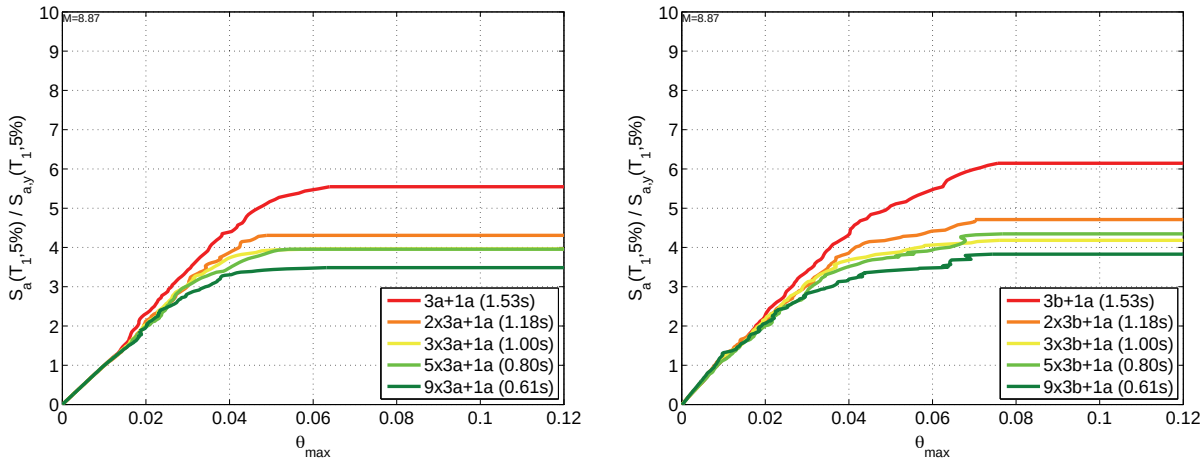

Figure 4-21 Median IDA curves plotted versus the normalized intensity measure $S_a(T,5\%)/S_{ay}(T,5\%)$ for systems Nx3a+1a and Nx3b+1a with a mass of 8.87 tons.

4.5.4 Effects of the Lateral Strength of Multi-Spring Systems

Plotting of results using absolute (non-normalized) intensity measures allows for comparison of results based on the relative strengths of different systems. Non-normalized intensity measures of S_a(1s,5%) for stiff systems and S_a(2s,5%) for flexible systems were used to identify the effects of the lateral strength of the multi-spring system on the lateral dynamic stability of the system.

Figure 4-22 shows median IDA curves for multi-spring systems Nx2a+1a and Nx3a+1a tuned with a mass of 8.87 tons. They are plotted versus S_a(1s,5%), which is an intensity measure keyed to a period of T=1.0s, located in the middle of the range of periods for the relatively stiff set of multi-spring systems. Figure 4-23 shows median IDA curves for same set of systems Nx2a+1a and Nx3a+1a, tuned with a mass of 35.46 tons. In this figure, the curves are plotted versus S_a(2s,5%), which is keyed to a period of T=2.0s, located in the middle of the range of periods for the relatively flexible set of multi-spring systems.

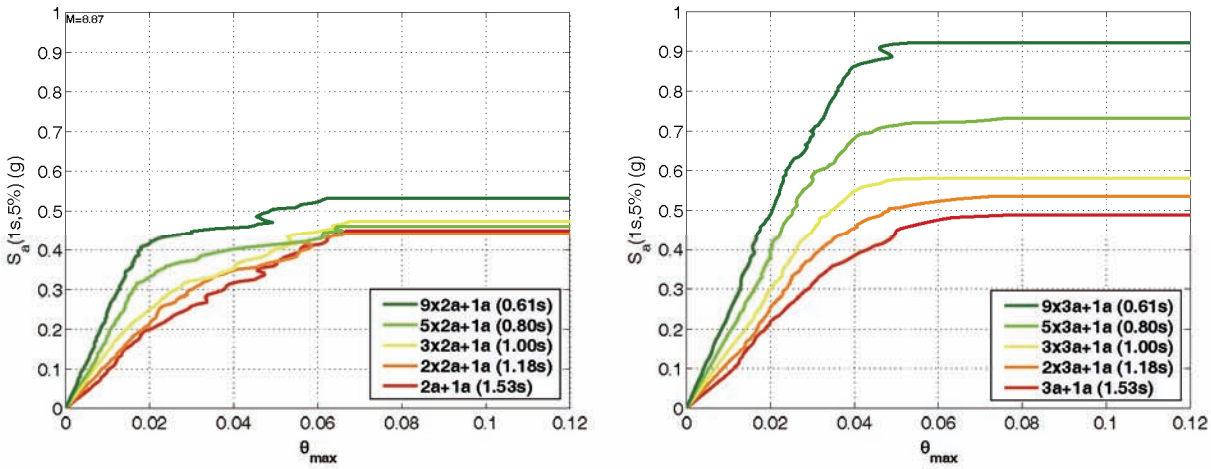

Figure 4-22 Median IDA curves plotted versus the common intensity measure S_a(1s,5%) for systems Nx2a+1a and Nx3a+1a with a mass of 8.87 tons.

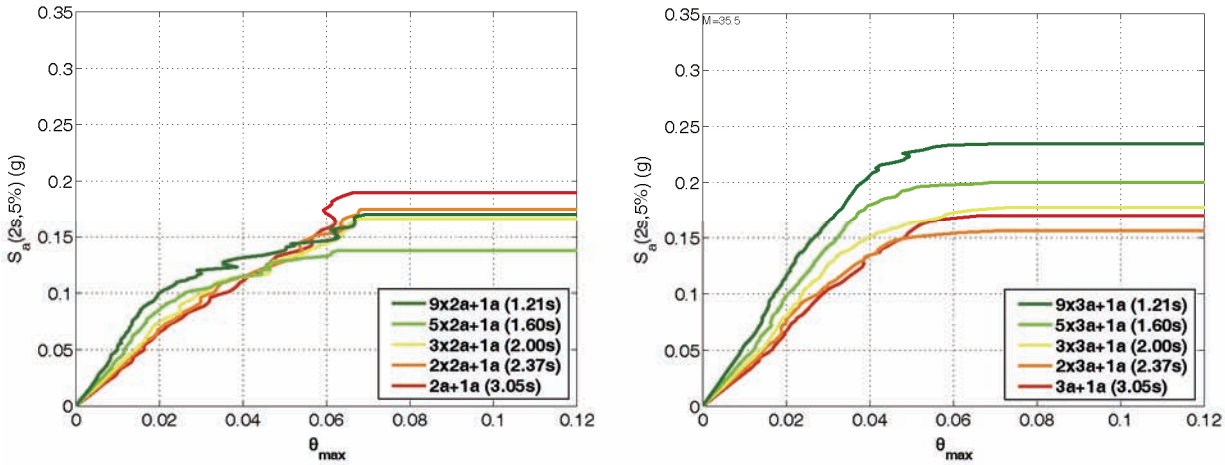

Figure 4-23 Median IDA curves plotted versus the common intensity measure S_a(2s,5%) for systems Nx2a+1a and Nx3a+1a with a mass of 35.46 tons.

In comparing non-normalized plots of IDA curves for various multi-spring combinations, the following observations were made:

- Increases in the lateral strength of a system change the intensity that initiates yielding in the system as well as the intensity at collapse (lateral dynamic instability). The incremental change in collapse capacity, however, is less than proportional to the increase in yield strength.
- The effectiveness of increasing the lateral strength of a system is a function of the shape of the force-displacement capacity boundary. Incremental changes in yield strength are more effective for ductile systems than they are for systems with less ductile behavior.

- The effectiveness of increasing the lateral strength of a system is also a function of the period of system. Incremental changes in yield strength are more effective for stiff systems than they are for flexible systems.

These effects can be observed by comparing the combined force-displacement capacity boundaries in Figure 4-18 with the resulting IDA curves in Figure 4-22 and Figure 4-23. Figure 4-22 shows that as "N" increases, the yield intensity increases significantly, however, increases in intensity at lateral dynamic instability are not as significant. For example, Figure 4-18 shows that the yield strength of system 9x3a+1a is approximately 6.5 times higher than the yield strength of system 3a+1a, but Figure 4-22 shows that the collapse capacity is only about two times higher.

Comparing results between systems Nx2a+1a and Nx3a+1a in Figure 4-22 shows that increases in collapse capacity that do occur as a result of changes in lateral strength are more pronounced for the more ductile Spring 3a than they are for the less ductile Spring 2a. For example, the increase in collapse capacity for system Nx3a+1a, as "N" increases from 1 to 9, is a factor of approximately 2.0. For system Nx2a+1a the corresponding increase in collapse capacity is a factor of approximately 1.25.

Comparing results between Figure 4-22 and Figure 4-23 shows that as the period increases, the increment in collapse capacity caused by a change in lateral strength decreases. For example, the increase in collapse capacity shown in Figure 4-22 for the relatively stiff combinations of system Nx3a+1a is a factor of approximately 2.0. The increase in collapse capacity shown in Figure 4-23 for the relatively flexible combinations of system Nx3a+1a is a factor of approximately 1.3.

4.5.5 Effects of Secondary System Characteristics

The contribution of a secondary ("gravity") system acting in parallel with a primary lateral-force-resisting system always results in an improvement in post-yield performance, especially close to collapse. This result was observed both qualitatively and quantitatively (i.e., both in normalized and non-normalized coordinates).

The improvement is larger when considering secondary systems with larger ultimate deformation capacities. Figure 4-24 shows median IDA curves plotted versus the normalized intensity measure $R = S_a(T,5\%)/S_{ay}(T,5\%)$ for multi-spring systems Nx2a+1a and Nx2a+1b with a mass of 8.87 tons. In the figure it can be seen that combinations with Spring 1b (with a larger ultimate deformation capacity) perform significantly better than combinations with

Spring 1a. This result was observed in combinations with all lateral-force-resisting springs.

Near collapse, secondary systems with larger deformation capacities have an even greater influence, even if the lateral strength is small compared to that of the primary system. This can be observed by comparing differences between systems 9x2a+1a and 9x2a+1b in Figure 4-24. Even though the relative contribution of Spring 1 in these combinations is small, the resulting collapse capacity is increased significantly.

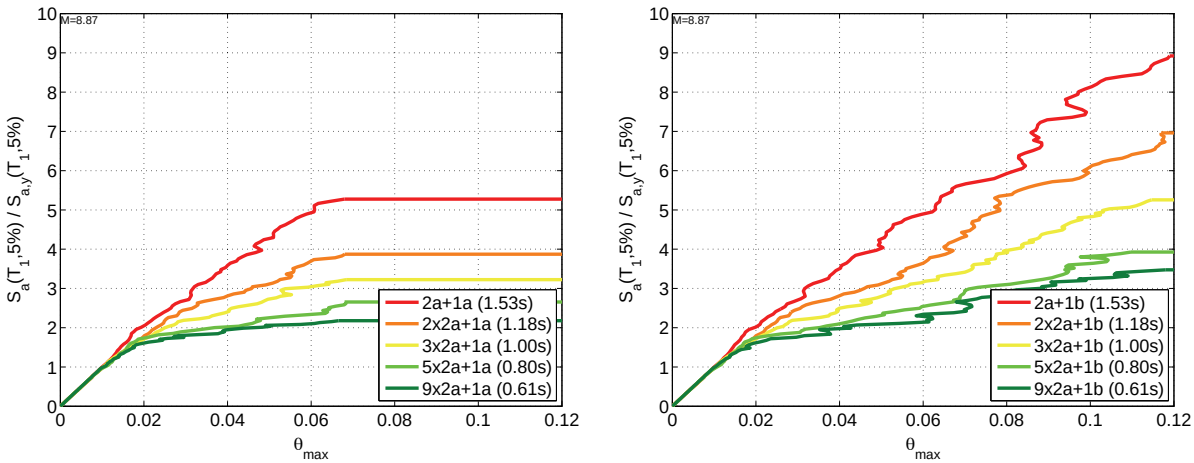

Figure 4-24 Median IDA curves plotted versus the normalized intensity measure $S_a(T,5\%)/S_{ay}(T,5\%)$ for systems Nx2a+1a and Nx2a+1b with a mass of 8.87 tons.

The contribution of the secondary system is more noticeable and significant in systems where the primary lateral resisting system is less ductile. Figure 4-25 shows median IDA curves plotted versus the normalized intensity measure $R = S_a(T,5\%)/S_{ay}(T,5\%)$ for multi-spring systems Nx2a+1a and Nx3a+1a with a mass of 8.87 tons.

Comparing the systems in Figure 4-25 shows a much wider spread between the median IDA curves for system Nx2a+1a than the curves for system Nx3a+1a. This means that the behavior of Spring 2a is more heavily influenced by the combination with Spring 1a than Spring 3a. The reason for this can be explained by the relative contributions of each spring to the combined force-displacement capacity boundaries in Figure 4-17.

Spring 2a, which represents a non-ductile moment frame system, has less favorable post-yield behavior in its force-displacement capacity boundary than does Spring 3a, which represents a ductile moment frame system. As such, Spring 2a is more favorably impacted by the characteristics of Spring 1a, and combinations with Spring 1a result in greater changes in performance. However, as "N" increases from 1 to 9, system Nx2a+1a

becomes more like Spring 2a, and the positive influences of Spring 1a diminish.

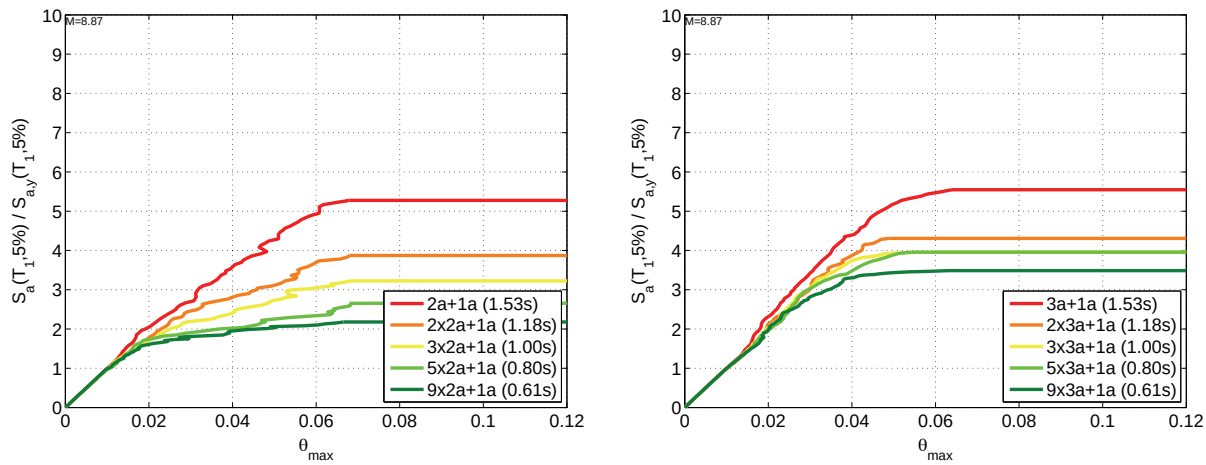

Figure 4-25 Median IDA curves plotted versus the normalized intensity measure Sa(T,5%)/Say(T,5%) for systems Nx2a+1a and Nx3a+1a with a mass of 8.87 tons.

4.6 Comparison with FEMA 440 Limitations on Strength for Lateral Dynamic Instability

In FEMA 440, a minimum strength requirement (maximum value of *R*) was developed as an approximate measure of the need to further investigate the potential for lateral dynamic instability caused by in-cycle strength degradation and P-delta effects. The recommended limitation is shown in Equation 4-1, with terms defined in Equation 4-2 and Equation 4-3, and illustrated in Figure 4-26:

$$R_{max} = \frac{\Delta_d}{\Delta_y} + \frac{\alpha_e^{-t}}{4} \tag{4-1}$$

where

$$t = 1 + 0.15 \ln T \tag{4-2}$$

and

$$\alpha_e = \alpha_{P-\Delta} + \lambda\left(\alpha_2 - \alpha_{P-\Delta}\right) \tag{4-3}$$

for $0 < \lambda < 1.0$.

In-cycle strength degradation caused by P-delta is represented by $\alpha_{P-\Delta}$. The effects from all other sources of cyclic and in-cycle strength and stiffness degradation are represented by the term $\left(\alpha_2 - \alpha_{P-\Delta}\right)$. At the time, it was apparent that modeling rules specified the use of hysteretic envelopes idealized from cyclic test results and would, consequently, overestimate

actual in-cycle losses. For this reason, these effects were reduced by factor λ, which was less than 1.0.

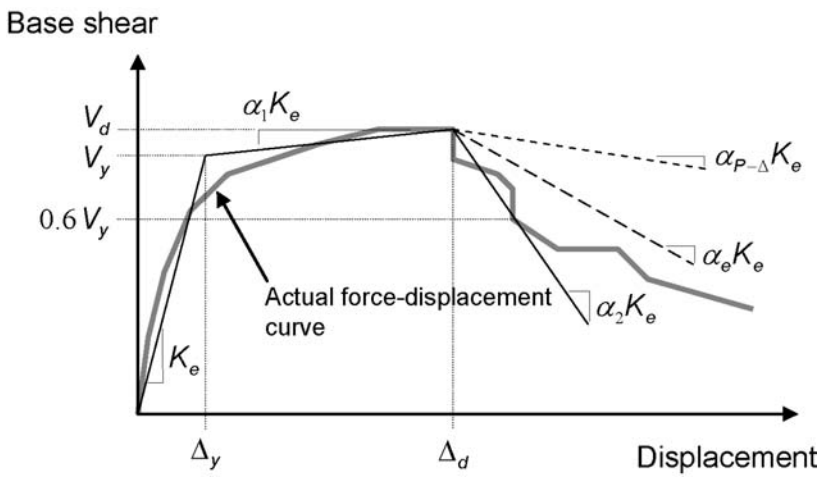

Figure 4-26 Idealized force-displacement curve for nonlinear static analysis (from FEMA 440).

According to FEMA 440, the idealized force-displacement relationship (Figure 4-26) and the factor λ were based on judgment, and significant variability should be expected in the value predicted using the equation for R_{max}. As such, R_{max} was intended only for identification of cases where further investigation using nonlinear response history analysis should be performed, and not as an accurate measure of the strength required to avoid lateral dynamic instability.

To further investigate correlation between the FEMA 440 equation for R_{max} and lateral dynamic instability, the results of this equation were compared to quantile IDA curves for selected multi-spring systems included in this investigation. In making this comparison, parameters in the FEMA 440 equation for R_{max} were estimated from multi-spring force-displacement capacity boundaries idealized as shown in Figure 4-27.

Results from this comparison indicate that values predicted by the FEMA 440 equation for R_{max} are variable, but generally plot between the median and 84th percentile results for lateral dynamic instability of the systems investigated. The trends observed in this comparison indicate that an improved equation, in a form similar to R_{max}, could be developed as a more accurate and reliable (less variable) predictor of lateral dynamic instability for use in current nonlinear static analysis procedures.

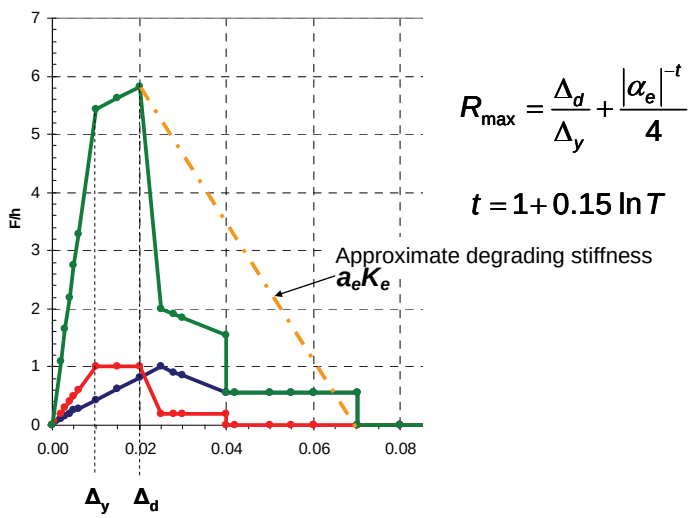

$$R_{max} = \frac{\Delta_d}{\Delta_y} + \frac{|\alpha_e|^{-t}}{4}$$

$$t = 1 + 0.15 \ln T$$

Figure 4-27 Idealization of multi-spring force-displacement capacity boundaries to estimate effective negative stiffness for use in the *FEMA 440* equation for R_{max}.

4.6.1 Improved Equation for Evaluating Lateral Dynamic Instability

An improved estimate for the strength ratio at which lateral dynamic instability might occur was developed based on nonlinear regression of the extensive volume of data generated during this investigation. In performing this regression, results were calibrated to the median response of the SDOF spring systems studied in this investigation.

A median-targeted strength ratio for lateral dynamic instability, R_{di}, is defined as:

$$R_{di} = \left(\frac{\Delta_c}{\Delta_y}\right)^a + b\frac{T_e}{3|\gamma|} + \frac{F_r}{F_c}\left(\frac{\Delta_u - \Delta_r}{\Delta_y}\right)\sqrt[3]{T_e} \tag{4-4}$$

where T_e is the effective fundamental period of vibration of the structure, Δ_y, Δ_c, Δ_r, and Δ_u are displacements corresponding to the yield strength, F_y, capping strength, F_c, residual strength, F_r, and ultimate deformation capacity at the end of the residual strength plateau, as shown in Figure 4-28. Parameters a and b are functions given by:

$$a = 1 - \exp(-dT_e) \tag{4-5}$$

$$b = 1 - \left(\frac{F_r}{F_c}\right)^2 \tag{4-6}$$

where the parameter *d* is a constant equal to 4 for systems with stiffness degradation, and 5 for systems without stiffness degradation. The parameter γ is the ratio of the post-capping slope (degrading stiffness) to the initial effective slope (elastic stiffness).

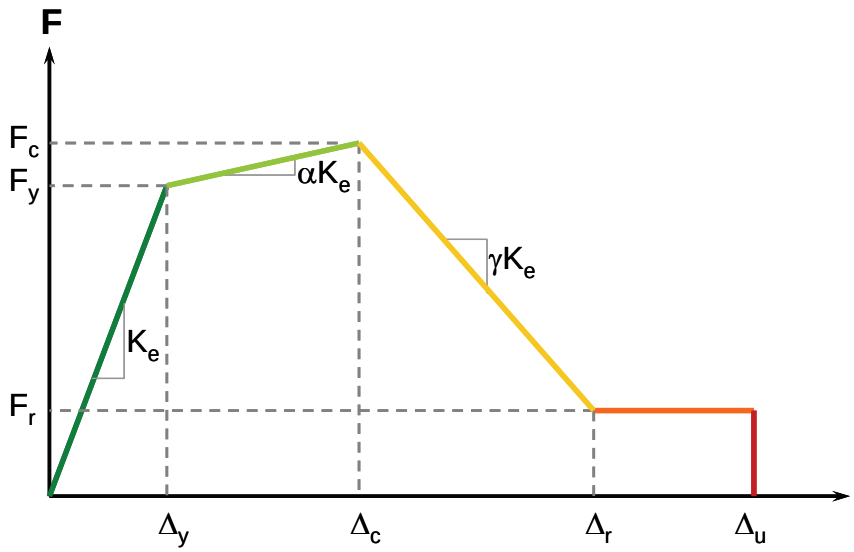

Figure 4-28 Simplified force-displacement boundary for estimating the median collapse capacity associated with lateral dynamic instability.

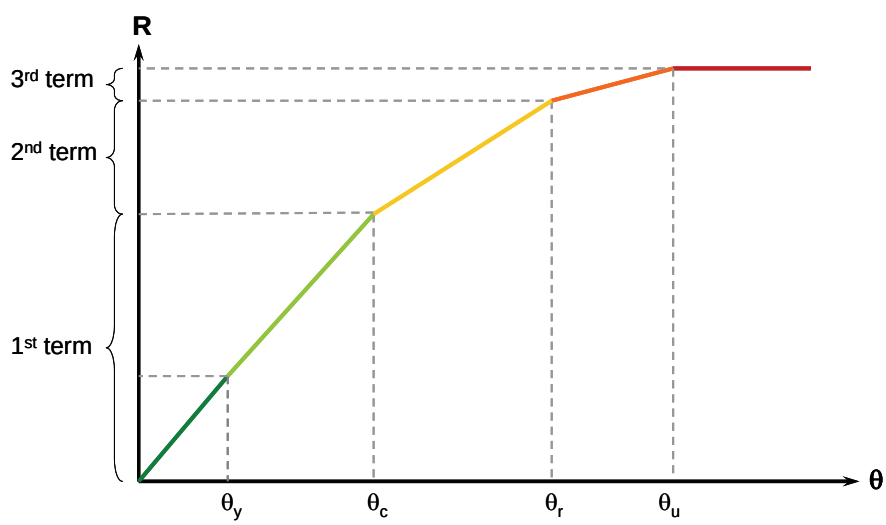

Figure 4-29 Relationship between Equation 4-4 and the segments of a typical IDA curve.

The three terms in Equation 4-4 relate to the segments of a typical force-displacement capacity boundary (Figure 4-28) and typical IDA curve (Figure 4-29). The first term provides an estimate of the median ground motion intensity corresponding to the end of the pseudo-linear segment of an IDA

curve (i.e., intensity at the onset of degradation). The second term provides an estimate of the increment in ground motion intensity required to push the structure onto the residual strength plateau. The third term provides an estimate of the increment in ground motion intensity required produce lateral dynamic instability (collapse).

As developed, the equation for R_{di} is intended to be a more reliable (less variable) predictor of median response at lateral dynamic instability. The resulting equation was compared to the FEMA 440 equation for R_{max} and overlaid onto results for selected multi-spring systems. With few exceptions, Figure 4-30 through Figure 4-35 show that the equation for R_{di} consistently predicts median response over a range of system types and periods of vibration.

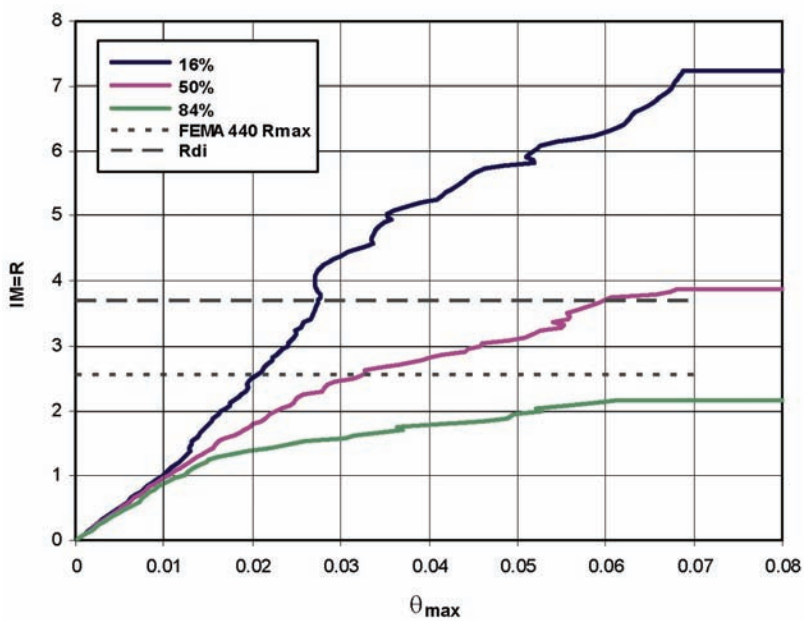

Figure 4-30 Comparison of R_{di} with FEMA 440 R_{max} and IDA results for system 2x2a+1a with T=1.18s.

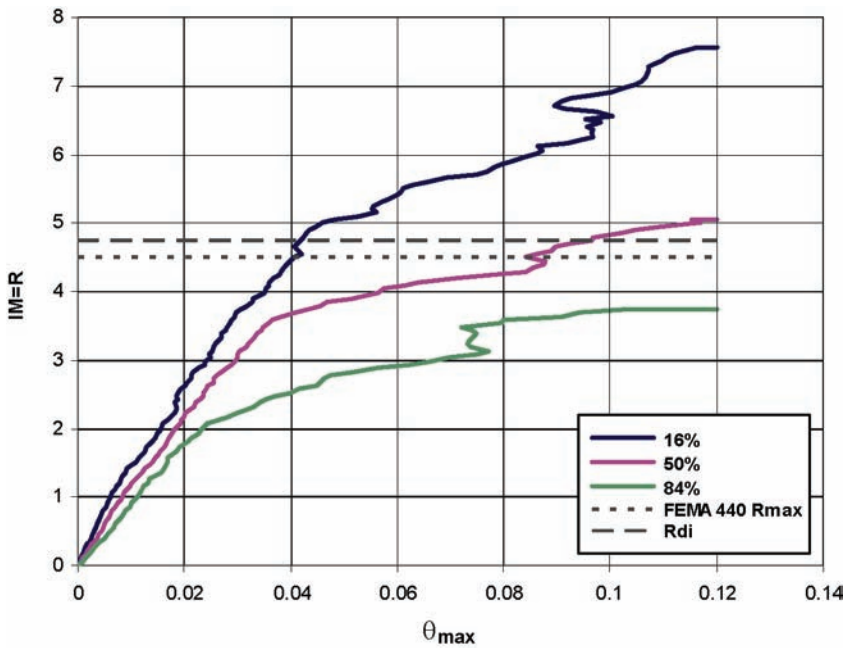

Figure 4-31 Comparison of R_{di} with FEMA 440 R_{max} and IDA results for system 3x3b+1b with T=1.0s.

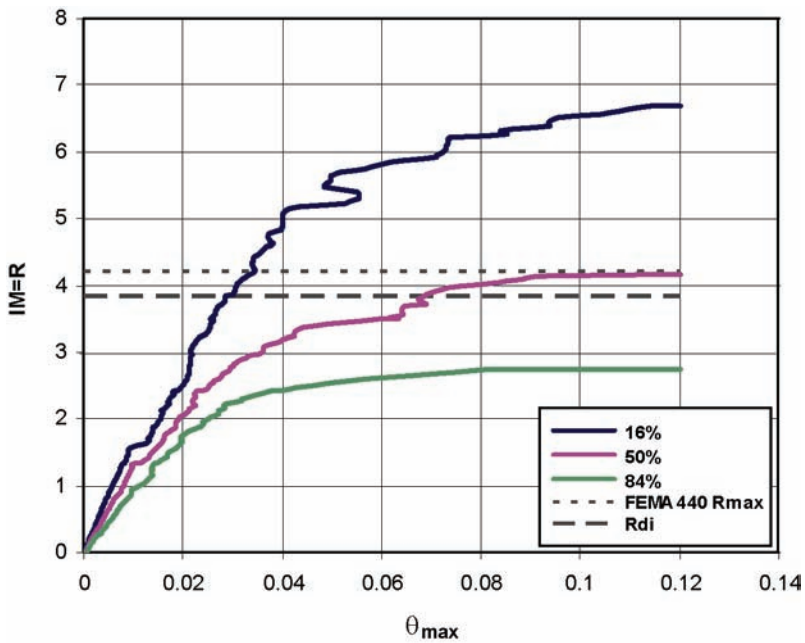

Figure 4-32 Comparison of R_{di} with FEMA 440 R_{max} and IDA results for system 9x3b+1b with T=0.61s.

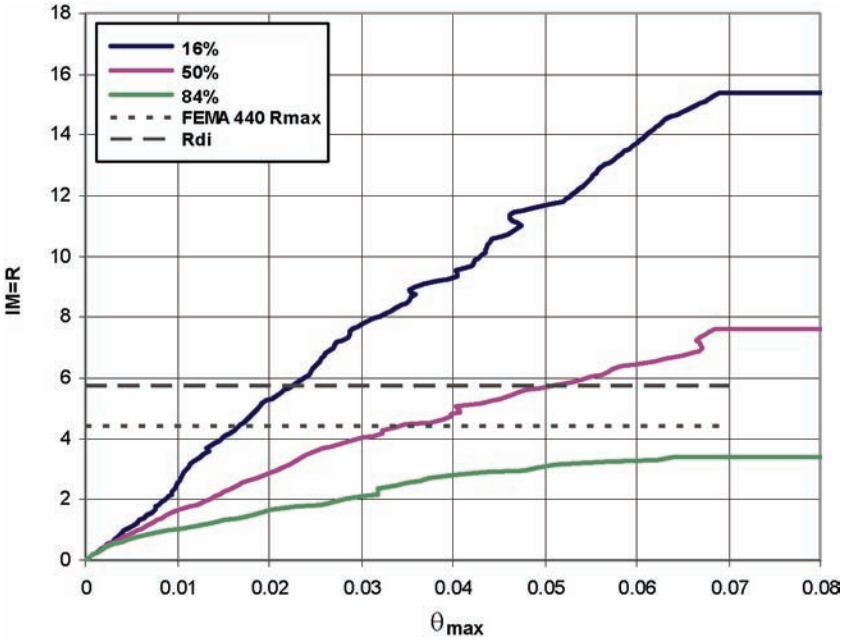

Figure 4-33 Comparison of R_{di} with FEMA 440 R_{max} and IDA results for system 5x5a+1a with T=1.15s.

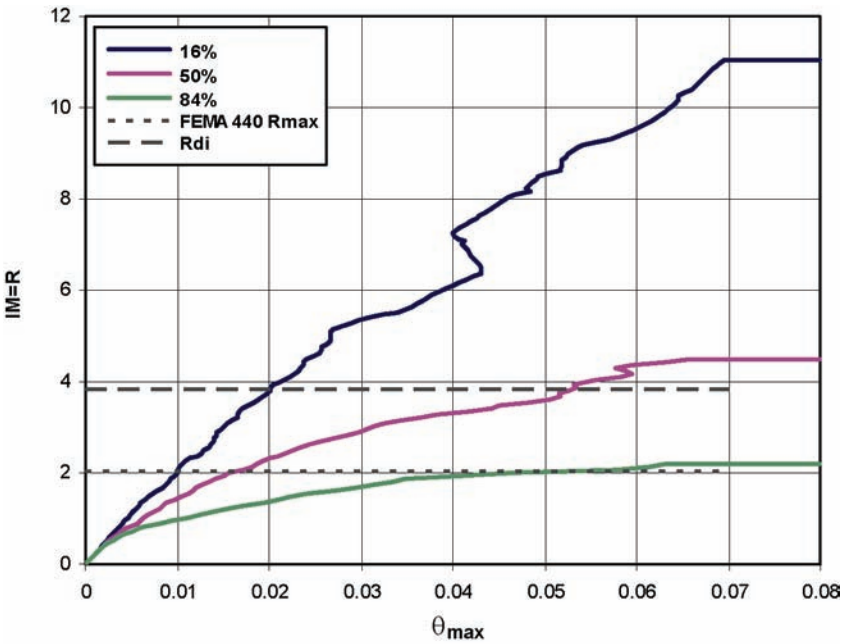

Figure 4-34 Comparison of R_{di} with FEMA 440 R_{max} and IDA results for system 5x5a+1a with T=0.58s.

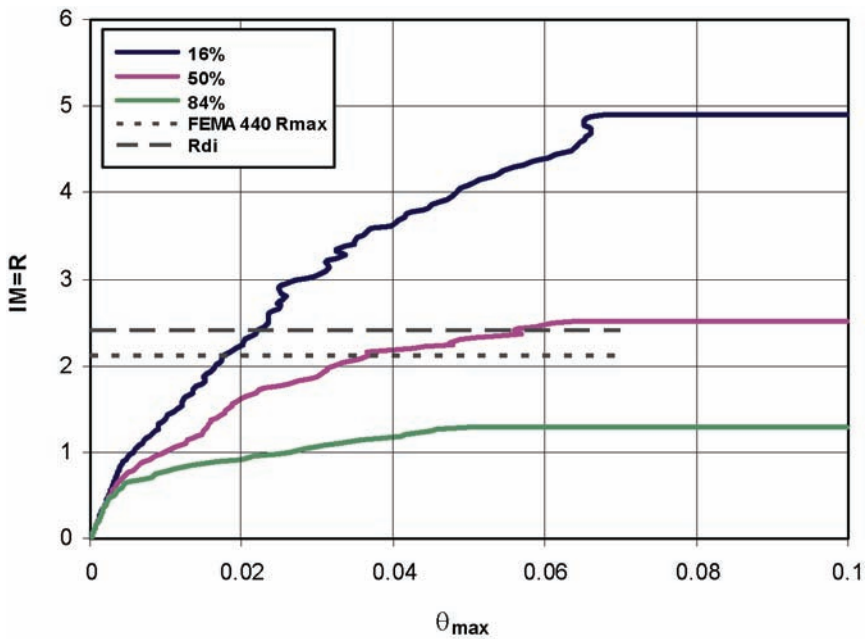

Figure 4-35 Comparison of R_{di} with FEMA 440 R_{max} and IDA results for system 9x5a+1a with T=0.34s.

Chapter 5
Findings, Conclusions, and Recommendations

This chapter summarizes the findings, conclusions, and recommendations resulting from the literature review and focused analytical studies of this investigation. Information from other chapters is collected and repeated here for ease of reference. In this chapter, findings have been grouped into the following categories:

- Findings related to improved understanding of nonlinear degrading response and judgment in implementation of nonlinear analysis results in engineering practice.
- Recommended improvements to current nonlinear analysis procedures
- Suggestions for further study

From the literature review, it is apparent that in-cycle strength and stiffness degradation are real phenomena that have been observed and documented to cause instability in individual components. Focused analytical studies have shown that larger assemblies of components of mixed hysteretic behavior experience similar negative stiffness that can lead to lateral dynamic instability. These studies have been able to link nonlinear dynamic response to major characteristics of component and system degrading behavior.

These studies have also confirmed many of the conclusions regarding degradation and lateral dynamic instability presented in FEMA 440: (1) in-cycle strength degradation is a significant contributor to dynamic instability; (2) cyclic degradation can increase the potential for dynamic instability, but its effects are far less significant in comparison with in-cycle degradation; and (3) an equation, such as R_{max}, could be used as an indicator of potential lateral dynamic instability for use in current nonlinear static analysis procedures.

5.1 Findings Related to Improved Understanding and Judgment

This section summarizes observations and conclusions related to improved understanding of nonlinear degrading response and judgment in implementation of nonlinear analysis results in engineering practice. Findings, and practical ramifications for engineering practice, are summarized in the sections that follow.

5.1.1 Sidesway Collapse versus Vertical Collapse

Lateral dynamic instability is manifested in structural systems as sidesway collapse caused by loss of lateral-force-resisting capacity. Most sidesway collapse mechanisms can be explicitly simulated in nonlinear response history analyses. It should be noted, however, that inelastic deformation of structural components can result in shear and flexural-shear failures in members, and failures in joints and connections, which can lead to an inability to support vertical loads (vertical collapse) long before sidesway collapse can be reached.

5.1.1.1 Practical Ramifications

Behavior of real structures can include loss of vertical-load-carrying capacity at lateral displacements that are significantly smaller than those associated with sidesway collapse. Use of the findings of this investigation with regard to lateral dynamic instability (sidesway collapse) in engineering practice should include consideration of possible vertical collapse modes that could be present in the structure under consideration.

5.1.2 Relationship between Loading Protocol, Cyclic Envelope, and Force-Displacement Capacity Boundary

Historically, the term “backbone curve” has referred to many different things. For this reason, two new terms have been introduced to distinguish between different aspects of hysteretic behavior. These are the *force-displacement capacity boundary*, and *cyclic envelope*.

5.1.2.1 Force-Displacement Capacity Boundary

A force-displacement capacity boundary defines the maximum strength that a structural member can develop at a given level of deformation, resulting in an effective “boundary” for the strength of a member in force-deformation space (Figure 5-1). In many cases, the force-displacement capacity boundary corresponds to the monotonic force-deformation curve.

A cyclic load path cannot cross a force-displacement capacity boundary. If a member is subjected to increasing deformation and the boundary is reached, then the strength that can be developed in the member is limited and the response must continue along the boundary (in-cycle strength degradation). Only displacement excursions intersecting portions of the capacity boundary with a negative slope will result in in-cycle strength degradation.

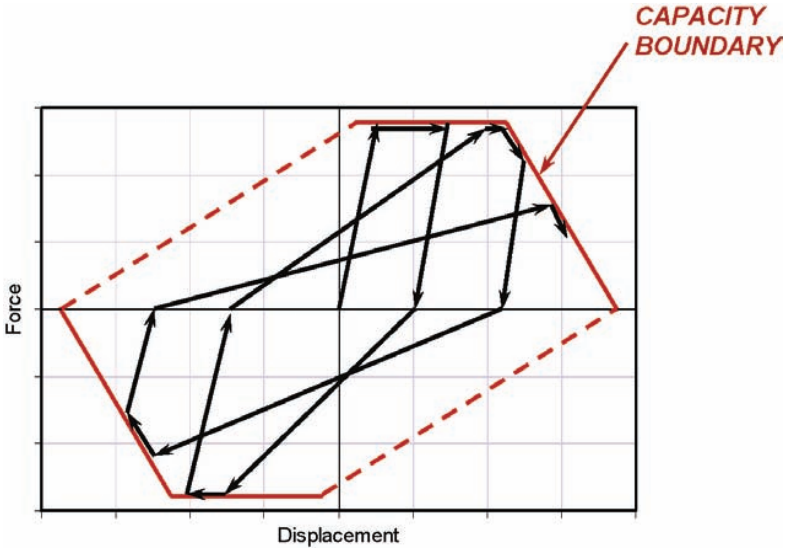

Figure 5-1 Example of a force-displacement capacity boundary.

5.1.2.2 Cyclic Envelope

A cyclic envelope is a force-deformation curve that envelopes the hysteretic behavior of a component or assembly that is subjected to cyclic loading (Figure 5-2).

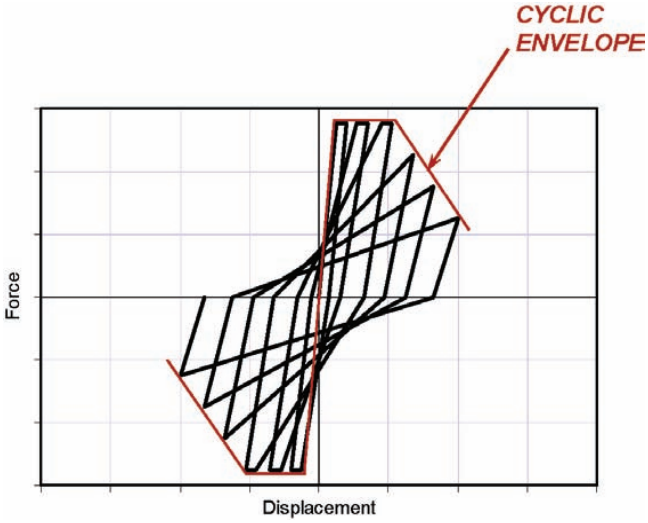

Figure 5-2 Example of a cyclic envelope.

The characteristics of the cyclic envelope are strongly influenced by the points at which unloading occurs in a test, and are therefore strongly influenced by the loading protocol that was used in the experimental program. Nominally identical specimens loaded with different loading protocols will have different cyclic envelopes depending on the number of cycles used in the loading protocol, the amplitude of each cycle, and the sequence of the loading cycles, as illustrated in Section 2.2.3.

Under lateral deformations that are less than or equal to those used to generate the cyclic envelope, differences between the cyclic envelope and the force-displacement capacity boundary are of no consequence. However, under larger lateral displacements these differences will affect the potential for in-cycle degradation to occur, and will significantly affect system behavior and response (Figure 5-3).

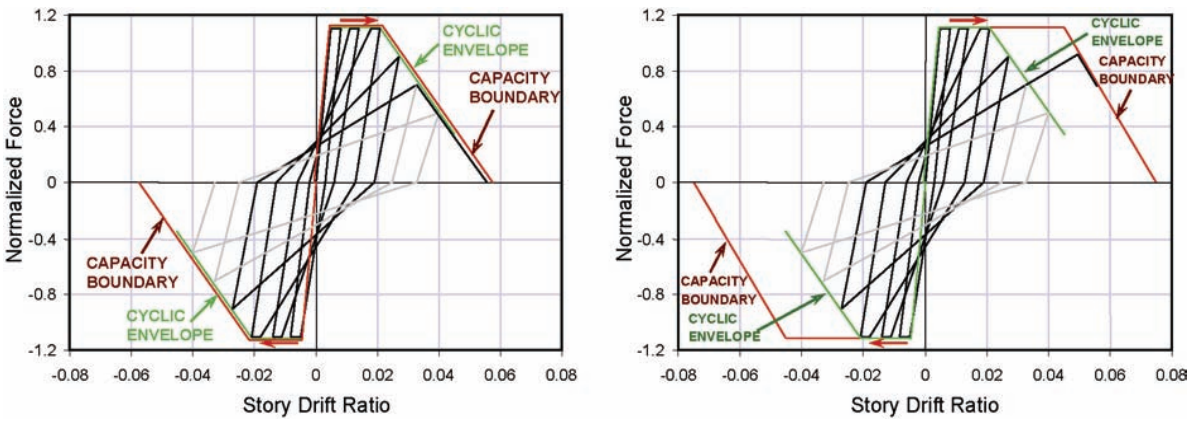

(a) (b)

Figure 5-3 Comparison of hysteretic behavior when the force-displacement capacity boundary is: (a) equal to the cyclic envelope, and (b) extends beyond the cyclic envelope.

Constraining nonlinear hysteretic behavior within the limits of a cyclic envelope that does not capture the full range of permissible force-deformation response, as defined by the force-displacement capacity boundary, will result in overly pessimistic predictions of the nonlinear dynamic response of a system.

5.1.2.3 Practical Ramifications

Nonlinear component parameters should be based on the force-displacement capacity boundary, which is different from a cyclic envelope. Determining the force-displacement capacity boundary from test results using a single cyclic loading protocol can result in significant underestimation of the actual capacity for force-deformation response and subsequent overestimation of nonlinear displacement demands.

5.1.3 Characteristics of Median IDA Curves

Observed relationships between IDA curves and degrading component characteristics suggest that dynamic response is directly influenced by the features of a force-displacement capacity boundary. This relationship, which is dependent upon the period of vibration of the system, is depicted in the idealized graphical representation of Figure 5-4.

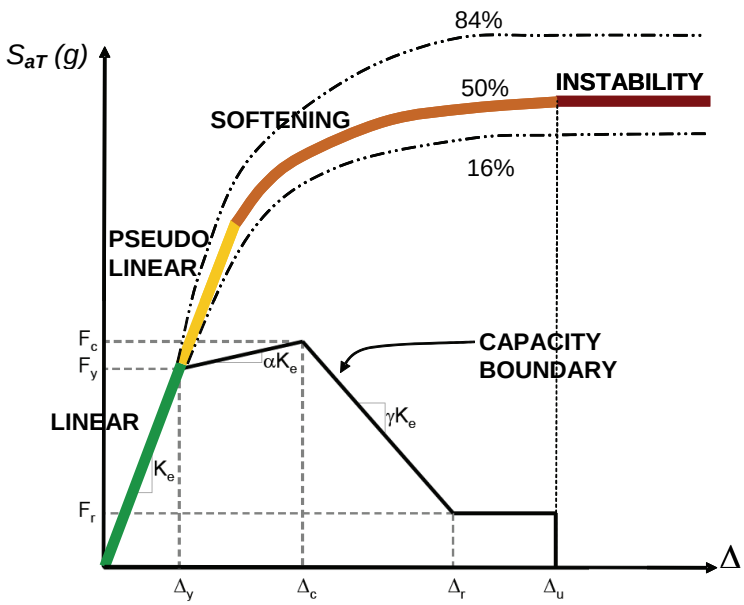

Figure 5-4 Relationship between IDA curves and the features of a typical force-displacement capacity boundary.

In general, median IDA curves were observed to exhibit the following characteristics:

- An initial linear segment corresponding to linear-elastic behavior in which in lateral deformation demand is proportional to ground motion intensity, regardless of the characteristics of the system or the ground motion. This segment extends from the origin to the onset of yielding.
- A second curvilinear segment corresponding to inelastic behavior in which lateral deformation demand is no longer proportional to ground motion intensity. As intensity increases, lateral deformation demands increase at a faster rate. This segment corresponds to softening of the system, or reduction in stiffness (reduction in the slope of the IDA curve). In this segment, the system "transitions" from linear behavior to eventual dynamic instability. Although a curvilinear segment is always present, in some cases the transition can be relatively long and gradual, while in other cases it can be very short and abrupt.

- A final linear segment that is horizontal, or nearly horizontal, in which infinitely large lateral deformation demands occur at small increments in ground motion intensity. This segment corresponds to the point at which a system becomes unstable (lateral dynamic instability). For SDOF systems, this point corresponds to the ultimate deformation capacity at which the system loses all lateral-force-resisting capacity.

In some systems, the initial linear segment can be extended beyond yield into the inelastic range. In this pseudo-linear segment, lateral deformation demand is approximately proportional to ground motion intensity, which is consistent with the familiar equal-displacement approximation for estimating inelastic displacements. The range of lateral deformation demands over which the equal-displacement approximation is applicable depends on the characteristics of the force-displacement capacity boundary of the system and the period of vibration.

5.1.3.1 Practical Ramifications

The observed relationships support the conclusion that it is possible to estimate nonlinear dynamic response based on knowledge of the characteristics of the force-displacement capacity boundary.

5.1.4 Dependence on Period of Vibration

In general, moderate and long period systems with zero or positive post-yield stiffness in the force-displacement capacity boundary follow the equal displacement trend well into the nonlinear range, as shown for Spring 3a in Figure 5-5. For systems with periods longer than 0.5s, Spring 3a exhibits an extension of the initial linear segment well beyond the yield drift of 0.01. In contrast, the short period system (T=0.2s) diverges from the initial linear segment just after yielding, even at deformations within the strength-hardening segment of the force-displacement capacity boundary (drifts between 0.01 and 0.04 in the figure).

5.1.4.1 Practical Ramifications

It is important to consider the dependence on period of vibration in conjunction with the effects of other parameters identified in this investigation. The generalized effect of any one single parameter can be misleading.

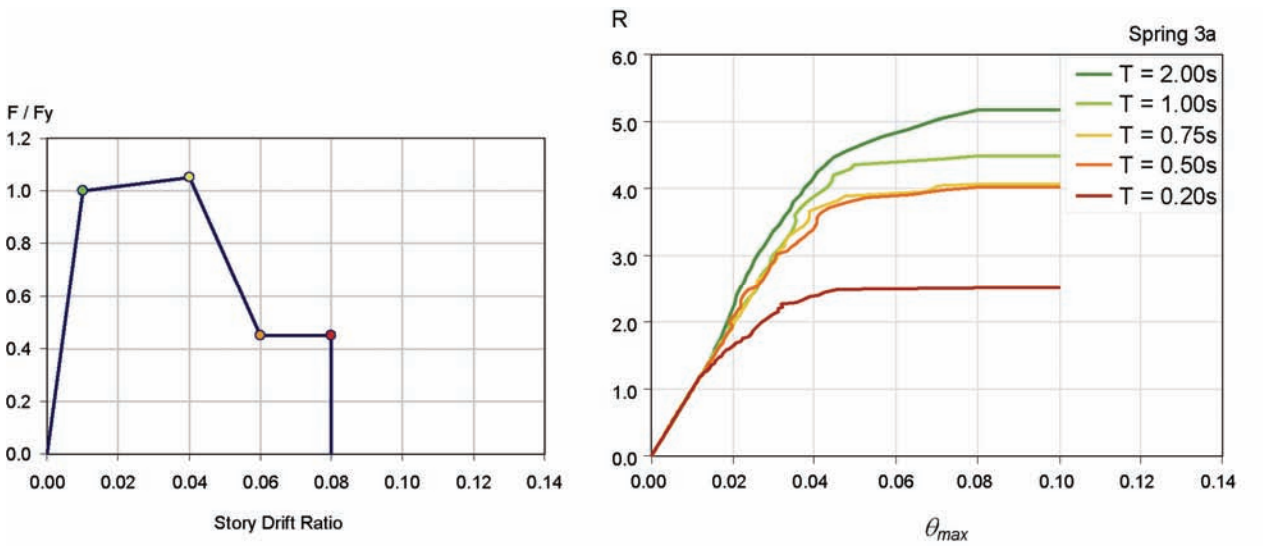

Figure 5-5 Force-displacement capacity boundary and median IDA curves for Spring 3a with various periods of vibration.

5.1.5 Dispersion in Response

Nonlinear response is sensitive to the characteristics of the ground motion record, and will vary from one ground motion to the next, even when scaled to the same intensity (Figure 5-6). For a given level of ground motion intensity, the lateral deformation demand can be significantly smaller or significantly larger than the value shown on median IDA curves, as indicated by the 16th and 84th percentile curves in the figure. As the level of ground motion intensity increases, the dispersion in response tends to increase.

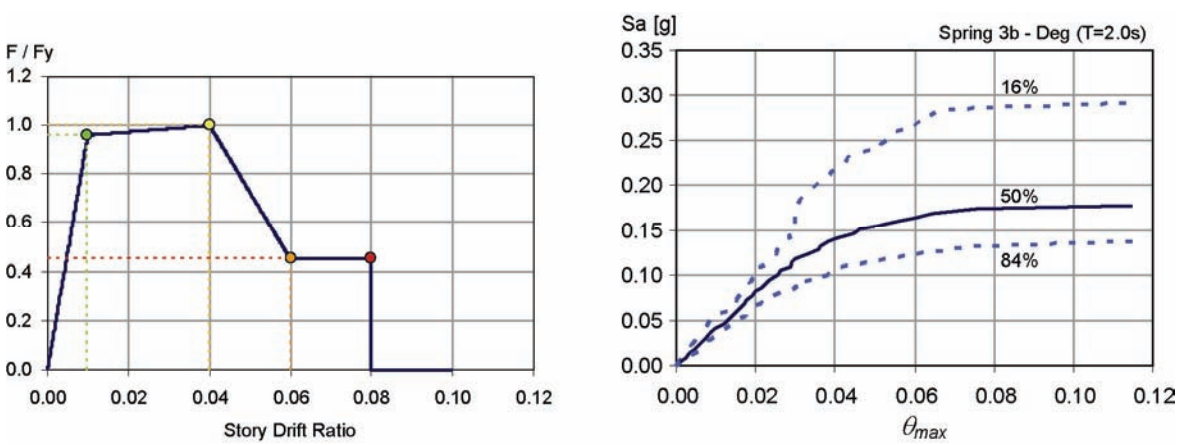

Figure 5-6 Force-displacement capacity boundary and 16th, 50th and 84th percentile IDA curves for Spring 3b with a period of vibration T=2.0s.

5.1.5.1 Practical Ramifications

It is important to recognize the level of uncertainty that is inherent in nonlinear analysis, particularly regarding variability in response due to

ground motion uncertainty. It may not be sufficient to rely on median (50%) estimates of response for certain design or evaluation quantities of interest, unless the intensity of the ground motion is associated with an appropriately rare probability of exceedance.

5.1.6 Influence of the Force-Displacement Capacity Boundary

Key features of a force-displacement capacity boundary that were observed to influence the shape of median IDA curves included post-yield behavior and onset of degradation, slope of degradation, ultimate deformation capacity, and presence of cyclic degradation. Systems in which the force-displacement capacity boundary had more favorable post-yield characteristics (e.g., delayed onset of degradation, more gradual slope of degradation, higher residual strength, and higher ultimate deformation capacity) were observed to perform better.

5.1.6.1 Post-Yield Behavior and Onset of Degradation

The presence of a non-negative post-yield slope and delay before the onset of degradation reduced potential in-cycle strength degradation and significantly improved the collapse capacity of a system (Figure 5-7).

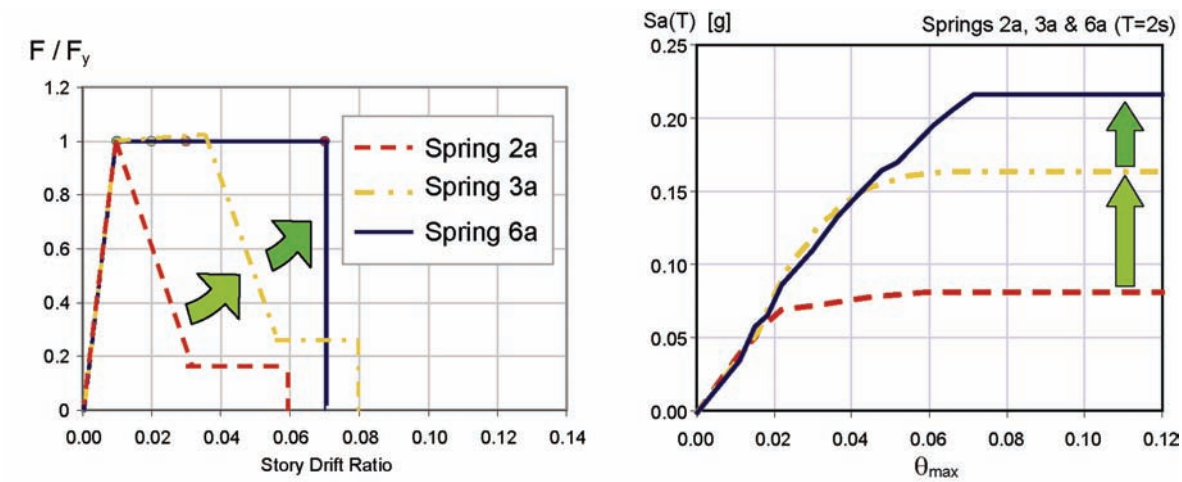

Figure 5-7 Effect of post-yield behavior on the collapse capacity of a system (Springs 2a, 3a and 6a with T=2.0s).

5.1.6.2 Slope of Degradation

Differences in the negative slope of the strength-degrading segment significantly affected the collapse capacity of a system. Systems with more shallow degrading slopes reached higher collapse capacities than systems with steeper degrading slopes (Figure 5-8). Changes in negative slope changed the magnitude of potential in-cycle strength degradation, and overshadowed any changes in other parameters (e.g., the residual strength plateau), as long as the ultimate deformation capacity remained the same.

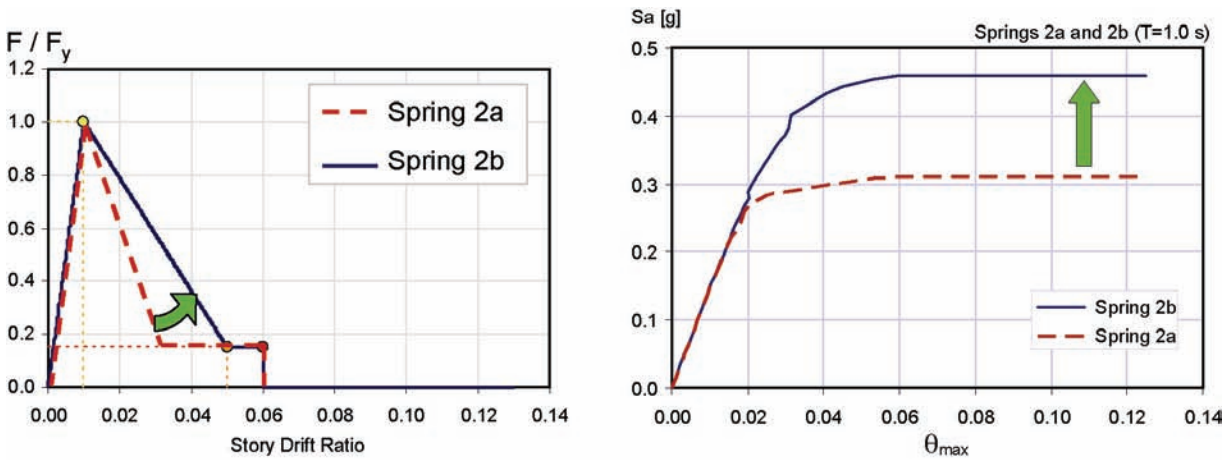

Figure 5-8 Effect of slope of degradation on the collapse capacity of a system (Springs 2a and 2b with T=1.0s).

5.1.6.3 Ultimate Deformation Capacity

Increasing the ultimate deformation capacity resulted in significant increases in collapse capacity (Figure 5-9). The key parameter related to the observed change in response is the increment in the ultimate deformation capacity. Observed changes in collapse capacity resulting from increases in the ultimate deformation capacity were insensitive to other characteristics of the post-yield behavior of the springs.

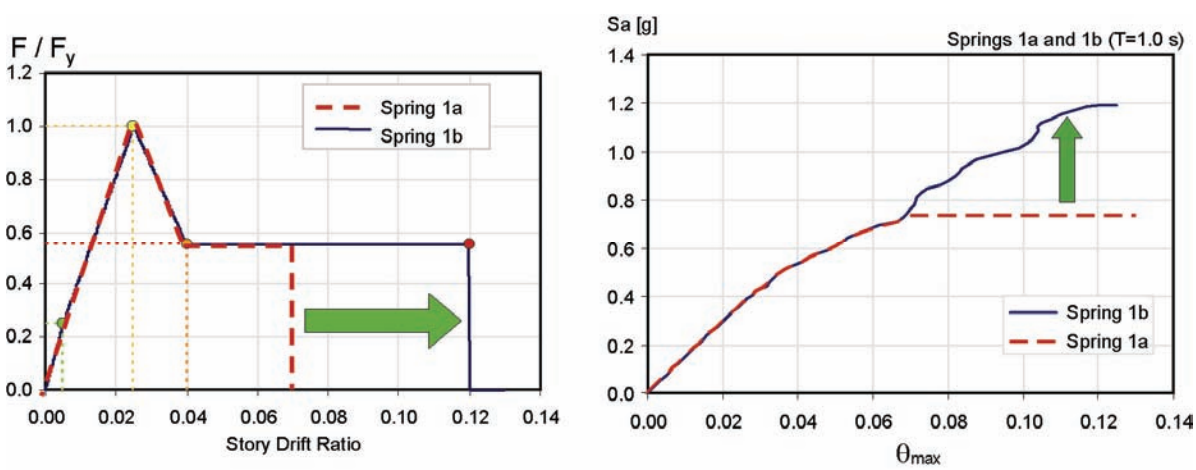

Figure 5-9 Effect of ultimate deformation capacity on the collapse capacity of a system (Springs 1a and 1b with T=1.0s).

5.1.6.4 Practical Ramifications

Observed relationships between selected features of the force-displacement capacity boundary and the resulting characteristics of median IDA curves support the conclusion that the nonlinear dynamic response of a system can be correlated to the parameters of the force-displacement capacity boundary of that system. Of particular interest is the relationship between global

deformation demand and the intensity of the ground motion at lateral dynamic instability (collapse). Results indicate that it is possible to use nonlinear static procedures to estimate the potential for lateral dynamic instability of systems exhibiting in-cycle degradation.

5.1.7 Cyclic Degradation of the Force-Displacement Capacity Boundary

In general, most components will exhibit some level of cyclic degradation. Consistent with observations from past studies, comparison of results between springs both with and without cyclic degradation show that the effects of cyclic degradation (as measured by gradual movement of the capacity boundary) are relatively unimportant in comparison with in-cycle degradation (as measured by the extent and steepness of negative slopes in the capacity boundary). This trend is illustrated for Spring 3b in Figure 5-10, but can be observed in the results for many spring systems in Appendix B.

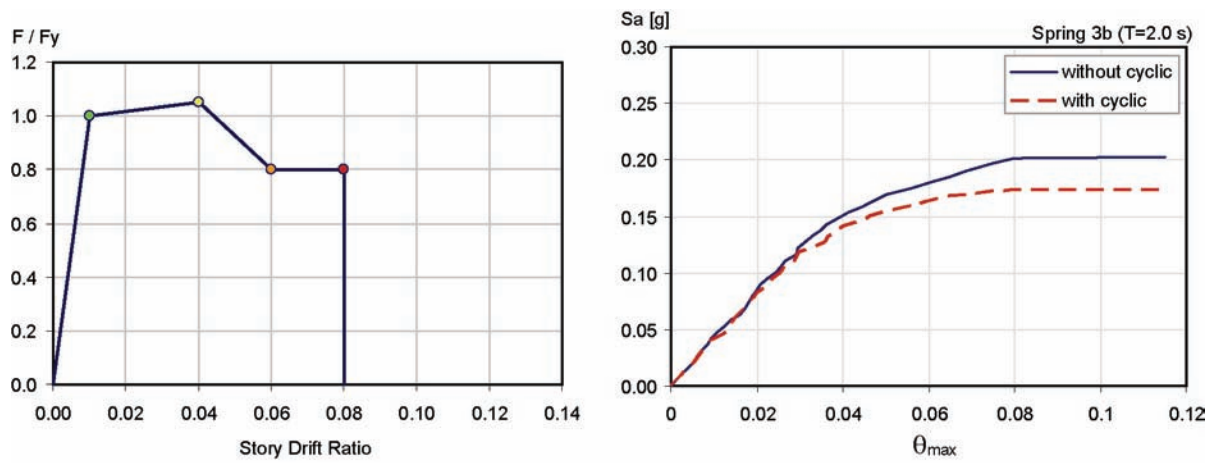

Figure 5-10 Effect of degradation of the force-displacement capacity boundary on the collapse capacity of a system (Spring 3b, T=2.0s, with and without cyclic degradation).

5.1.7.1 Practical Ramifications

In most cases the effects of in-cycle strength degradation dominate the nonlinear dynamic behavior of a system. This suggests that in many cases the effects of cyclic degradation can be neglected. Instead, the focus should be on more accurately characterizing the force-displacement capacity boundary, which controls the onset of in-cycle degradation (where it occurs).

Two situations in which the effects of cyclic degradation were observed to be important include: (1) short period systems; and (2) systems with very strong in-cycle strength degradation effects (very steep and very large drops in lateral strength). In these cases, the effects of cyclic degradation can be important and should be considered.

5.1.8 Effects of Secondary System Characteristics

The contribution of a secondary ("gravity") system acting in parallel with a primary lateral-force-resisting system always resulted in an improvement in nonlinear response, especially close to collapse. This result was observed both qualitatively and quantitatively (i.e., both in normalized and non-normalized coordinates).

The improvement was larger when considering secondary systems with larger ultimate deformation capacities, even if the lateral strength of the secondary system was small in comparison to that of the primary system. This result is illustrated in Figure 5-11, and is supported by results described in Section 5.1.6.3. In the figure, as the system combination ratio increases, the relative combination of the secondary system diminishes, yet the resulting collapse capacities for combinations with Spring 1b (larger ultimate deformation capacity) are significantly higher than combinations with Spring 1a (smaller ultimate deformation capacity).

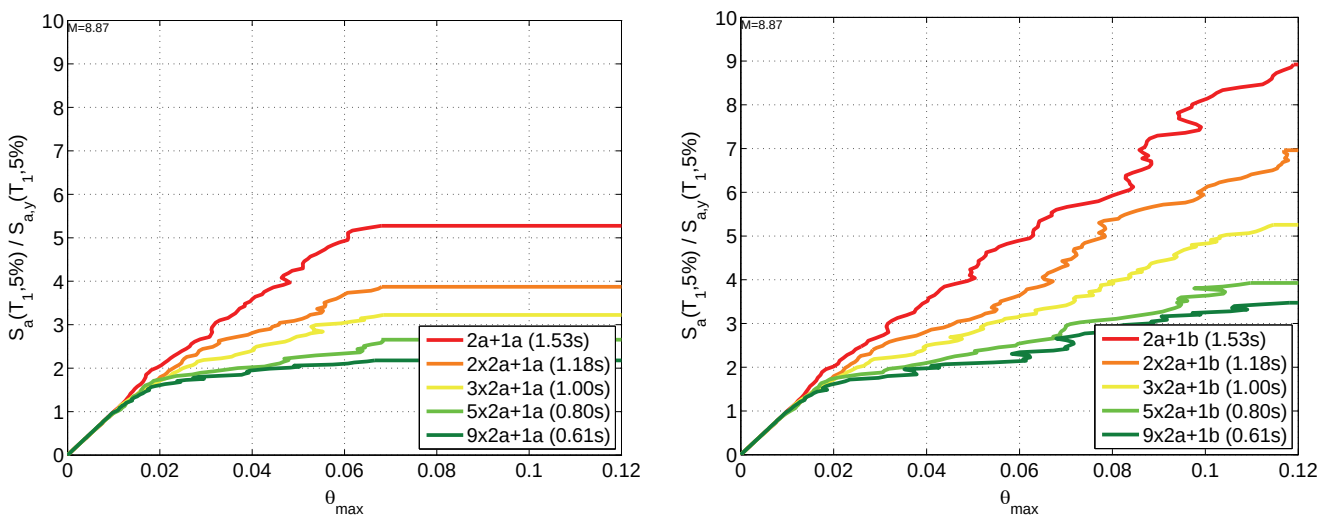

Figure 5-11 Median IDA curves plotted versus the normalized intensity measure $S_a(T,5\%)/S_{ay}(T,5\%)$ for systems Nx2a+1a and Nx2a+1b with a mass of 8.87 tons.

5.1.8.1 Practical Ramifications

Consideration of the contribution of secondary ("gravity") systems acting in parallel with primary lateral resisting systems is important and should be included in nonlinear modeling for collapse simulation. For seismic retrofit of existing structures, this suggests that adding a relatively weak (but ductile) system in parallel with the primary system could substantially increase collapse capacity and delay the onset of lateral dynamic instability. The introduction of such a secondary system could be significantly less complicated and less expensive than direct improvements to the strength, stiffness and deformation capacity of the primary system.

5.1.9 Effects of Lateral Strength

Increasing the lateral strength of a system was observed to increase collapse capacity, with the following limitations:

- Increases in the lateral strength of a system changed the intensity that initiated yielding in the system and the intensity at collapse (lateral dynamic instability). The incremental change in collapse capacity, however, was less than proportional to the increase in yield strength (Figure 5-12).

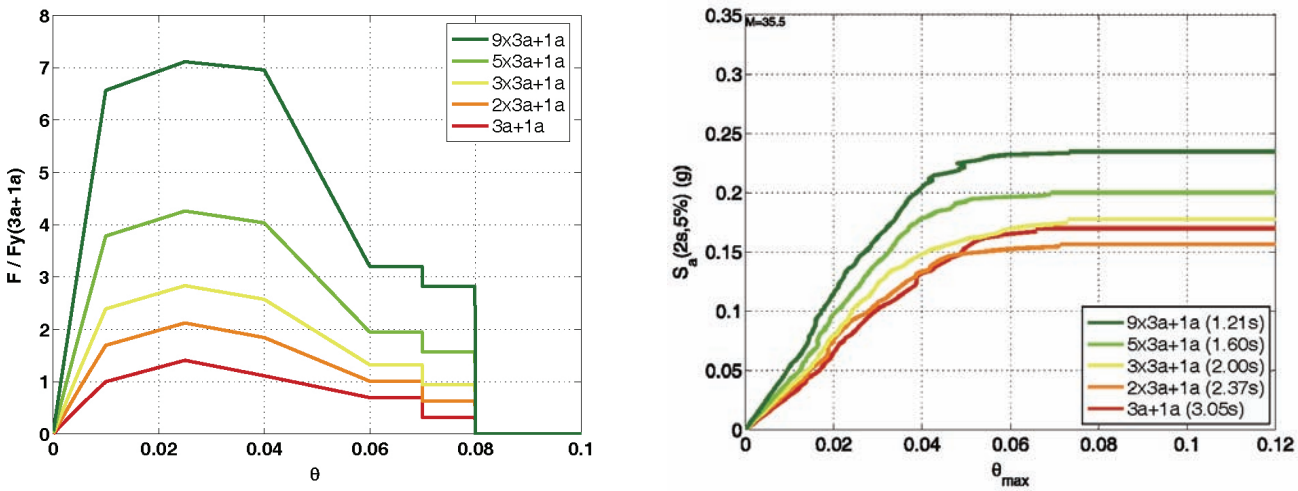

Figure 5-12 Force-displacement capacity boundaries and median IDA curves plotted versus the common intensity measure S_a(2s,5%) for system Nx3a+1a with a mass of 35.46 tons.

- The effectiveness of increasing the lateral strength of a system was a function of the shape of the force-displacement capacity boundary. Incremental changes in yield strength were more effective for ductile systems than they were for systems with less ductile behavior.
- The effectiveness of increasing the lateral strength of a system was also a function of the period of system. Incremental changes in yield strength were more effective for stiff systems than they were for flexible systems.

5.1.9.1 Practical Ramifications

Increasing the lateral strength of a system can improve collapse behavior, but will not result in equal increases in collapse capacity. The effectiveness of seismic retrofit strategies that involve increasing the lateral strength will depend on the characteristics of the force-displacement capacity boundary of the existing system as well as the period of vibration.

5.2 Recommended Improvements to Current Nonlinear Analysis Procedures

Prevailing practice for performance-based seismic design is based on the FEMA 273 *NEHRP Guidelines for the Seismic Rehabilitation of Buildings* (FEMA, 1997) and its successor documents, FEMA 356 *Prestandard and Commentary for the Seismic Rehabilitation of Buildings* (FEMA, 2000), and ASCE/SEI Standard 41-06 *Seismic Rehabilitation of Existing Buildings* (ASCE, 2006b). Recommendations contained in FEMA 440 *Improvement of Nonlinear Static Seismic Analysis Procedures* (FEMA, 2005) were incorporated into the developing ASCE/SEI Standard 41-06 in 2005. ASCE/SEI Standard 41-06 Supplement No. 1 was published in 2007. Together these resource documents form the basis of nonlinear analysis in current engineering practice. This section summarizes recommended clarifications and improvements to current nonlinear analysis procedures as characterized in these documents.

5.2.1 Current Nonlinear Static Procedures

The Coefficient Method is one method of estimating maximum inelastic displacements of a system. The process begins with the generation of an idealized force-deformation curve (i.e., static pushover curve) relating base shear to roof displacement. From this curve, an effective period, T_e, is obtained, and the maximum global displacement (target displacement) for a specified level of ground motion intensity is estimated using Equation 5-1:

$$\delta_t = C_0 C_1 C_2 S_a \frac{T_e^2}{4\pi^2} g \qquad (5\text{-}1)$$

In this expression the first three terms are coefficients that modify the elastic displacement of the system. C_0 is the first mode participation factor. This coefficient essentially converts from spectral ordinates to roof displacement. This C_1 coefficient (Equation 5-2) increases elastic displacements in short period systems, essentially accounting for exceptions to the equal displacement approximation.

$$C_1 = 1 + \frac{R-1}{aT_e^2} \qquad (5\text{-}2)$$

where:

$$R = \frac{S_a}{V_y / W} \cdot C_m \qquad (5\text{-}3)$$

and C_m is the effective mass factor to account for higher mode mass participation effects. The C_2 coefficient (Equation 5-4) increases elastic displacements in short period and weak systems to account for stiffness degradation, hysteretic pinching, and cyclic strength degradation.

$$C_2 = 1 + \frac{1}{800}\left(\frac{R-1}{T_e}\right)^2 \tag{5-4}$$

Importantly, C_2 does not account for displacement amplification due to in-cycle strength degradation, which can result in lateral dynamic instability. In-cycle strength degradation is addressed by a minimum strength requirement (maximum value of R) used as a trigger for the need to further investigate the potential for lateral dynamic instability using nonlinear response history analysis. The minimum strength requirement in current nonlinear analysis procedures was described in Section 4.6 (and is repeated in the equations that follow):

$$R_{max} = \frac{\Delta_d}{\Delta_y} + \frac{\alpha_e^{-t}}{4} \tag{5-5}$$

where

$$t = 1 + 0.15 \ln T \tag{5-6}$$

and

$$\alpha_e = \alpha_{P-\Delta} + \lambda\left(\alpha_2 - \alpha_{P-\Delta}\right) \tag{5-7}$$

for $0 < \lambda < 1.0$.

Values of R (Equation 5-3) are compared to R_{max}. Systems in which $R < R_{max}$ are deemed to meet the minimum strength requirement to avoid lateral dynamic instability, and nonlinear response history analysis is not required.

5.2.2 Clarification of Terminology and Use of the Force-Displacement Capacity Boundary for Component Modeling

For nonlinear analysis, ASCE/SEI 41-06 specifies component modeling and acceptability criteria based on the conceptual force-displacement relationship ("backbone") depicted in Figure 5-13. Since the term "backbone curve" has been used to refer to many different things, its definition related to nonlinear component modeling is not clear. In Section 2.8 of the standard, it is permitted to derive modeling parameters and acceptance criteria using experimentally obtained cyclic response characteristics from subassembly

testing. So defined, the standard can be interpreted to condone the use of cyclic envelopes from component tests to generate the necessary force-displacement relationships.

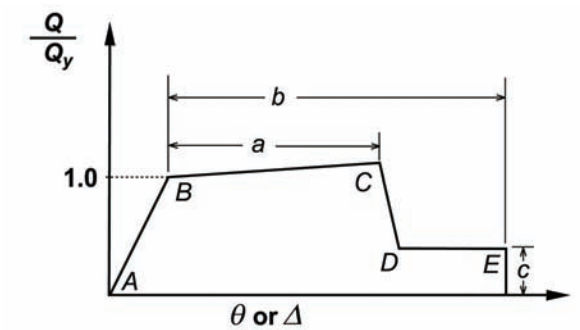

Figure 5-13 Conceptual force-displacement relationship ("backbone") used in ASCE/SEI 41-06 (adapted from FEMA 356).

The use of a cyclic envelope, as opposed to a force-displacement capacity boundary, has been shown to result in underestimation of the actual capacity for force-deformation response and subsequent overestimation of nonlinear deformation demands. In some cases the resulting conservatism can be very large.

For this reason, introduction and use of two new terms are recommended to distinguish between different aspects of hysteretic behavior. These are the *force-displacement capacity boundary*, and *cyclic envelope*, defined in Section 5.1.2. Important conceptual differences between the force-displacement capacity boundary and a loading protocol-specific cyclic envelope should be clarified in future revisions to ASCE/SEI 41, and the use of an appropriate force-displacement capacity boundary should be specified for characterizing component hysteretic behavior.

Proper definition of the hysteretic behavior in a component model requires an understanding of: (1) the initial force-displacement capacity boundary; and (2) how the force-displacement capacity boundary degrades under cyclic loading. The ideal method for establishing an initial force-displacement capacity boundary is through monotonic testing. Once the initial force-displacement capacity boundary is defined, degradation parameters should be established based on results from cyclic tests.

There is no recognized testing protocol that incorporates realistic consideration of the force-displacement capacity boundary. The use of several cyclic loading protocols is desirable to ensure that the degradation parameters are properly identified and the calibrated component model is general enough to represent response under any type of loading.

In Commentary Section C6.3.1.2.2 of ASCE/SEI 41-06 Supplement No. 1, it is suggested that the sudden drop from Point C to Point D (in Figure 5-10) can be overly pessimistic, and that a more gradual slope from Point C to Point E might be more realistic for concrete components. Some experimental results suggest that such an adjustment could be applicable for other types of components. If the actual monotonic curve is not available, or cannot be estimated, use of a force-displacement capacity boundary with this alternate slope can be considered.

5.2.3 Improved Equation for Evaluating Lateral Dynamic Instability

In comparison with results for selected multi-spring systems in this investigation, the FEMA 440 equation for R_{max} was shown to predict values that are variable, but generally fall between the median and 84th percentile results for lateral dynamic instability. This result suggests that the current equation for R_{max} would be conservative if used in conjunction with a capacity boundary generated from a pushover analysis. It could be very conservative if the pushover curve was based on component modeling parameters determined using a cyclic envelope rather than a force-displacement capacity boundary.

The trends observed in this comparison indicate that an improved equation, in a form similar to R_{max}, could be developed as a more accurate and reliable (less variable) predictor of lateral dynamic instability for use in current nonlinear static analysis procedures. An improved estimate for the strength ratio at which lateral dynamic instability might occur was developed based on nonlinear regression of the extensive volume of data generated during this investigation. In performing this regression, results were calibrated to the median response of the SDOF spring systems studied in this investigation.

A median-targeted minimum strength requirement (maximum value of R) for lateral dynamic instability, R_{di}, is proposed in Equation 5-8:

$$R_{di} = \left(\frac{\Delta_c}{\Delta_y}\right)^a + b\frac{T_e}{3|\gamma|} + \frac{F_r}{F_c}\left(\frac{\Delta_u - \Delta_r}{\Delta_y}\right)\sqrt[3]{T_e} \qquad (5\text{-}8)$$

where T_e is the effective fundamental period of vibration of the structure, Δ_y, Δ_c, Δ_r, and Δ_u are displacements corresponding to the yield strength, F_y, capping strength, F_c, residual strength, F_r, and ultimate deformation capacity at the end of the residual strength plateau, as shown in Figure 5-14. Parameters a and b are functions given by:

$$a = 1 - \exp(-dT_e) \qquad (5\text{-}9)$$

$$b = 1 - \left(\frac{F_r}{F_c} \right)^2 \tag{5-10}$$

The parameter d is a constant equal to 4 for systems with stiffness degradation, and 5 for systems without stiffness degradation. The parameter γ is the ratio of the post-capping slope (degrading stiffness) to the initial effective slope (elastic stiffness).

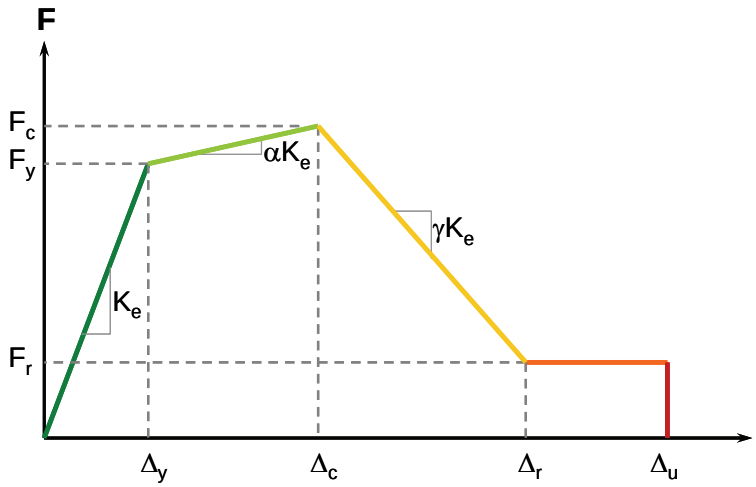

Figure 5-14 Simplified force-displacement boundary for estimating the median collapse capacity associated with dynamic instability.

5.2.3.1 Practical Ramifications

Since R_{di} has been calibrated to median response, use of this equation could eliminate some of the conservatism built into the current R_{max} limitation on use of nonlinear static procedures. Calibrated using the extensive volume of data generated during this investigation, use of this equation could improve the reliability of current nonlinear static procedures with regard to cyclic and in-cycle degradation.

In conjunction with a pushover curve used as a system force-displacement capacity boundary, the equation for R_{di} could be used to determine if a system is susceptible to lateral dynamic instability for a specified level of spectral acceleration, S_{aT}. Similar to R_{max}, use of R_{di} would involve comparison with R (Equation 5-3). If $R < R_{di}$ the system could be deemed satisfactory without additional nonlinear dynamic analysis. This capability is, of course, limited to systems for which the assumption of SDOF behavior is appropriate (i.e., MDOF effects are not significant).

Calculated values of R_{di} should be viewed carefully with respect to the intensity measure (S_{aT}) considered. Collapse limit states (i.e., lateral dynamic

instability) should be evaluated for intensities associated with rare ground motions (long return periods). Evaluation of collapse limit states at lower ground motion intensities leaves open the possibility that collapse could occur during events in which those intensities are exceeded.

In addition, the development of the proposed equation for R_{di} targeted median response, which was intentionally less conservative than the level at which the FEMA 440 equation for R_{max} appeared to be predicting. Median response implies a fifty percent chance of being above or below the specified value. Use of R_{di} in engineering practice should consider whether or not a median predictor represents an appropriate level of safety against the potential for lateral dynamic instability. If needed, a reduction factor could be applied to Equation 5-8 to reduce the resulting values of R_{di} and ultimately achieve a correspondingly higher level of safety.

5.2.4 Simplified Nonlinear Dynamic Analysis Procedure

From empirical relationships for characteristic segments of IDA curves for many systems, Vamvatsikos and Cornell (2006) suggested that static pushover curves could be used to estimate nonlinear dynamic response. The open source software tool, *Static Pushover 2 Incremental Dynamic Analysis* (SPO2IDA), was created as a product of that research, and can be obtained at http://www.ucy.ac.cy/~divamva/software.html. A Microsoft Excel version of the SPO2IDA application has also been provided on the CD accompanying this report.

As the name suggests, SPO2IDA transforms static pushover (SPO) curves to incremental dynamic analysis (IDA) plots. It utilizes a large database of IDA results to fit representative 16th, 50th, and 84th percentile IDA curves to a given idealized single-degree-of-freedom (SDOF) oscillator subjected to a static pushover analysis. The relationships between force-displacement capacity boundaries and IDA curves observed in this investigation are consistent with this notion.

Focused analytical studies comparing force-displacement capacity boundaries to incremental dynamic analysis results led to the concept of a simplified nonlinear dynamic analysis procedure. In this procedure, a nonlinear static analysis is used to generate an idealized force-deformation curve (i.e., static pushover curve). The resulting curve is then used as a force-displacement capacity boundary to constrain the hysteretic behavior of an equivalent SDOF oscillator. This SDOF oscillator is then subjected to incremental dynamic analysis (or approximate IDA results are obtained using SPO2IDA).

The concept of a simplified nonlinear dynamic analysis procedure is described in the steps outlined below.

- **Develop an analytical model of the system.**

  Models can be developed in accordance with prevailing practice for seismic evaluation, design, and rehabilitation of buildings described in ASCE/SEI 41-06. Component properties should be based on force-displacement capacity boundaries, rather than cyclic envelopes.

- **Perform a nonlinear static pushover analysis.**

  Subject the model to a conventional pushover analysis in accordance with prevailing practice. Lateral load increments and resulting displacements are recorded to generate an idealized force-deformation curve.

- **Conduct an incremental dynamic analysis of the system based on an equivalent SDOF model.**

  The idealized force-deformation curve is, in effect, a system force-displacement capacity boundary that can be used to constrain a hysteretic model of an equivalent SDOF oscillator. This SDOF oscillator is then subjected to incremental dynamic analysis to check for lateral dynamic instability and other limit states of interest. Alternatively, an approximate incremental dynamic analysis can be accomplished using the idealized force-deformation curve and SPO2IDA.

- **Determine probabilities associated with limit states of interest.**

  Results from incremental dynamic analysis can be used to obtain response statistics associated with limit states of interest in addition to lateral dynamic instability. SPO2IDA can also be used to obtain median, 16th, and 84th percentile IDA curves relating displacements to intensity. Using the fragility relationships described in Appendix E in conjunction with a site hazard curve, this information can be converted into annual probabilities of exceedance for each limit state. Probabilistic information in this form can be used to make enhanced decisions based on risk and uncertainty, rather than on discrete threshold values of acceptance.

The procedure is simplified because only a SDOF oscillator is subjected to nonlinear dynamic analysis. Further simplification is achieved through the use of SPO2IDA, which avoids the computational effort associated with incremental dynamic analysis. This simplified procedure has several advantages over nonlinear static analysis procedures: (1) lateral dynamic instability is investigated explicitly; (2) results include the effects of record-to-record variability in ground motion; (3) response can be characterized

probabilistically; and (4) uncertainty can be considered explicitly. Results can be investigated for any limit state that can be linked to the demand parameter of interest (e.g. roof displacement).

Use of the procedure is explained in more detail in the example application contained in Appendix F.

5.3 Suggestions for Further Study

This section summarizes suggestions for further study that will expand the application of results to more complex systems, fill in gaps in existing knowledge, and enhance future practice.

5.3.1 Application of Results to Multiple-Degree-of-Freedom Systems

Multi-story buildings are more complex dynamic systems whose seismic response is more difficult to estimate than that of SDOF systems. Recent studies have suggested that it may be possible to estimate the collapse capacity of multiple-degree-of-freedom (MDOF) systems through dynamic analysis of equivalent SDOF systems.

As part of the focused analytical work, preliminary studies of MDOF systems were performed as summarized in Appendix G. These studies investigated the use of nonlinear static analyses combined with incremental dynamic analyses of equivalent SDOF systems to evaluate dynamic instability of multi-story buildings ranging in height from 4 to 20 stories. Preliminary results indicate that many of the findings for SDOF systems in this investigation (e.g., the relationship between force-displacement capacity boundary and IDA curves; the equation for R_{di}) may be applicable to MDOF systems. More detailed study of the application of these results to MDOF systems is recommended as a result of this investigation, and additional MDOF investigations are planned under a project funded by the National Institute of Standards and Technology (NIST).

5.3.2 Development of Physical Testing Protocols for Determination of Force-Displacement Capacity Boundaries

Important conceptual differences exist between force displacement capacity boundaries and loading protocol-specific cyclic envelopes. Proper definition of hysteretic behavior in a component model requires an understanding of the initial force-displacement capacity boundary and how that boundary degrades under cyclic loading. The use of several loading protocols is desirable, but there is no recognized testing procedure that accomplishes this.

The loading protocol for experimental investigations described in Section 2.8 of ASCE/SEI 41-06 is not specific enough to produce a true force-displacement capacity boundary. For a set of identical specimens, necessary testing could conceivably include: (1) monotonic loading to get an initial capacity boundary; (2) multiple symmetric cyclic loading cases to calibrate cyclic degradation; (3) high frequency or long duration cyclic loading cases to check for fracture or fatigue; (4) cyclic loading followed by a monotonic push to more clearly observe changes due to cyclic degradation; and (5) unsymmetrical cyclic loading. Development of a specification for physical testing protocols necessary to generate appropriate force-displacement capacity boundaries is recommended.

5.3.3 Development and Refinement of Tools for Approximate Nonlinear Dynamic Analysis

Nonlinear dynamic analysis has obvious advantages over nonlinear static analysis procedures. Disadvantages are related to increased computational effort. Studies have shown that the characteristics of nonlinear dynamic response can be estimated through simplified approximate relationships based on the results of static pushover analyses.

Software tools such as SPO2IDA have the capability to estimate dynamic response without the computational effort associated with incremental dynamic analysis. This approximation facilitates the use of dynamic analysis results to supplement and inform more simplified analysis procedures (e.g., nonlinear static procedures). Development and refinement of similar approximate tools for performing nonlinear dynamic analyses is recommended.

5.4 Concluding Remarks

Using FEMA 440 as a starting point, this investigation has advanced the understanding of degradation and lateral dynamic instability by:

- Investigating and documenting currently available empirical and theoretical knowledge on nonlinear cyclic and in-cycle strength and stiffness degradation, and their affects on the stability of structural systems
- Supplementing and refining the existing knowledge base with focused analytical studies

This investigation has resulted in an extensive collection of available research on component modeling of degradation, and a database of analytical results from over 2.6 million nonlinear response history analyses

documenting the effects of a variety of parameters on the overall response of SDOF systems with degrading components.

Results have confirmed conclusions regarding degradation and dynamic instability presented in FEMA 440, provided updated information on modeling to differentiate between cyclic and in-cycle strength and stiffness degradation, and linked nonlinear dynamic response to major characteristics of component and system degrading behavior. This information has resulted in:

- an improved understanding of nonlinear degrading response and the practical ramifications of this information for engineering practice
- recommendations to better account for nonlinear degrading response in the context of current nonlinear analysis procedures
- suggestions for further study

Results from this investigation will ultimately improve the modeling of structural components considering cyclic and in-cycle degrading behavior, improve the characterization of lateral dynamic instability, and reduce the conservatism in current analysis procedures making it more cost-effective to strengthen existing buildings for improved seismic resistance in the future.

Appendix A

Detailed Summary of Previous Research

This appendix contains a detailed summary of the development of hysteretic models for nonlinear analysis. It also contains summaries of publications that were extensively reviewed for guidance on appropriately targeting and scoping focused analytical studies.

A.1 Summary of the Development of Hysteretic Models

A.1.1 Non-Deteriorating Models

Early studies that incorporated nonlinear behavior in seismic response of structures assumed the structure to have an elastoplastic hysteretic behavior or a bilinear hysteretic behavior (e.g., Berg and Da Deppo, 1960; Penzien 1960a, 1960b; Iwan 1961). These might be perfectly plastic with no post-elastic stiffness or with some strain hardening. More accurate models were also developed with smooth rounded transitions from elastic to plastic regions. (Ramberg and Osgood, 1943; Pinto and Guiffre, 1970; Menegotto and Pinto, 1973). Ramberg-Osgood and Giuffre-Menegotto-Pinto models continue to be used today for modeling non-degrading structures such as steel moment-frame structures when fracture and buckling do not occur, and have recently been used successfully to model the hysteretic behavior of buckling-restrained braces (e.g., Lin *et al*., 2004).

Other examples of non-degrading smooth hysteretic models commonly used are the Bouc-Wen model (Bouc, 1967a, 1967b; Wen, 1976, 1989) and the Ozdemir model (1976). Unlike the Ramberg-Osgood and Giuffre-Menegotto-Pinto models in which the force-deformation relationship is described by an algebraic equation, in the Bouc-Wen and Ozdemir models the force-displacement relationship and the force-deformation characteristics are described by a differential equation. These models are relatively easy to implement and are capable of describing, relatively well, non-degrading hysteretic behavior. An extension of smooth models to a three-dimensional tensorial idealization of Prager's model was developed by Casciati and Faravelli (1985, Casciati, 1989). Although models based on differential

equations with smooth loading curves, such as the Bouc-Wen or Ozdemir models, are relatively easy to implement, they generally exhibit a local violation of Drucker's stability postulate. In particular, Thyagarajan and Iwan (1990) concluded that the Wen-Bouc model tends to exhibit a pronounced drift, particularly when post-yield stiffness is small.

A.1.2 Piecewise Linear Deteriorating Models

Many structural materials and structural elements will exhibit some level of degradation of stiffness or strength or both, or may also exhibit other phenomena such as pinching, when subjected to cyclic reversed loading, this is especially true for reinforced concrete elements subjected to several large cyclic reversals. Deterioration can be the result of, for example, cracking, crushing, rebar buckling, crack or gap opening and closing, loss of bond, and interaction with high shear or axial stresses. The level of degradation depends, on the one hand, on the characteristics of the structural element such as properties of the materials, geometry, level of detailing, and type and characteristics of the connections, and on the other hand, on the loading history (e.g., loading intensity on each cycle, number of cycles, and sequence of loading cycles).

One of the earliest attempts to model deterioration of structural elements subjected to cyclic reversals was conducted by Jacobsen (1958) who proposed a behaviorist model to study the response of connections to cyclic loading. His model consisted of a combination of sliding blocks arranged in series which experienced frictional forces of different amplitudes and which were joined by Hookean springs with different elastic stiffnesses. Although this model allowed the mathematical description of observed static behavior, earthquake response of deteriorating structures was not studied until 1962, when Hisada proposed a degrading model (Hisada, Nakagawa and Izumi, 1962) for studying earthquake response of degrading structures.

Concerned with the stiffness degradation observed in reinforced concrete elements, Clough and Johnston (Clough, 1966; Clough and Johnston, 1966) developed a degrading model which incorporated stiffness degradation after reloading. In this model unloading occurred with a stiffness equal to the initial stiffness but reloading was aimed towards the largest excursion in previous cycles. They used the model to study the response of SDOF systems subjected to four recorded acceleration time histories. In particular, this study computed ratios of maximum deformation of elastoplastic systems to maximum deformation of stiffness-degrading systems. When evaluating these ratios they wrote "*these ratios demonstrate conclusively that there is no*

significant difference between the yield amplitudes generated in the two materials. The ratios vary between 0.8 and 1.2 except in a few cases." They concluded that "*earthquake ductility requirements in the degrading stiffness systems are not materially different from those observed in ordinary elastoplastic structures, except for structures having a period of vibration less than ½ second.*" Based on their study they also concluded that "*the ductility required in the members of reinforced concrete frame buildings will be about the same as is required in equivalent steel frame buildings.*"

An unrealistic feature of the Clough model when experiencing large load reversals followed by small load reversals was pointed out by Mahin and Bertero (1976) and by Riddell and Newmark (1979) who showed that after a small unloading the model would unrealistically reload toward the point of maximum deformation. They modified the model to reload along the same unloading branch until the reloading branch was reached and then aim toward the point of peak deformation. Mahin and Bertero (1976) also made the model more versatile by incorporating a positive post-yield stiffness and variable unloading stiffness as a function of the peak deformation. The model proposed by Mahin and Bertero (1972), which is often referred to as the modified-Clough model, has been incorporated in several general nonlinear analysis programs and has been used extensively to model the behavior of flexurally controlled reinforced concrete elements.

An early model proposed for nonlinear analysis of reinforced concrete is the Takeda model (Takeda, Sozen and Nielsen, 1970). This model incorporated some of the features of the Clough model but also added other features such as a trilinear loading curve to incorporate pre-cracking and post-cracking stiffnesses, a variable unloading stiffness which was a function of the peak deformation, and improved hysteretic rules for inner cyclic loops. This model has also been incorporated in several general analysis programs and has been extensively used in earthquake engineering to study the seismic response of reinforced concrete structures.

A slight modification to the Takeda model was proposed by Otani and Sozen (1972) who replaced the trilinear initial loading segments of the Takeda model by a bilinear relationship. The resulting model is known as bilinear Takeda model. Otani (1981) compared the response of six different hysteretic models (Ramberg-Osgood, degrading bilinear, modified-Clough, bilinear Takeda, Takeda and degrading trilinear) when subjected to horizontal components of the 1940 El Centro and the 1954 Taft records. He concluded

that "*maximum response amplitudes are not as sensitive to details in the differences in hysteretic rules of these models.*"

Other early models developed specifically for reinforced concrete structures include the model developed by Nielsen and Imbeault (1970) who proposed a degrading bilinear system whose stiffness would change only when a prior maximum displacement was exceeded, and the degrading model proposed by Anagnostopoulos (1972) which combines Nielsen's degrading bilinear model and the Clough model. Models where reloading is aimed at the point of maximum deformation in prior cycles are sometimes also referred to as "peak-oriented" models (Rahnama and Krawinkler, 1993; Medina and Krawinkler, 2004). The Clough model, the modified-Clough, Takeda, bilinear Takeda and Anagnostopoulos models are all peak-oriented models.

Iwan developed a general class of stiffness-degrading and pinching models (Iwan, 1973, 1977, 1978). Similar to prior models developed by him (Iwan, 1966, 1967) and by Jacobsen (1958), this model consisted of a collection of linear elastic and Coulomb slip elements. He then studied the response of a wide range of stiffness-degrading and pinching models when subjected to an ensemble of 12 accelerograms recorded in various earthquakes (Iwan and Gates, 1979a, 1979b). After comparing the response of the various degrading and non-degrading systems they noted "*despite the quite different load deformation characteristic the overall effect for a given ductility is nearly the same. This is a rather surprising result which may be useful in design, for it implies that it may not be necessary to know the precise details of the load-deflection behavior of a structure in order to make a reasonably accurate estimate of its response.*" In another study aimed at estimating inelastic spectra from elastic spectra using equivalent linear methods, Iwan (1980) concluded that "*the differences in hysteretic behavior considered herein appear to have only a secondary effect on the accuracy of the results.*"

Chopra and Kan (1973) studied the effects of stiffness degradation on ductility requirements of two idealized multistory buildings, one having a period of vibration of 0.5 s and the other 2.0 s. They concluded that "*stiffness degradation has little influence on ductility requirements for flexible buildings, but it leads to increased ductility requirements for stiff buildings.*"

Riddell and Newmark (Riddell and Newmark, 1979; Newmark and Riddell, 1980) studied the influence of hysteretic behavior on inelastic spectral ordinates. They considered an elastoplastic system, a bilinear system and a stiffness degrading system. They compared average inelastic spectral

ordinates for the three systems for ground motions scaled to peak ground acceleration, peak ground velocity and peak ground displacement in the acceleration, velocity and displacement-controlled spectral regions, respectively. They arrived at similar conclusions to those of Clough or those of Iwan; in particular they concluded that "*the ordinates of the average spectra do not vary significantly when various nonlinear models are used*." They also noted "*It is particularly significant that, on the average, the stiffness degradation phenomenon is not as critical as one might expect* " and concluded that "*the use of the elastoplastic idealization provides, in almost every case, a conservative estimate of the average response to a number of earthquake ground motions*."

Mahin and Bertero (1981) used the modified Clough model to also study the difference in response of elastoplastic systems and stiffness-degrading systems. They noted that "*ductility demands for a stiffness degrading system subjected to a particular ground motion can differ significantly from those obtained for elastoplastic systems in some period ranges. However, it appears that, on average, the differences are generally small*." Similar conclusions were also reached by Powel and Row (1976) who studied the influence of analysis assumptions on computed inelastic response of three different types of reinforced concrete ten-story buildings. They concluded that "*degrading stiffness appears to have no substantial influence on interstory drift demands*." Nassar and Krawinkler (1991), used the modified Clough model to study the difference of strength reduction factors associated to increasing levels of ductility demands in bilinear and stiffness degrading models. In their report they wrote "*... except for very short period systems, the stiffness-degrading models allow higher reduction factors than the bilinear model, for systems without strain hardening. This difference diminishes with strain hardening. This is a very interesting result in that it suggests that the stiffness degrading model behaves "better" than the bilinear model, i.e., it has a smaller inelastic strength demand for the same ductility ratio*."

Other piece-wise models that incorporate degradation include the Park and Ang mechanistic model (Park and Ang, 1985) and the three-parameter model (Park, Reinhorn and Kunnath, 1987; Valles et al., 1996). The three-parameter model includes strain hardening, variable unloading stiffness, pinching and cyclic load degradation (that is, decreasing yielding strength as a function of maximum deformation, hysteretic energy demand, or a combination of the two). The model was further improved in Kunnath and Reinhorn (1990). Rahnama and Krawinkler (1993) developed a general piece-wise linear

hysteretic model which was incorporated into a SDOF analysis program referred to as SNAP (SDOF Nonlinear Analysis Program). The model has a bilinear skeleton relationship and includes variable unloading stiffness, peak-oriented stiffness degradation at reloading, pinching, cyclic strength deterioration as a function of hysteretic energy demands, and also the capability of accelerating the degradation of loading stiffness beyond the peak-oriented degradation.

They used this model to study the influence of hysteretic behavior of SDOF systems subjected to 15 recorded ground motions recorded at firm sites during California earthquakes to study constant-ductility strength-reduction factors. Their results confirmed observations of Nassar and Krawinkler (1991) and of previous investigators who noted that the effect of stiffness degradation was small, on average, leading to smaller displacement demands except for short-period structures where displacement demands in systems with stiffness degradation were larger than those in bilinear systems. In their study they also noted that cyclic strength deterioration increased displacement demands but that the increase was not large unless the strength deteriorates to a small value, and noted that further research was needed before quantitative conclusions could be drawn.

Rahnama and Krawinkler also studied the effect of in-cyclic degradation by considering a negative post-elastic slope (that is, negative strain hardening) in bilinear and degrading models. They concluded that "*ratios of reduction factors for degrading and bilinear systems become significantly larger than 1.0 when negative hardening is present, particularly if the periods of vibration are short and the ductility demands are high*."

Gupta and Krawinkler (1998, 1999) investigated the effects of pinching and stiffness degradation in SDOF and MDOF structures using the hysteretic model previous developed by Rahnama (Rahnama and Krawinkler, 1993) which was incorporated in the DRAIN-2DX analysis program (Allahabadi and Powell, 1988). They concluded that "*for SDOF systems, pinching leads to a relatively small amplification of the displacement response for systems with medium and long periods, regardless of the yielding strength. For short period structures, which are subject to a larger number of cycles, the displacement amplification increases significantly*." They also noted that "*the effect of the pinched force-deformation relationship on the displacement ratio is not very sensitive to the severity of the ground motion*." For MDOF structures they concluded that "*pinching of the force-deformation characteristics of inelastic systems has a global (roof) drift similar to that*

observed in SDOF systems." They also investigated the effect of negative post-yield stiffness in SDOF and MDOF systems. They concluded that "*for SDOF systems a negative post-yield stiffness (which could represent P-Δ effects) has a large effect on the displacement demand for systems with bilinear characteristics. The effect increases rapidly with an increase in the negative stiffness ratio α, with decrease in the yield strength of the system, and a decrease in the period. Dynamic instability, caused by attainment of zero lateral resistance, is a distinct possibility and was observed under several of the ground motion records*." For systems with negative strain hardening they noted that the pinching model exhibits better behavior than the bilinear model.

Recently, Ruiz-Garcia and Miranda (2005) examined the effect of hysteretic behavior on maximum deformations of SDOF systems subjected to an ensemble of 240 ground motions recorded in California. They considered seven different types of hysteretic behavior: elastoplastic, bilinear, modified Clough, Takeda, origin-oriented, moderate degrading, and severely degrading. The modified Clough, Takeda and origin-oriented models only exhibit stiffness degradation while the moderate degrading and severely degrading systems exhibit both stiffness and cyclic strength degradation. They found that the effect of positive post-yield stiffness was relatively small except for systems with very short periods of vibration (T<0.2s). When subjected to firm soil records they found that the effects of hysteretic behavior were relatively small for structures with periods of vibration larger than about 0.7s.

The same authors used the modified Clough model to examine the effect of stiffness degradation on single-degree-of-freedom systems subjected to ground motions recorded on soft soil sites (Miranda and Ruiz-Garcia, 2002, Ruiz-Garcia and Miranda, 2004, 2006b). They concluded that the effects of stiffness degradation were larger for structures on soft soil sites than those observed for structures on firm sites. In particular, they concluded that for structures with periods of vibration shorter than the predominant period of the ground motion, the lateral displacement demands in stiffness degrading systems on average are 25% larger than those of non-degrading systems and that, in order to control lateral deformations to comparable levels of those in non-degrading structures, stiffness-degrading structures in this spectral region need to be designed for higher lateral forces.

A model similar to the one developed by Krawinkler and his coworkers but with additional capabilities to model connection fracture was developed and

incorporated into DRAIN-2DX by Shi and Foutch (Shi and Foutch, 1997; Foutch and Shi, 1998). They studied the influence of hysteretic behavior on the seismic response of buildings by considering seven different hysteretic behaviors, which included non-degrading and degrading models, and nine steel moment-resisting frame models of buildings with three, six, and nine stories. They concluded that "*Hysteresis type has only a minimum effect on ductility demands of structures*." When evaluating ratios of deformations of degrading to bilinear behavior they noted that "*For the non-pinching hysteresis models, the maximum ratios of ductility demand to the bilinear hysteresis model range from 1.10 to 1.15 when the period of the structure is less than 1.0 second. For pinching hysteresis types the maximum ratios are on the order of 1.25 to 1.30*."

Gupta and Kunnath (1998) arrived at similar conclusions. More recently Medina and Krawinkler (2004) studied the effects of hysteretic behavior (i.e., bilinear, peak oriented and pinching) in the evaluation of peak deformation demands and their distribution over the height for regular frame structures over a wide range of stories (from 3 to 18) and fundamental periods (from 0.3 s. to 3.6 s.). The study did not consider monotonic in-cycle deterioration. The ground motions used were those with frequency content characteristic of what they referred to as "ordinary ground motions" (that is, no near-fault or soft soil effects). They concluded that "*the degree of stiffness degradation is important for the seismic performance evaluation of regular frames because systems with a large degree of stiffness degradation tend to exhibit larger peak drift demands and a less uniform distribution of peak drifts over the height*."

Based on the general class of non-degrading and degrading models developed by Iwan (1966, 1967, 1973), Mostaghel (1998, 1999) developed a general hysteretic model by providing an analytical description (that is, with differential equations) of physical models consisting of a series of linear springs, dashpots, and sliders. The model includes the effects of pinching, stiffness degradation, and load deterioration. He showed that complex multi-linear hysteretic behavior can be obtained by solving ($2n$-1) differential equations where n is the number of linear segments in the model.

A.1.3 Smooth Deteriorating Hysteretic Models

Degradation and pinching have also been incorporated in smooth hysteretic models. Some examples of degrading smooth models are the Baber model (Baber and Wen, 1981; Baber and Noori 1985, 1986) which extends the Bouc-Wen model to include stiffness degradation and pinching.

More recently, Sivaselvan and Reinhorn (1999, 2000) developed a versatile hysteretic model that is conceptually based on a general class of non-degrading and degrading models developed by Iwan (1966, 1967, 1973) but extended the model developed by Mostaghel (1998, 1999) to include smooth curvilinear segments. Stiffness degradation is incorporated using a pivot rule analogous to the one incorporated in the three-parameter model (Park, Reinhorn and Kunnath, 1987). Cyclic strength degradation is modeled by reducing the capacity in the backbone curve while pinching is achieved by adding an additional slip-lock spring in series with the main smooth hysteretic spring, which is similar to the Bouc-Wen model. The hysteretic behavior is then described by the solution of four time-independent differential equations which are solved using Runge-Kutta's method. Although they provided specific rules for controlling stiffness degradation, cyclic degradation, and pinching, they showed that other rules could be implemented as well. This hysteretic model has been incorporated in recent versions of IDARC (Valles et al., 1996).

A.1.4 Hysteretic Models for Steel Braces

Experimental research on the behavior of steel braces has shown that their behavior under severe cyclic loading is complicated and not fully understood. Cyclic nonlinear behavior of steel brace members is complex as a result of various phenomena occurring in the braces and their connections, such as yielding in tension, buckling in compression, post-buckling deterioration of compressive load capacity, deterioration of axial stiffness with cycling, low-cycle fatigue fractures at plastic hinge regions, Bauschinger effect, and buckling and fracture in the gusset plates. As in the models previously described, element models for steel braces can be classified as either phenomenological models in which the load-deformation behavior of steel braces is described through a series of hysteretic rules that try to reproduce behavior observed experimentally, or material-based models such as finite element models and fiber element models where the steel brace is discretized into small elements and the overall behavior of the brace is obtained from uniaxial, biaxial or triaxial material behavior of the material.

A significant amount of both experimental and analytical work on the behavior of steel bracing has been conducted at the University of Michigan under the direction of Professors Goel and Hanson. One of the first analytical models for predicting the force-deformation behavior of axially-loaded members with intermediate slenderness ratios was developed by Higginbotham and Hanson (1976). Prathuangsit, Goel, and Hanson, (1978) proposed a model with rotational end springs to simulate the end restraint

resulting from the flexural rigidity of the connections of axially loaded (that is, bracing) members. They showed that members with balanced strength connections, (that is, which form plastic hinges simultaneously at midspan and at the ends), have more efficient compressive load and energy dissipation capacities than members of the same length and same cross-sectional properties with unbalanced strength connections. They concluded that the hysteresis behavior of a balanced strength member can be represented adequately by that of a pin-connected member of the same cross section and same effective slenderness ratio

Jain, Goel, and Hanson tested 17 tube specimens and eight angle specimens under repeated axial loading (Jain, Goel and Hanson, 1976, 1978a, b). The objective of this experimental investigation was to quantify the reduction in maximum compressive loads and increase in member length, and to study the influence of the buckling mode and the shape of the cross-section on the hysteretic behavior and dissipation of energy through the hysteretic cycles. They concluded that local buckling and shape of the cross section can have a significant influence on the hysteretic behavior of axially loaded steel members. Based on their experimental results they developed a hysteresis model for steel tubular members that included a reduction in compressive strength and an increase in member length with the number of cycles (Jain and Goel, 1978, 1980) which was then incorporated in the DRAIN-2D analysis program. This model has been extensively used by investigators at the University of Michigan and elsewhere to study the seismic response of concentrically braced steel frames.

Astaneh-Asl and Goel investigated the behavior of double-angle bracing members subjected to out-of-plane buckling due to severe cyclic load reversals (Astaneh-Asl *et al*. 1982; Astaneh-Asl and Goel 1984). Nine full-size test specimens were subjected to severe inelastic axial deformations. Test specimens were made of back-to-back A36 steel angle sections connected to the end gusset plates by fillet welds or high-strength bolts. Five of the test specimens were designed according to current design procedures and code requirements. These specimens experienced fracture in gusset plates and stitches during early cycles of loading. Based on observations and analysis of the behavior of the specimens, new design procedures were proposed for improved ductility and energy dissipation capacity of double-angle bracing members. Goel and El-Tayem (1986) investigated the behavior of angle cross-bracing.

Gugerili and Goel (1982) tested nine commercially available wide-flange shapes and structural tubes with different slenderness and width-to-thickness ratios in order to investigate the effects of cross section and slenderness ratio. A general rule was developed for transitioning between compression and tension mechanism lines of constant shape and elastic segments. The new rule also included the effects of residual elongation. The theoretical model was used as a basis for a developing a semi-empirical model for predicting experimental hysteresis loops more accurately than previous models. This model included the decrease in compressive strength with cumulative plastic hinge deformation.

Tang and Goel (1987) developed a procedure to predict the fracture life of bracing members. Their empirically based procedure was refined with an energy approach using Jain's hysteresis model and was then also incorporated in the the DRAIN-2D program. Based on the experimental results of previous researchers Hassan and Goel (1991) formulated a refined and practical hysteresis model for bracing the members of concentrically (chevron) braced steel structures subjected to severe earthquakes. A more recent model was implemented in a Structural Nonlinear Analysis Program (SNAP) (Rai et al, 1996), which eliminates the brace once it is estimated that it has fractured (while this program has the same name, it is different from the program developed by Krawinkler and his coworkers).

Professors Popov and Mahin at the University of California at Berkeley have also conducted a significant amount of experimental and analytical research on steel braces. Zayas, Popov, and Mahin, (1979, 1980) conducted a series of experimental tests on scaled tubular brace members subjected to severe inelastic cyclic loading. The tubular brace specimens considered were one-sixth scale models of braces of the type used for offshore platforms. A method of predicting the reduction in buckling load was presented. Maison and Popov (1980) performed an experimental and analytical investigation of the behavior of structural steel frames with K-braces subjected to severe cyclic loadings simulating seismic effects. They developed an empirical brace model to analyze steel frames with K-braces.

Black and Popov, E.P. (1980, 1981) conducted an experimental study on 24 commercially available steel struts, commonly used as bracing members. They investigated the effects of loading patterns, end conditions, cross-sectional shapes, and slenderness ratios on the hysteresis response of members. A large variety of shapes were tested, including wide flanges, structural tees, double-angles, a double-channel, and thick-walled and thin-

walled square and round tubes. Two types of boundary conditions were considered, pinned-pinned and fixed-pinned, with effective slenderness ratios of 40, 80, and 120. An explanation was provided regarding the fundamental mechanisms responsible for the observed degradation in the buckling load capacity during inelastic cycling.

Ikeda and Mahin (1984) developed an analytical model for simulation of the inelastic buckling behavior of steel braces. In their model, buckling is simulated by the use of predefined straight-line segments and simple rules regarding factors such as buckling load deterioration and plastic growth. The model, based on the approach of Maison and Popov (1980) overcomes some of the limitations of earlier models. They proposed a systematic method for selecting input parameters along with several rules governing the values of certain parameters. The model was subsequently refined in 1986 by combining analytical formulations describing plastic hinge behavior with empirical formulas that are based on a study of experimental data. Analytical expressions for the axial force versus axial deformation behavior of braces were derived as solutions of the basic beam-column equation based on specified assumptions. While analytical expressions form the basis of this model, several empirical behavioral characteristics were implemented in the modeling to achieve better representation of observed cyclic inelastic behavior.

Khatib and Mahin (1987, 1988) conducted an analytical investigation on concentrically braced frames. Their study stressed that concentrically braced steel frames designed by conventional methods may exhibit several undesirable modes of behavior. In particular, they showed that chevron-braced frames have an inelastic cyclic behavior that is often characterized by a rapid redistribution of internal forces, a deterioration of strength, a tendency to form soft stories, and fracture due to excessive deformation demand. They identified parameters having a significant influence on these phenomena and provided recommendations for preferable ranges of brace slenderness, approaches for designing beams, and a simplified capacity design approach for proportioning columns and connections. They also proposed several alternative brace configurations with improved behavior including zipper bracing systems which incorporate vertical linkage elements in a conventional chevron-braced frame to decrease concentrations of interstory drift demands.

More recently Uriz and Mahin (2004, Uriz, 2005) conducted experimental testing of a nearly full-size, two-story Special Concentric Braced Frame

(SCBF) specimen. They also conducted an analytical investigation using the same reliability framework used to assess Special Moment Resisting Frame (SMRF) structures during the FEMA/SAC Steel Project in order to assess the confidence with which SCBFs might achieve the seismic performance expected of new SMRF construction.

Other institutions have also been actively involved in research on the behavior of steel braces. For example, Nonaka (1973, 1977) at Kyoto University, conducted elastic, perfectly plastic analyses of a bar under repeated axial loading. The bar was taken as a one-dimensional continuum with both ends simply supported. His analysis considered the plastic interaction for the combined action of bending and axial deformation, based on a piecewise-linear yield condition. With a number of simplifying assumptions, a closed form solution was derived that can describe the hysteretic behavior of a bar, such as a structural brace or a truss member, under any given history of tension and/or compression or of corresponding displacements. Nonaka's closed form solution was later extended by Shibata (1982) for a bar of ideal I-section with bilinear stress-strain relationship. For a bar of arbitrary solid cross-section with a piecewise linear stress-strain relationship, an incremental load-displacement relationship was also obtained in analytical form.

At the University of Canterbury in New Zealand, Remennikov and Walpole (1997a, 1997b) developed an analytical model for the inelastic response analysis of braced steel structures. Their model combines the analytical formulation of plastic hinge behavior with empirical formulas developed on the basis of experimental data. The brace is modeled as a pin-ended member, with a plastic hinge located at the midspan and braces with other end conditions are handled using the effective length concept. Step-wise regression analysis is employed to approximate the plastic conditions for the steel UC section. Verification of the brace model is performed on the basis of quasi-static analyses of individual struts and a one-bay one-story cross-braced steel frame.

At the Ecole Polytechnique de Montreal in Canada, Archambault, Tremblay, and Filiatrault, (1995, 2003) conducted experimental and analytical studies on the seismic performance of concentrically braced steel frames made with cold-formed rectangular tubular bracing members. They tested a total of 24 quasi-static cyclic tests on full scale X bracing and single diagonal bracing systems. They developed simplified models to predict the out-of-plane deformation of the braces as a function of the ductility level. They then used

their models to develop an empirical expression to assess the inelastic deformation capacity before fracture of bracing members made of rectangular hollow sections.

More recently, Jin and El-Tawil, (2003) developed a beam-column element to model the inelastic cyclic behavior of steel braces. In their model a bounding surface plasticity model in stress-resultant space coupled with a backward Euler algorithm is used to keep track of the spread of plasticity through the cross-section. Deterioration of the cross-section stiffness due to local buckling is accounted for through a damage model.

Further information on the experimental and analytical response of steel bracing is available in Tremblay (2002), Jin and El-Tawil, (2003) and Uriz (2005), which provide summaries of experimental and analytical work. In particular Tremblay (2002) conducted a survey of past experimental studies on the inelastic response of diagonal steel bracing members subjected to cyclic inelastic loading to collect data for the seismic design of concentrically braced steel frames for which a ductile response is required during earthquakes. He examined the buckling strength of the bracing members, the brace post-buckling compressive resistance at various ductility levels, the brace maximum tensile strength including strain hardening effects, and the lateral deformations of the braces upon buckling. Additionally he proposed equations for each of these parameters and examined the maximum ductility that can be achieved by rectangular hollow bracing members.

Nakashima and Wakabayashi (1992) provide an overview of Japanese experimental and analytical research on steel braces and braced frames. Current Japanese practice is also briefly summarized.

A.2 Detailed Summaries of Relevant Publications

This section presents summaries of publications that were judged to be particularly relevant to the subject of nonlinear degrading response, and were, therefore, reviewed in detail. Each summary includes the list of authors, an abstract, a narrative summary of the work, relevant figures, a summary of important findings, and a listing of relevant publications included in the list of references. The following publications were selected for detailed review:

- Bernal, D., 1998, “Instability of buildings during seismic response,” *Engineering Structures*, Vol. 20, No. 4-6, pp. 496-502.

- Pincheira, J.A, Dotiwala, F.S., and D' Souza J.T., 1999, "Spectral displacement demands of stiffness- and strength-degrading systems," *Earthquake Spectra*, 15(2), 245–272.
- Song, J.-K., and Pincheira, J.A, 2000, "Seismic analysis of older reinforced concrete columns," *Earthquake Spectra*, 16(4), 817–851.
- Miranda, E. and Akkar, S.D., 2003 "Dynamic instability of simple structural systems," *Journal of Structural Engineering*, ASCE, 129(12), pp 1722-1727.
- Vian, D. and Bruneau, M., 2003, "Tests to structural collapse of single-degree-of-freedom frames subjected to earthquake excitations," *Journal of Structural Engineering*, ASCE, 129(12), 1676-1685.
- Kanvinde, A.M., 2003, "Methods to evaluate the dynamic stability of structures – shake table tests and nonlinear dynamic analyses," EERI Annual Student Paper Competition, *Proceedings of 2003 EERI Annual Meeting*, Portland, Oregon.
- Vamvatsikos, D. and Cornell, C.A., 2005, *Seismic performance, capacity and reliability of structures as seen through incremental dynamic analysis*, John A. Blume Earthquake Engineering Research Center, Report No. 151, Department of Civil and Environmental Engineering, Stanford University, Stanford, California.
- Ibarra, L., Medina, R., and Krawinkler, H., 2005, "Hysteretic models that incorporate strength and stiffness deterioration, *Earthquake Engineering and Structural Dynamics*, Vol. 34, no. 12, pp. 1489-1511.
- Ibarra, L.F., and Krawinkler, H., 2005, *Global collapse of frame structures under seismic excitations*, John A. Blume Earthquake Engineering Research Center, Report No. 152, Department of Civil and Environmental Engineering, Stanford University, Stanford, California.
- Kaul, R., 2004, *Object-oriented development of strength and stiffness degrading models for reinforced concrete structures*, Ph.D. Thesis, Department of Civil and Environmental Engineering, Stanford University, Stanford, California.
- Elwood, K.J., 2002, *Shake table tests and analytical studies on the gravity load collapse of reinforced concrete frames*, Ph.D. Dissertation, University of California, Berkeley, California.
- Lee, L.H., Han, S.W., and Oh, Y.H., 1999, "Determination of ductility factor considering different hysteretic models," *Earthquake Engineering and Structural Dynamics*, Vol. 28, 957–977.

- Foutch, D.A. and Shi, S., 1998, "Effects of hysteresis type on the seismic response of buildings," *Proc. 6th U.S. National Conference on Earthquake Engineering*, Seattle, Washington, Earthquake Engineering Research Institute, Oakland, California.
- Ruiz-Garcia, J. and Miranda, E., 2003, "Inelastic displacement ratio for evaluation of existing structures," *Earthquake Engineering and Structural Dynamics*. 32(8), 1237-1258.
- Dolsek, M. and Fajfar, P., 2004, "Inelastic spectra for infilled reinforced concrete frames," *Earthquake Engineering and Structural Dynamics*, Vol. 33, 1395–1416.

A.2.1 Instability of Buildings During Seismic Response

Authors:

Bernal, D. (1998)

Abstract:

The issue of gravity-induced instability during response to severe seismic excitation is examined. While static instability is fully determined by the existence of at least one negative eigenvalue in the second-order tangent stiffness, this condition is necessary but not sufficient for instability during dynamic response. The likelihood of collapse is strongly dependent on the shape of the mechanism that controls during the critical displacement cycle and this shape can be reasonably identified using a pushover analysis with an appropriately selected lateral load distribution. A characterization of the instability limit state based on the reduction of a multistory building to an equivalent SDOF system is presented

Summary:

Dynamic instability is a phenomenon whereby the response changes from vibration to drift in a single direction. In this study a structure is defined as stable if small increases in the ground motion intensity result in small changes in the response. The study shows that the distribution of inelastic action along the height of the building plays a critical role in the likelihood of instability. The study emphasizes that gravity generally has little effect on the dynamic response of structures, except when failure from instability is near. In particular, the study shows that the static based approach of accounting for second-order effects through amplifications of the first-order solution is not appropriate in a dynamic setting. Specifically, design in a region where

amplifications from *P-Δ* are significant implies unacceptably low safety factors.

Representative Figures:

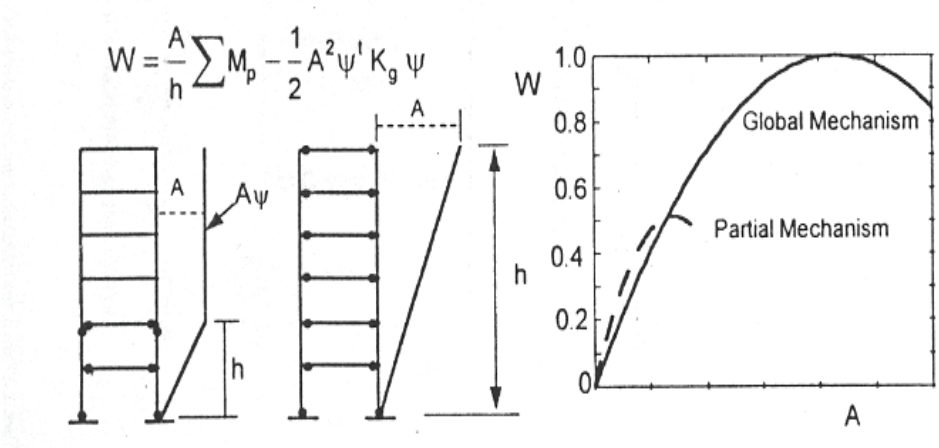

Figure A-1 Effect of mechanism shape on the monotonic work *vs*. amplitude relationship.

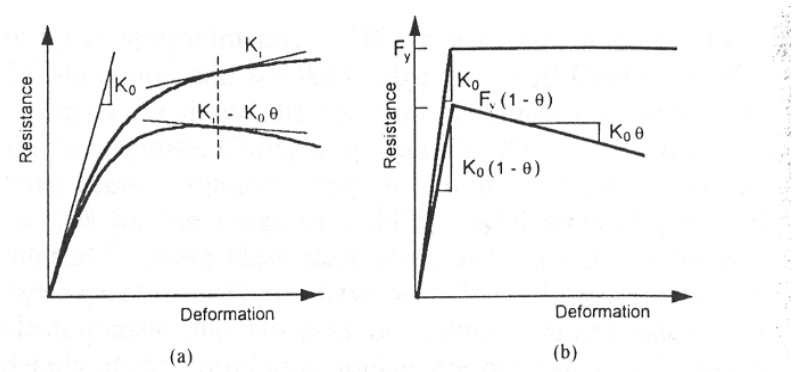

Figure A-2 Illustration of the definition of stability coefficient: (a) general load deformation relationship, (b) elasto-plastic system.

Summary of Findings:

Dynamic instability takes place when the strength of the structure is below a certain threshold and is strongly dependent on the shape of the failure (or collapse) mechanism that controls. Safety against dynamic instability cannot be guaranteed by placing controls on initial elastic stiffness; a rational check of the safety against collapse must contemplate the strength and shape of the critical mechanism. In particular, a rational approach is to estimate the strength level associated with the instability threshold and to ensure that the strength level provided exceeds the required limit by an appropriate safety margin.

Relevant Publications:

Bernal, D., 1998, "Instability of buildings during seismic response," *Engineering Structures*, Vol. 20, No. 4-6, pp. 496-502.

Bernal, D., 1992, "Instability of buildings subjected to earthquakes." *Journal of Structural Engineering* , ASCE, Vol. 118, No. 8, pp. 2239-2260.

Bernal, D., 1987, “Amplification factors for inelastic dynamic *P-Δ* effects in earthquake analysis,” *Earthquake Eng. Struct. Dyn*., 15(5), pp. 117-144.

A.2.2 Seismic Analysis of Older Reinforced Concrete Columns

Authors:

Pincheira, J.A., Dotiwala, F.S., and D’Souza J.T. (1999)

Abstract:

A nonlinear model and an analytical procedure for calculating the cyclic response of nonductile reinforced concrete columns are presented. The main characteristics of the model include the ability to represent flexure or shear failure under monotonically increasing or reversed cyclic loading. Stiffness degradation with cyclic loading can also be represented. The model was implemented in a multipurpose analysis program and was used to calculate the response of selected columns representative of older construction. A comparison of the calculated response with experimental results shows that the strength, failure mode and general characteristics of the measured cyclic response can be well represented by the model.

Summary:

A beam-column element was created in order to simulate the behavior of older non-ductile or shear-critical reinforced concrete columns in 2D frames. This is a lumped plasticity element using two flexural springs at the beam ends and a shear spring at the midpoint (Figure A-3). For the flexural springs a Takeda hysteresis law is used together with a quadrilinear backbone curve that incorporates a hardening post-yield segment followed by a negative post-peak slope that stops at a residual plateau; essentially, only in-cycle strength degradation is considered (Figure A-4a). On the other hand, the shear spring uses a similar quadrilinear backbone but a pinching hysteresis together with cyclic degradation of the post-peak strength (Figure A-4b).

The element was incorporated in the Drain-2D analysis program, resulting in important limitations in its implementation and applicability. The solution

algorithm of Drain-2D cannot handle negative stiffness, thus necessitating the use of numerical techniques to find an approximate solution. Specifically, on a negative slope (for any of the three springs), the load steps are performed first with an arbitrary positive stiffness, and the load unbalance is then subtracted from the resulting increased load to move down to the actual negative slope (Figure A-5). The results can be considered reliable only under small load-steps and they may indeed lead to gross numerical errors and possible numerical instabilities at the MDOF level. Furthermore, the use of Drain-2D means that only a load-control pushover is possible, thus severely reducing the applicability of this element for anything but time-history analysis with small time steps.

Significant effort has gone into the definition of the spring backbones, using modified compression field theory for the shear backbone, and considering anchorage slip, lap-splice slip, and section degradation for the flexural springs. Calibration and testing of the element were performed with regard to the experimental results.

Representative Figures:

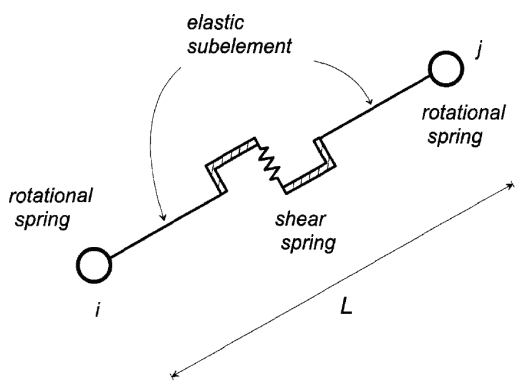

Figure A-3 The RC column element formulation.

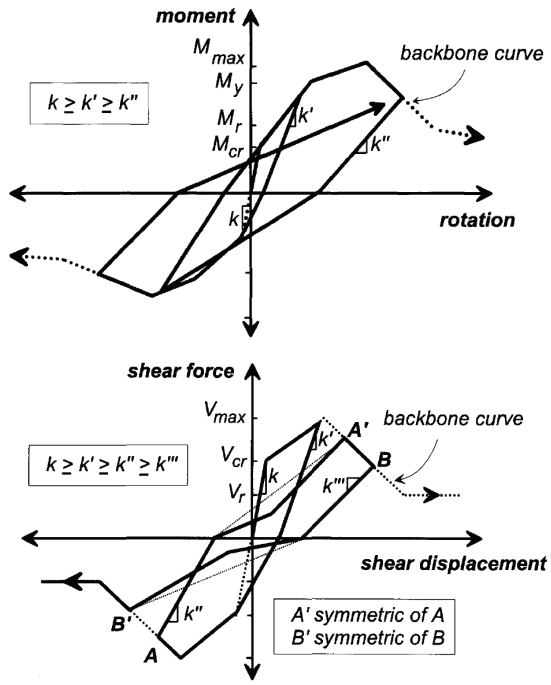

Figure A-4 The hysteretic laws for shear and moment springs.

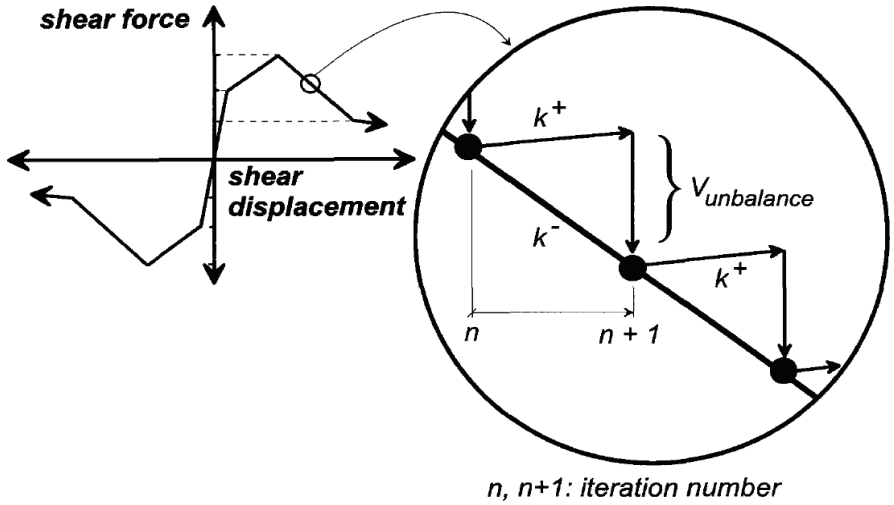

Figure A-5 The force (or moment) unbalance is subtracted after an arbitrary positive stiffness step towards the "correct" displacement. Very small load steps are needed for accuracy, even at the SDOF level.

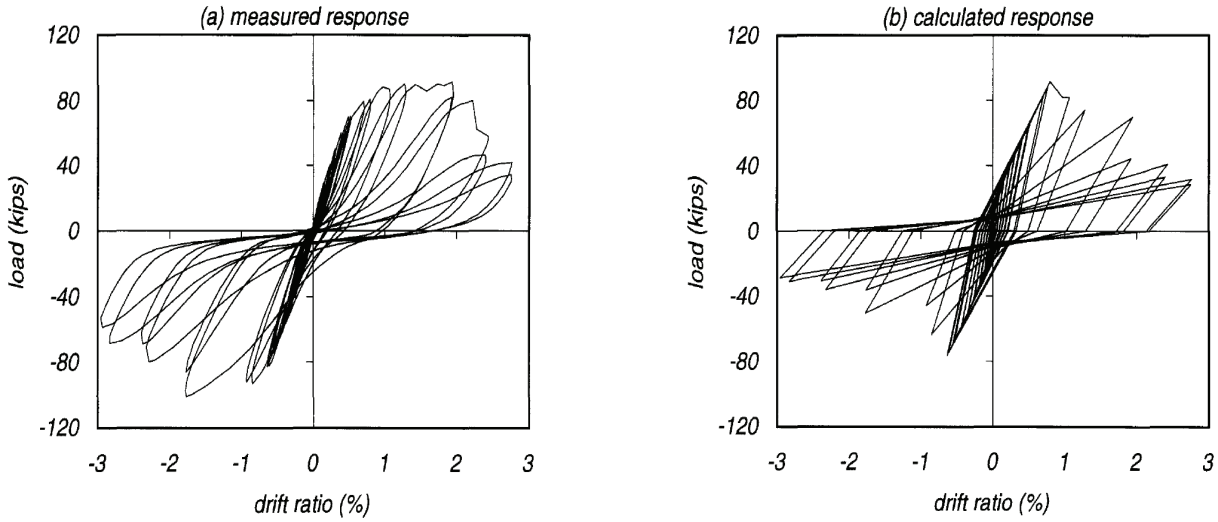

Figure A-6 Observed versus calculated response for a column specimen SC3 (shear critical).

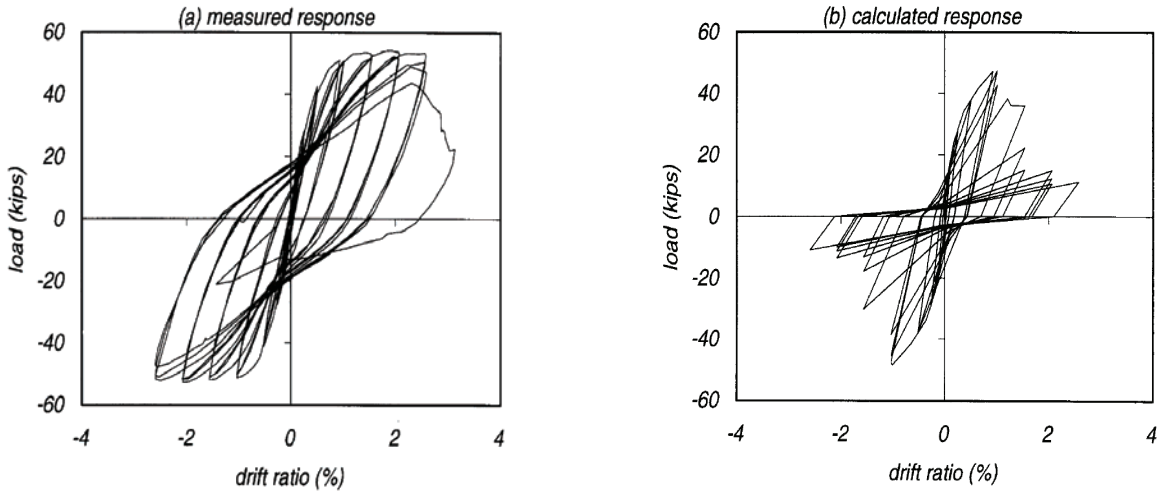

Figure A-7 Observed *versus* calculated response for a column specimen 2CLH18 (fails in shear after considerable flexural deformation).

Summary of Findings:

The comparison with experimental results showed that good correlation of the observed versus the calculated post-peak response was in many cases not possible (Figures A-6, A-7). The cyclic degradation parameters were shown to have a large influence on the post-peak response while significant epistemic uncertainty was identified in the cyclic degradation.

The column failure mode was captured in every test considered, but the estimated failure loads and drifts were generally conservative. Nonetheless, the model was able to capture satisfactorily the overall strength degradation,

stiffness degradation, and in-cycle and cyclic degradation properties of the specimens.

Relevant Publications:

Pincheira, J.A, Dotiwala, F.S., and D'Souza J.T., 1999, "Spectral displacement demands of stiffness- and strength-degrading systems," *Earthquake Spectra*, 15(2), 245–272.

Song J.-K., and Pincheira, J.A., 2000, "Seismic analysis of older reinforced concrete columns," *Earthquake Spectra*, 16(4), 817–851.

Dotiwala, F.S., 1996, *A nonlinear flexural-shear model for RC columns subjected to earthquake loads*, MS Thesis, Department of Civil and Environmental Engineering, University of Wisconsin-Madison.

Pincheira, J.A., and Dotiwala, F.S., 1996, "Modeling of nonductile R/C columns subjected to earthquake loading," *Proc. 11th World Conf. on Earthquake Engineering*, Paper No. 316, Acapulco, Mexico.

A.2.3 Spectral Displacement Demands of Stiffness- and Strength-Degrading Systems

Authors:

Song, J.-K., and Pincheira, J.A. (2000)

Abstract:

The effect of stiffness and strength degradation on the maximum inelastic displacement of single-degree-of-freedom (SDOF) systems was investigated. The SDOF model included strength and stiffness degradation with increasing deformation amplitude and upon reversal of loading cycles. Pinching of the hysteresis loops was also considered. Spectral displacements were calculated for oscillators with a range of degrading characteristics subjected to twelve ground motions on rock, firm, and soft soils. The results show that the maximum displacements of degrading oscillators are, on average, larger than those of non-degrading systems. The displacement amplification depends significantly with the period, strength coefficient, degradation rate, and ground motion considered. Nonetheless, the amplification due to the degradation characteristics of the system is more important in the short-period range where average amplification factors of two or three are credible. The amplification factors proposed in the FEMA 273 report by the ATC-33 project provided conservative estimates for oscillators with periods greater than 0.3 seconds subjected to motions on rock or firm soil. On soft soils, a

good correlation was found for periods greater than 1.5 seconds. At shorter periods, the ATC 33 factors underestimate the displacement amplification.

Summary:

About 7,600 SDOF dynamic analyses were performed for 12 ground motions including rock, firm soil, soft soil, and near-field and far-field records. The oscillator had a quadrilinear backbone with a hardening, a softening and a residual strength segment. Still, only a limited set of backbones were considered, all having hardening stiffness 5% of the elastic, residual strength 10% of yield strength and reaching 1.25 ductility at peak strength. Some gentle negative slopes were investigated, namely -1% and -3% of the elastic. The oscillator had 5% damping and used a pinching hysteresis with or without cyclic strength degradation. During the investigation an *ad hoc* collapse limit-state was considered when the post-peak strength reached 10% of the yield strength.

Representative Figures:

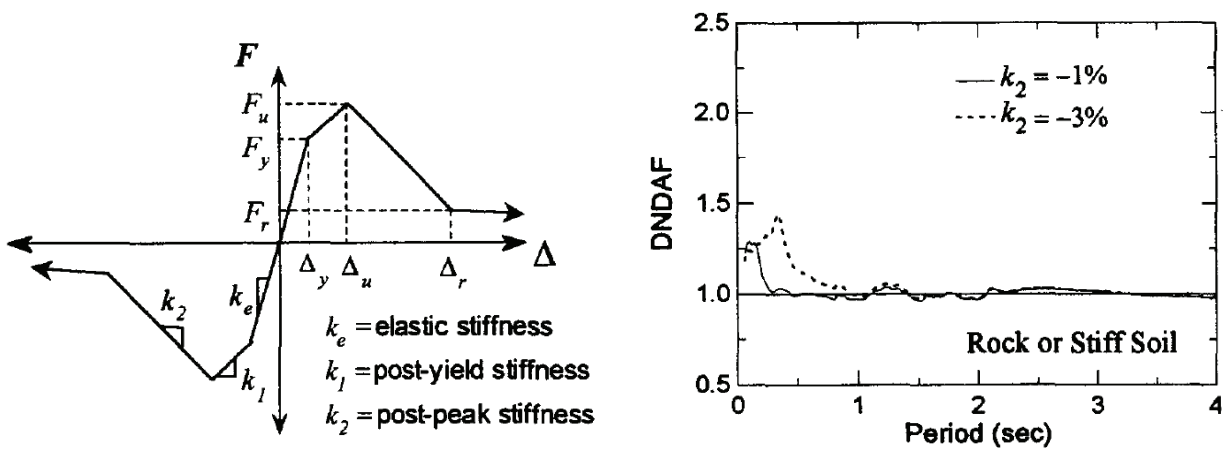

Figure A-8 (a) Hysteresis law used for the SDOF system and (b) ratio of degrading to non-degrading displacement amplification factors for the post-peak stiffness equal to -1% or -3% of the elastic stiffness.

Summary of Findings:

The post-peak stiffness and the unloading stiffness were found to be the most important parameters, while the degree of pinching was important except for soft-soil records. Cyclic degradation generally increases the dynamic response, but mostly for the short periods. Significant differences in the SDOF response and its dependence on cyclic degradation were found between soft soil and firm soil (or rock) and maybe between near-field versus far-field record response, although only one near-source record was used.

Finally, for a given strength reduction factor, collapse (as defined in the paper) was consistently observed below a certain oscillator period. Some duration effects were also reported.

The study seriously suffers from the lack of records. Only twelve were used and they were selected from soft and firm soil sites without differentiating between near-field and far-field. Thus, the statistics on the results are not reliable, although the general observations provided may prove useful.

Relevant Publications:

Song J.-K., and Pincheira, J.A., 2000, "Seismic analysis of older reinforced concrete columns," *Earthquake Spectra*, 16(4), 817–851.

Pincheira, J.A, Dotiwala, F.S., and D'Souza, J.T., 1999, "Spectral displacement demands of stiffness- and strength-degrading systems," *Earthquake Spectra*, 15(2), 245–272.

A.2.4 Dynamic Instability of Simple Structural Systems

Authors:

Miranda, E. and Akkar, S.D., (2003)

Abstract:

Lateral strengths required to avoid dynamic instability of SDOF systems are examined. Oscillators with a bilinear hysteretic behavior with negative post-yield stiffness are considered. Mean lateral strengths, normalized by the lateral strength required to maintain the system elastic, are computed for systems with periods ranging from 0.2 to 3.0 s when subjected to 72 earthquake ground motions recorded on firm soil. The effect of period of vibration and post-yield stiffness is investigated. Results indicate that mean normalized lateral strengths required to avoid dynamic instability decrease as negative post-yield stiffness increases, and that the reductions are much larger for small negative post-yield stiffness than for severe negative post-yield stiffness. It is concluded that there is a significant influence of the period of vibration for short-period systems and for systems with mildly negative post-yield stiffness. Dispersion of normalized lateral strengths required to avoid dynamic instability are found to increase as the negative post-yield stiffness decreases and as the period of vibration increases. Simple equations that capture the effects of period and post-yield stiffness to aid in the evaluation of existing structures are obtained through nonlinear regression analyses.

Summary:

The objective of this study was to assess the minimum lateral strength required to avoid dynamic instability in SDOF systems. The minimum lateral strength is computed as a function of linear elastic spectral ordinates, that is, the lateral strength required to maintain the system elastic. Specific goals of the study were: (a) to study the effect of the post-yield negative stiffness on the minimum strength required to avoid collapse, (b) to study the effect of period of vibration, (c) to compute mean normalized strengths required to avoid dynamic instability, and (d) to develop approximate expressions to assist practicing engineers in evaluating the minimum lateral strengths required in existing structures to avoid dynamic instability.

The study considered SDOF systems with a bilinear force displacement relationship characterized by a linear segment with initial stiffness K followed by a post-yield linear segment with negative stiffness $-\alpha K$. When subjected to earthquake ground motions the likelihood of experiencing dynamic instability in a system with a given negative slope increases as the lateral strength decreases. Lateral strengths required to avoid dynamic instability of bilinear SDOF systems with negative post-yield stiffness were investigated. Mean lateral strengths normalized by the lateral strength required to maintain the system elastic are computed for systems with periods ranging from 0.2 to 3.0 s and post-yield negative stiffness ratios ranging from 0.03 to 2.0 when subjected to 72 earthquake ground motions recorded on firm soil.

Representative Figures:

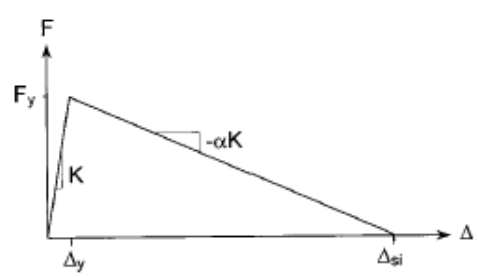

Figure A-9 Force-displacement characteristics of bilinear systems considered

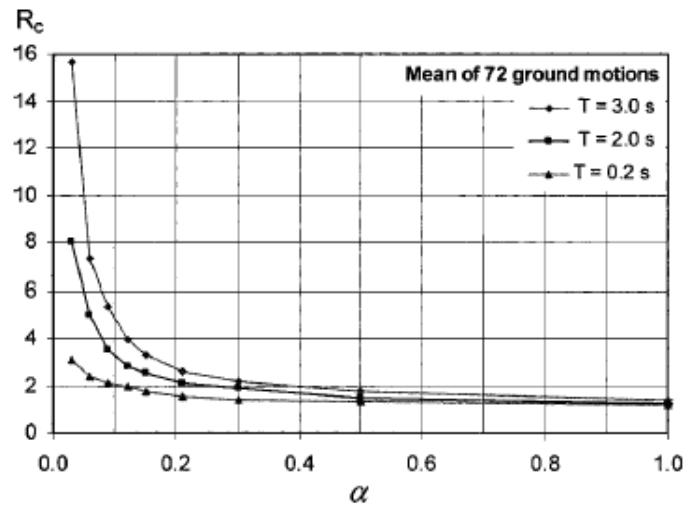

Figure A-10 Effect of period of vibration and post-yield stiffness on the mean strength ratio at which dynamic instability is produced.

Summary of Findings:

Lateral strengths required to avoid dynamic instability of bilinear SDOF systems with negative post-yield stiffness were investigated. Mean lateral strengths, normalized by the lateral strength required to maintain the system elastic, are computed for systems with periods ranging from 0.2 to 3.0 s and post-yield negative stiffness ratios ranging from 0.03 to 2.0 when subjected to 72 earthquake ground motions recorded on firm soil. The following conclusions are drawn from this study.

The strength ratio at which dynamic instability is produced decreases as the post-yield negative stiffness ratio α increases. This means that the lateral strength required to avoid collapse increases as the post-yield descending branch of the force-deformation relationship is steeper. When α is smaller than about 0.2 small increases in α can produce significant increases in required lateral strength to avoid instability. Meanwhile, for values of α >1, the system must remain practically elastic in order to avoid collapse.

The collapse strength ratio increases with increasing period, particularly for post-yielding negative stiffness ratios smaller than 0.3. Mean collapse strength ratios of short period structures are relatively strong, particularly when α >0.1. Dispersion of collapse strength ratios decreases as α increases and as the period of vibration decreases. Coefficients of variation of collapse strength ratios are particularly small for α >0.5. An approximate equation to estimate lateral strengths required to avoid dynamic instability of bilinear SDOF system is proposed.

Relevant Publications:

Miranda, E. and Akkar, S.D., 2003 "Dynamic instability of simple structural systems," *Journal of Structural Engineering*, ASCE, 129(12) , pp 1722-1727.

Vamvatsikos, D., and Cornell, C.A., 2005, *Seismic performance, capacity and reliability of structures as seen through incremental dynamic analysis*, John A. Blume Earthquake Engineering Research Center Report No. 151, Department of Civil and Environmental Engineering, Stanford University, Stanford, California.

A.2.5 Tests to Structural Collapse of Single-Degree-of-Freedom Frames Subjected to Earthquake Excitations

Authors:

Vian, D. and Bruneau, M. (2003)

Abstract:

This paper presents and analyzes experimental results of tests of 15 four-column frame specimens subjected to progressively increasing uniaxial ground shaking until collapse. The specimens were subdivided into groups of three different column slenderness ratios: 100, 150, and 200. Within each group, the column dimensions and supported mass varied. Ground motion of different severity was required to collapse the structures tested. The experimental setup is briefly described and results are presented. Test structure performance is compared with the proposed limits for minimizing $P–\Delta$ effects in highway bridge piers. The stability factor is found to have a strong relation to the relative structural performance in this regard. Performance is also compared with the capacity predicted by currently used design equations dealing with axial and moment interactions for strength and stability by expressing these capacities in terms of acceleration and maximum base shear (represented as a fraction of the system's weight). The experimental results exceeded the maximum spectral accelerations calculated when considering second-order effects, but did not when considering only member strength. Finally, an example of how to use the experimental data for analytical model verification is presented, illustrating the shortcomings and inaccuracies of using a particular simplified model with constant structural damping.

Summary:

Although the first and foremost objective of this project was to provide well-documented data (freely available on the web to be used by others) of tests to collapse, this paper includes results from a preliminary investigation of behavioral trends observed from the shake table results. In particular, peak responses are compared with limits proposed by others to minimize *P–Δ* effects in bridge piers. Specimen behavior is also investigated with respect to axial and moment interaction limits considering strength and stability. Finally, to illustrate how the generated experimental data could be used to develop or calibrate analytical models of inelastic behavior to collapse, experimental results are compared with those obtained using a simple analytical model. Progressive bilinear dynamic analyses are performed in two different ways and are compared with the shake table test results.

Representative Figures:

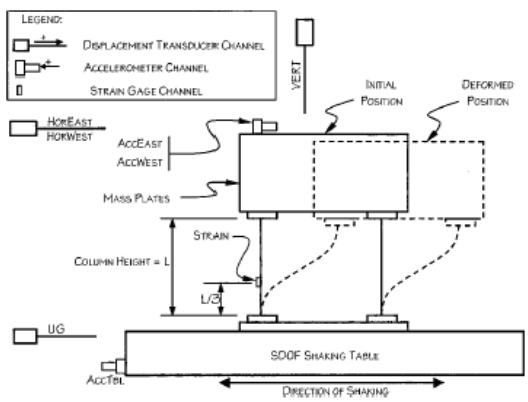

Figure A-11 (a) Schematic of test setup

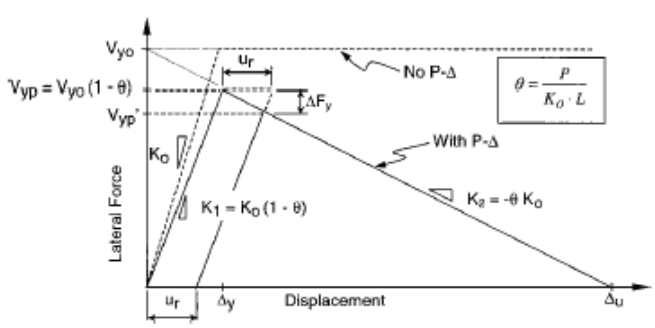

Figure A-12 Simplified bilinear force deformation model

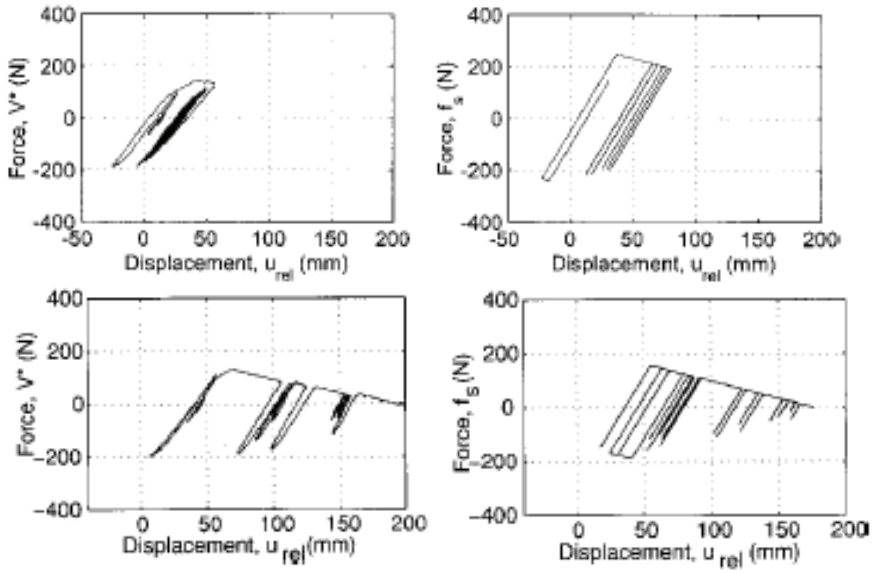

Figure A-13 Comparison of experimental (left) and analytical (right) results.

Summary of Findings:

Specimens showed an approximate bilinear behavior with a tendency to drift to one side and ultimately experience collapse. The stability factor, θ, was observed to have the most significant effect on the structure's propensity to collapse. As θ increases, the maximum attainable ductility, maximum sustainable drift, and maximum spectral acceleration reached before collapse, all decrease. When this factor θ was larger than 0.1, the ultimate values of maximum spectral acceleration, displacement ductility, and drift reached before collapse were all grouped below values of 0.75 g, 5, and 20%, respectively.

Relevant Publications:

Vian, D. and Bruneau, M., 2003, "Tests to structural collapse of single degree of freedom frames subjected to earthquake excitations." *Journal of Structural Engineering*, ASCE, 129(12), 1676-1685.

Bruneau, M. and Vian, D., 2002, "Tests to collapse of simple structures and comparison with existing codified procedures," *Proc. 7th U.S. National Conference on Earthquake Engineering*, Boston, MA.

Bruneau, M. and Vian, D., 2002, "Experimental investigation of $P-\Delta$ effects to collapse during earthquakes," *Proc. 12th European Conference on Earthquake Engineering*, London, UK.

Vian, D. and Bruneau, M., 2001, *Experimental investigation of P−Δ effects to collapse during earthquakes*, Report MCEER-01-0001, Multidisciplinary Research for Earthquake Engineering Research Center, Buffalo, N.Y.

A.2.6 Methods to Evaluate the Dynamic Stability of Structures – Shake Table Tests and Nonlinear Dynamic Analyses

Author:

Kanvinde, A.M. (2003)

Abstract:

This paper aims to understand the phenomenon of dynamic instability in structures better, and to suggest and evaluate methods to predict collapse limit states of structures during earthquakes, based on findings of recent shake table tests and nonlinear dynamic analyses conducted at Stanford University. Simple models that collapsed due to a story mechanism were used as test specimens. Data from nineteen experiments suggest that current methods of nonlinear dynamic analysis (using the OpenSees program in this case) are accurate and reliable for predicting collapse and tracing the path of the structure down to the ground during collapse. Moreover, it is found from the experiments that for non-degrading structures, an estimate of collapse drift based on a static pushover analysis can be successfully applied to predict the dynamic collapse or instability due to *P-Δ* effects. The rationale for this is that the structure has an elongated period at the point of global instability, virtually insulating it from the ground motion and justifying the use of a static-analysis-based drift. Finally, the paper directs the readers to a valuable database of test data from collapse tests of a "clean" structure, which can be used for further verification studies.

Summary:

This was a brief assessment of the collapse performance of two 2D single-story single-bay frames using results from static pushover and incremental dynamic analyses (IDA) and correlating them with experimental tests. The frames tested and simulated had a rigid beam that forced the creation of plastic hinges in the two columns. By using easily replaceable steel plates for the columns it was possible to repeat the shake table tests at various intensities and in effect experimentally reproduce IDA-like results. A total of 19 uniaxial shake table tests was performed using two ground motion records and two different structures (that is, two different column types).

Structure A was ductile and, having a ratio of yield base shear to weight of 1.03, was practically impossible to collapse. Structure B had weaker columns, produced by drilling holes at the bottom and top of the steel plates, and was thus prone to a story-mechanism collapse due to significant *P-Δ* effects (Figure A-14a). The two structures were also simulated in OpenSEES using a Giufre-Menegotto-Pinto hysteresis model for the column hinges (Figure A-14b) without any cyclic deterioration, and an exact corrotational formulation for geometric nonlinearities.

Representative Figures:

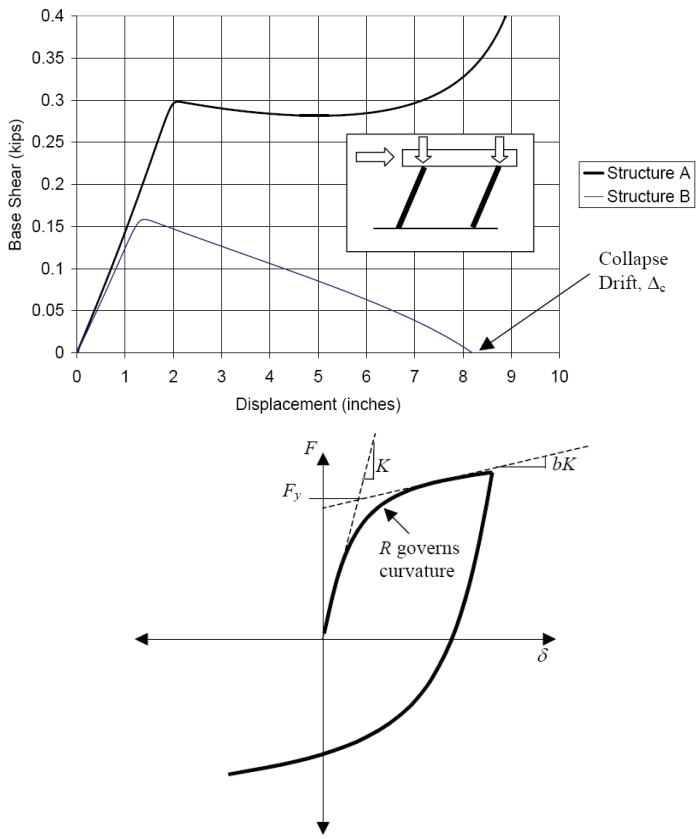

Figure A-14 (a) Static pushover curves for the two frames and (b) modeling of the column plastic hinges in OpenSEES.

Summary of Findings:

The evidence presented shows that nonlinear dynamic analysis is a reliable tool to predict the actual behavior of the two structures. The usefulness of static pushover was also proven, at least when cyclic deterioration is not an issue, as the collapse drift calculated statically was accurately matched by both incremental dynamic analysis and the shake table experiments. Compared to the response at lower intensities, larger scatter was observed

close to collapse both in the experiments and in the dynamic analyses, even when using the same earthquake record. This suggests an increased sensitivity of the actual results to the uncertainties in the initial condition of the structure, and an increased difficulty in predicting the collapse drift or intensity level even for such simple specimens.

Relevant Publications:

Kanvinde, A.M., 2003, "Methods to evaluate the dynamic stability of structures – shake table tests and nonlinear dynamic analyses," EERI Annual Student Paper Competition, *Proceedings of 2003 EERI Meeting*, Portland, OR.

Vian, D. and Bruneau, M., 2001, *Experimental investigation of P-Δ effects to collapse during earthquakes*, Report No. MCEER-01-0001, Multidisciplinary Research for Earthquake Engineering Research Center, Buffalo, N.Y.

A.2.7 Seismic Performance, Capacity and Reliability of Structures as Seen Through Incremental Dynamic Analysis

Authors:

Vamvatsikos, D. and Cornell, C.A. (2005)

Abstract:

Incremental Dynamic Analysis (IDA) is an emerging structural analysis method that offers thorough seismic demand and limit-state capacity prediction capability by using a series of nonlinear dynamic analyses under a suite of multiply scaled ground motion records. Realization of its opportunities is enhanced by several innovations, such as choosing suitable ground motion intensity measures and representative structural demand measures. In addition, proper interpolation and summarization techniques for multiple records need to be employed, providing the means for estimating the probability distribution of the structural demand given the seismic intensity. Limit-states, such as the dynamic global system instability, can be naturally defined in the context of IDA. The associated capacities are calculated so that when properly combined with probabilistic seismic hazard analysis, they allow the estimation of the mean annual frequencies of limit-state exceedance.

IDA is resource-intensive. Thus the use of simpler approaches becomes attractive. The IDA can be related to the computationally faster Static

Pushover (SPO), enabling a fast and accurate approximation to be established for SDOF systems. By investigating oscillators with quadrilinear backbones and summarizing the results into a few empirical equations, a new software tool, SPO2IDA, is produced here that allows direct estimation of the summarized IDA results. Interesting observations are made regarding the influence of the period and the backbone shape on the seismic performance of oscillators. Taking advantage of SPO2IDA, existing methodologies for predicting the seismic performance of first-mode-dominated, MDOF systems can be upgraded to provide accurate estimation well beyond the peak of the SPO.

The IDA results may display a large record-to-record variability. By incorporating elastic spectrum information, efficient intensity measures can be created that reduce such dispersions, resulting in significant computational savings. By employing either a single optimal spectral value, a vector of two or a scalar combination of several spectral values, significant efficiency is achieved. As the structure becomes damaged, the evolution of such optimally selected spectral values is observed, providing intuition about the role of spectral shape in the seismic performance of structures.

Summary:

The research presented is entirely based on the concept of incremental dynamic analysis (IDA). The methodology is established and is extensively used to derive (among others) the collapse capacity of MDOF frames. Of particular importance is the exploration of the connection between the fractile IDA curves and the pushover. The authors propose the use of a 5% damped SDOF oscillator with a complex quadrilinear backbone (including a hardening, a softening and a residual plateau segment) with moderately pinching hysteresis to capture the pushover curve shape of actual MDOF frames. No cyclic degradation was considered but in the process millions of nonlinear dynamic SDOF analyses are performed for 30 records and a wide variety of oscillator backbones and periods. The results are fitted and incorporated into a complex R-μ-T relationship, realized in the form of the SPO2IDA Excel tool.

The proposed tool is applied to the MDOF prediction problem using the worst-case pushover concept. This is defined as the pushover that leads to the earliest post-peak collapse, stipulating that it will also help find the collapse mechanism that a dynamic analysis would predict. By applying the SPO2IDA tool on the worst-case pushover the complete IDA curves of

MDOF frames are generated for a 5-story, a 9-story and a 20-story steel frame.

Representative Figures:

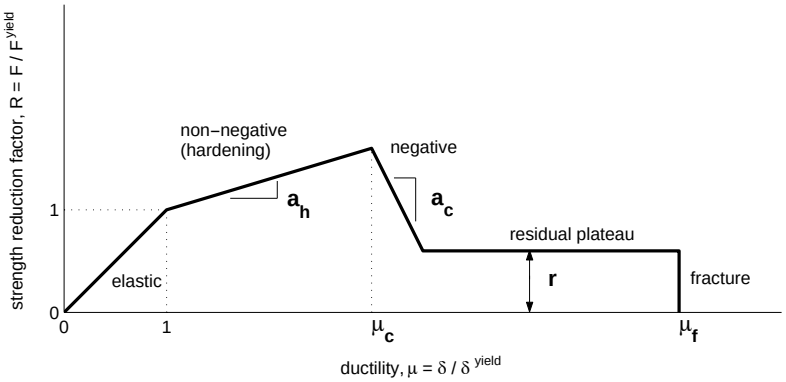

Figure A-15 The backbone of the studied oscillator.

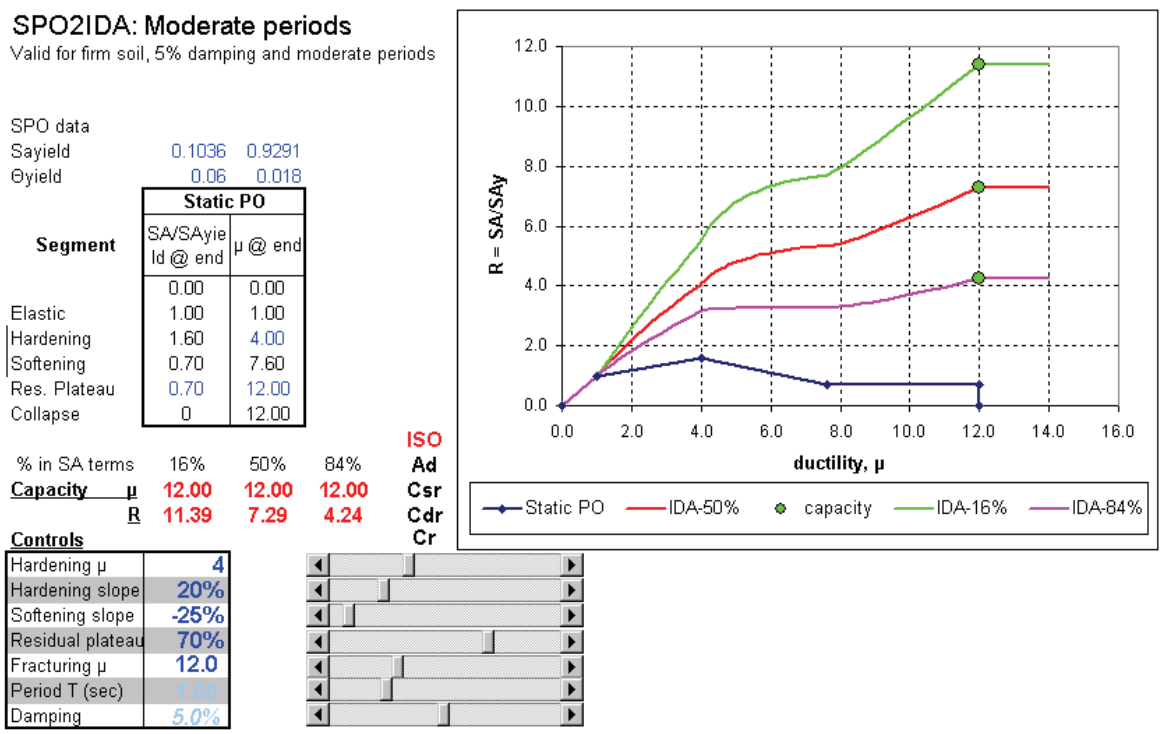

Figure A-16 The interface of the SPO2IDA tool for moderate periods.

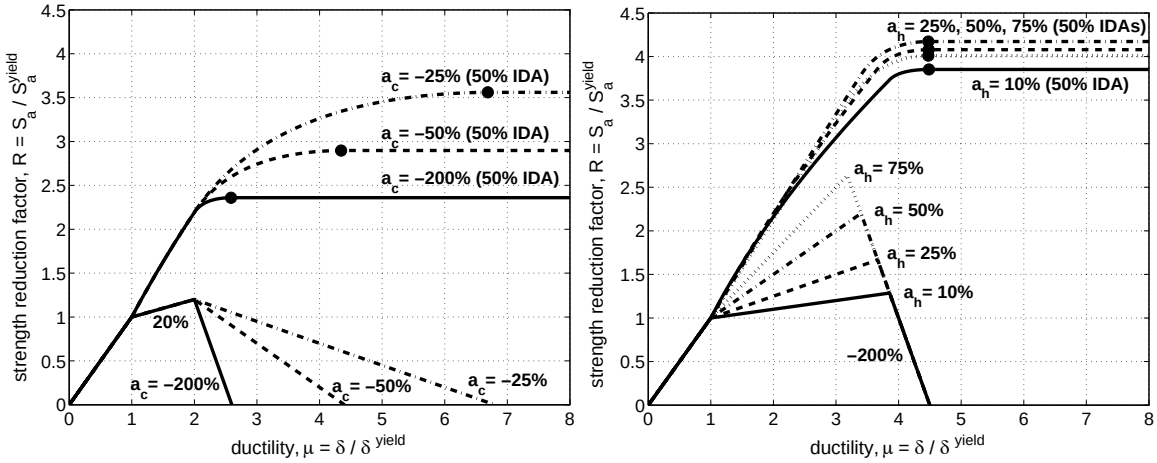

Figure A-17 Influence of (a) the post-peak and (b) post-yield stiffness on the median dynamic response of the oscillator. When the negative segment is the same then the hardening slope has a negligible effect.

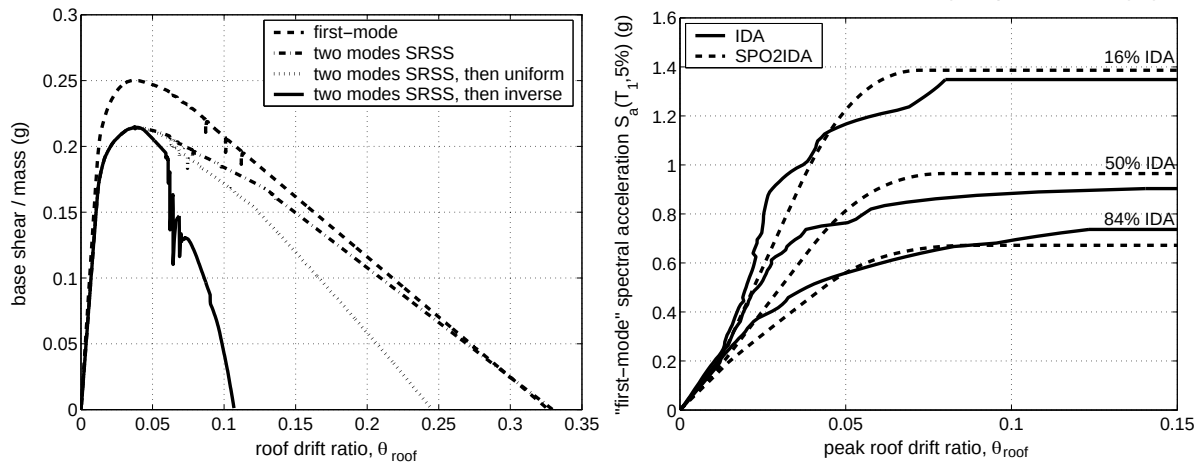

Figure A-18 (a) Influence of the load pattern on the pushover curve shape and (b) the predicted versus actual dynamic response for various intensity levels using SPO2IDA and the worst-case pushover for a 9-story steel moment frame.

Summary of Findings:

Regarding SDOF oscillators, it was found that the shape of the backbone curve has a very complex effect on the dynamic response. For example, the negative slope, the hardening deformation and the residual strength level are the three parameters that dominate (e.g. Figure A-17a). On the other hand, the hardening slope is not as important, while the residual plateau is significant only when long or high enough. Surprisingly, the peak strength of the oscillator is found to be relatively unimportant when the subsequent negative-slope segment is fixed. Thus some very different backbones exist that have almost the same performance (Figure A-17b).

For MDOF application, it was found that the worst-case pushover is not always easy to estimate. For a 9-story steel frame building, in order to find the dominant collapse mechanism it was necessary to change the load pattern after the peak of the pushover and actually try several combinations before getting an acceptable shape (Figure A-18a). Under this condition, the use of SPO2IDA was found to provide accurate results for first-mode-dominated frames. A test conducted on a 20-story frame, where higher modes are a significant issue, showed that it was impossible to get good agreement in the early inelastic range. Curiously, when close to collapse, this approach still managed to provide an accurate answer, leading to the observation that an SDOF can predict reliably the collapse capacity of complex buildings.

Relevant Publications:

Vamvatsikos, D., and Cornell, C.A., 2005, *Seismic performance, capacity and reliability of structures as seen through incremental dynamic analysis*, John A. Blume Earthquake Engineering Research Center, Report No. 151, Department of Civil and Environmental Engineering, Stanford University, Stanford, California.

Ibarra, L.F., and Krawinkler, H., 2005, *Global collapse of frame structures under seismic excitations*, John A. Blume Earthquake Engineering Research Center, Report No. 152, Department of Civil and Environmental Engineering, Stanford University, Stanford, California.

A.2.8 Hysteretic Models that Incorporate Strength and Stiffness Deterioration

Authors:

Ibarra, L., Medina, R.A., and Krawinkler, H., (2005)

Abstract:

This paper presents the description, calibration and application of relatively simple hysteretic models that include strength and stiffness deterioration properties, features that are critical for demand predictions as a structural system approaches collapse. Three of the basic hysteretic models used in seismic demand evaluation are modified to include deterioration properties: bilinear, peak-oriented, and pinching models. The modified models include most of the sources of deterioration, namely, various modes of cyclic deterioration and softening of the post-yielding stiffness, and they also account for a residual strength after deterioration. The models incorporate an energy-based deterioration parameter that controls four cyclic deterioration

modes: basic strength, post-capping strength, unloading stiffness, and accelerated reloading stiffness deterioration modes. Calibration of the hysteretic models on steel, plywood, and reinforced-concrete components demonstrates that the proposed models are capable of simulating the main characteristics that influence deterioration. An application of a peak-oriented deterioration model in the seismic evaluation of SDOF systems is illustrated. The advantages of using deteriorating hysteretic models for obtaining the response of highly inelastic systems are discussed.

Summary:

This study presents an improved piece-wise linear hysteretic model that is capable of considering stiffness degradation, pinching cyclic strength degradation as well as in-cycle strength degradation. The paper has a threefold objective: (a) to describe the properties of proposed hysteretic models that incorporate both monotonic and cyclic deterioration; (b) to illustrate the calibration of these hysteretic models on component tests of steel, plywood, and reinforced-concrete specimens; and (c) to exemplify the utilization of the hysteretic models in the seismic response evaluation of SDOF systems. In this study the term deteriorating hysteretic models refers to models that include strength deterioration of the backbone curve or cyclic deterioration or both.

As shown in Figure A-19, the model considers a backbone curve consisting of four linear segments: an elastic segment until a yield displacement, post-yield strain-hardening segment until the 'capping' displacement is reached, a post-capping segment with negative stiffness (that is, in-cycle degradation), and a final residual horizontal segment.

Representative Figures:

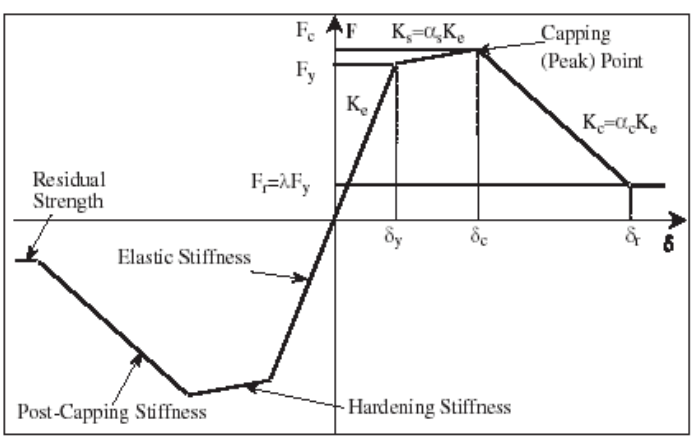

Figure A-19 The backbone of the proposed hysteretic model.

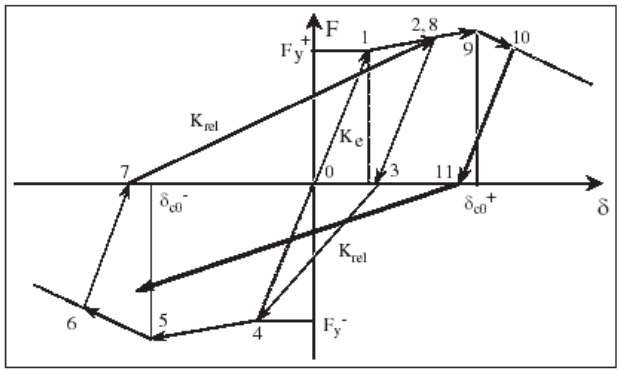

Figure A-20 Basic rules for peak-oriented hysteretic model.

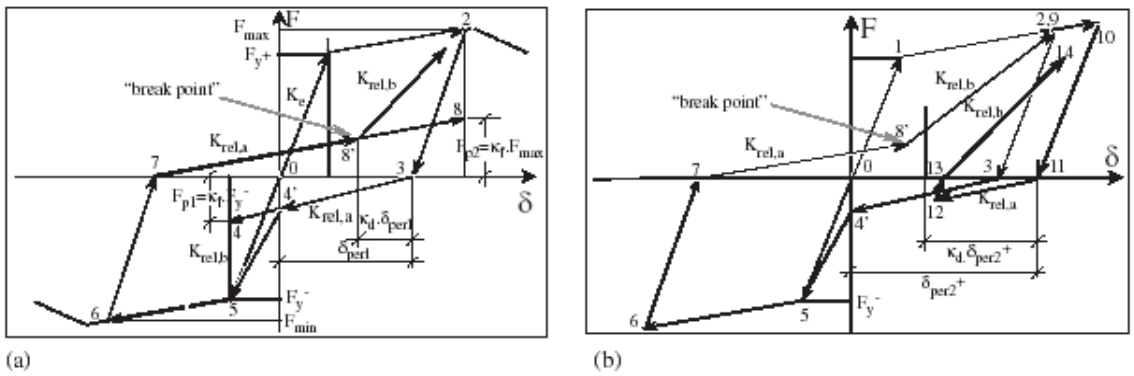

Figure A-21 Pinching hysteretic model: (a) basic model rules; and (b) modification if reloading deformation is to the right of break point.

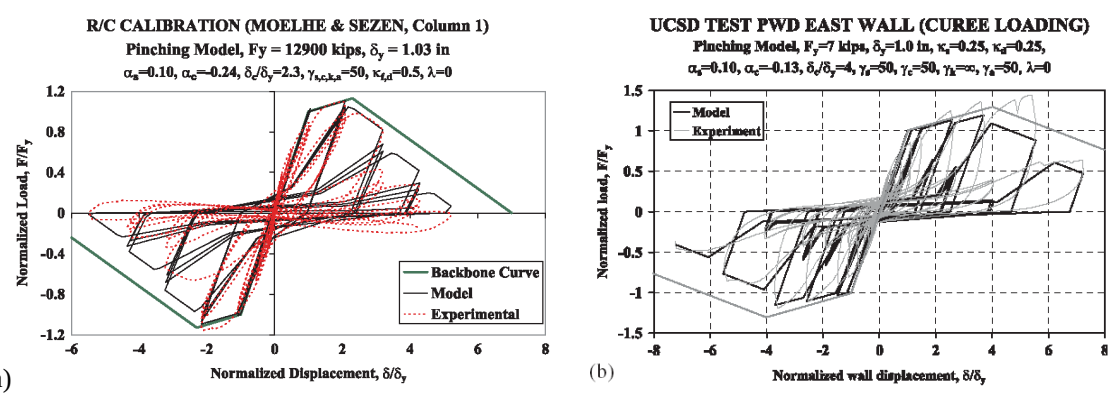

Figure A-22 Examples of comparisons between experimental and analytical results for (a) non-ductile reinforced concrete column; and (b) plywood shear wall.

Summary of Findings:

The hysteretic models include a post-capping softening branch, residual strength, and cyclic deterioration. Cyclic deterioration permits deterioration to be traced as a function of past loading history, the rate of deterioration (which depends on the hysteretic energy dissipated in past cycles), and on a

reference energy dissipation capacity. Four modes of cyclic deterioration can be simulated: basic strength, postcapping strength, unloading stiffness, and accelerated reloading stiffness deterioration. Based on calibrations performed with experimental data from component tests of steel, wood, and reinforced-concrete specimens, they concluded that it appears that, for a given component, the backbone characteristics and a single parameter that controls all four modes of cyclic deterioration are adequate to represent component behavior regardless of the loading history.

Results from the seismic evaluation of various SDOF systems demonstrate that strength deterioration becomes a dominant factor when the response of a structure approaches the limit state of collapse. At early stages of inelastic behavior, both deteriorating and nondeteriorating systems exhibit similar responses. The differences become important when the post-capping stiffness is attained in the response.

Relevant Publications:

Ibarra, L., Medina, R., Krawinkler, H., 2005, "Hysteretic models that incorporate strength and stiffness deterioration, *Earthquake Engineering and Structural Dynamics*, Vol. 34, no. 12, pp. 1489-1511.

Ibarra, L.F., and Krawinkler, H., 2005, *Global collapse of frame structures under seismic excitations*, John A. Blume Earthquake Engineering Research Center, Report No. 152, Department of Civil and Environmental Engineering, Stanford University, Stanford, California.

Ibarra, L., Medina, R., Krawinkler, H., 2002, "Collapse assessment of deteriorating SDOF systems," *Proc. 12th European Conference on Earthquake Engineering*, London, UK, Paper 665, Elsevier Science Ltd.

A.2.9 Global Collapse of Frame Structures Under Seismic Excitations

Authors:

Ibarra, L.F. and Krawinkler, H. (2005)

Abstract:

Global collapse in earthquake engineering refers to the inability of a structural system to sustain gravity loads in the presence of seismic effects. This research proposes a methodology for evaluating global incremental (sidesway) collapse based on a relative intensity measure instead of an Engineering Demand Parameter (EDP). The relative intensity is the ratio of

ground motion intensity to a structure strength parameter, which is increased until the response of the system becomes unstable, which means that the relative intensity - EDP curve becomes flat (that is, with zero slope). The largest relative intensity is referred to as “collapse capacity.”

In order to implement the methodology, deteriorating hysteretic models are developed to represent the monotonic and cyclic behavior of structural components. Parameter studies that utilize these deteriorating models are performed to obtain collapse capacities and quantify the effects of system parameters that most influence the collapse for SDOF and MDOF structural systems. The range of collapse capacity due to record-to-record variability and uncertainty in the system parameters is evaluated. The latter source of dispersion is quantified by means of the first order second moment (FOSM) method. The studies reveal that softening of the post-yield stiffness in the backbone curve (postcapping stiffness) and the displacement at which this softening commences (defined by the ductility capacity) are the two system parameters that most influence the collapse capacity of a system. Cyclic deterioration appears to be an important but not the dominant issue for collapse evaluation. *P-Δ* effects greatly accelerate collapse of deteriorating systems and may be the primary source of collapse for flexible, but very ductile, structural systems.

The dissertation presents applications of the proposed collapse methodology to the development of collapse fragility curves and the evaluation of the mean annual frequency of collapse.

An important contribution is the development of a transparent methodology for the evaluation of incremental collapse, in which the assessment of collapse is closely related with the physical phenomena that lead to this limit state. The methodology addresses the fact that collapse is caused by deterioration in complex assemblies of structural components that should be modeled explicitly.

Summary:

The authors used an oscillator with a quadrilinear backbone curve with hardening, softening and residual segment to conduct an extensive parametric study. Pinching, peak-oriented and (bilinear-like) kinematic hysteresis rules were considered, while the cyclic degradation of the backbone stiffness and strength and of the unloading/reloading stiffness were also included. The effects of P-Δ were added separately, as a rotation of the backbone around the center of the axes. The investigation used 40 “ordinary”

ground motion records and it was focused on determining the influence of all the parameters on the collapse capacity, which was considered to occur in an IDA (incremental dynamic analysis) fashion, when numerical instability occurred or when the IDA curve becomes horizontal.

Additionally a number of 2D single-bay frames with 3, 6, 9, 12, 15 and 18 stories was considered; they were designed according to a strong column, weak beam, concept, with the beam hinges having a hysteretic model of the same type as the one used for the SDOF studies. By maintaining a uniform hysteretic model for all beam hinges and globally varying its parameters, another parametric study was performed, focused now on the effect of the hysteretic parameters on the MDOF response.

Representative Figures:

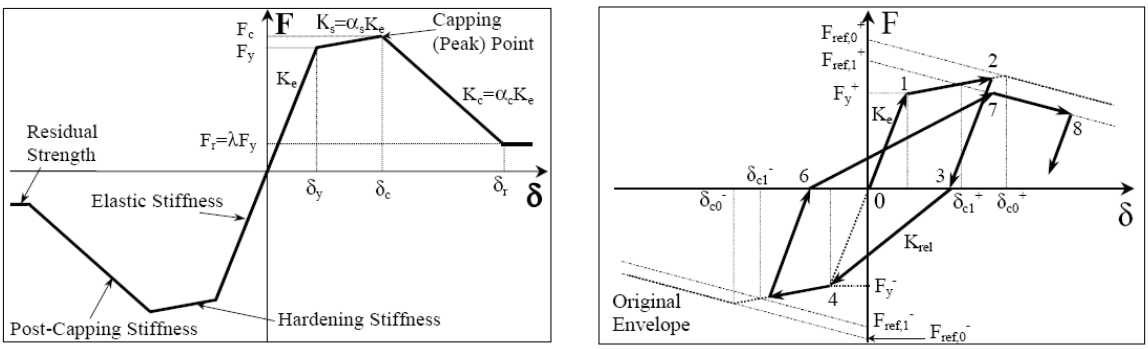

Figure A-23 (a) Backbone curve used for the investigations and (b) post-peak stiffness cyclic deterioration considered.

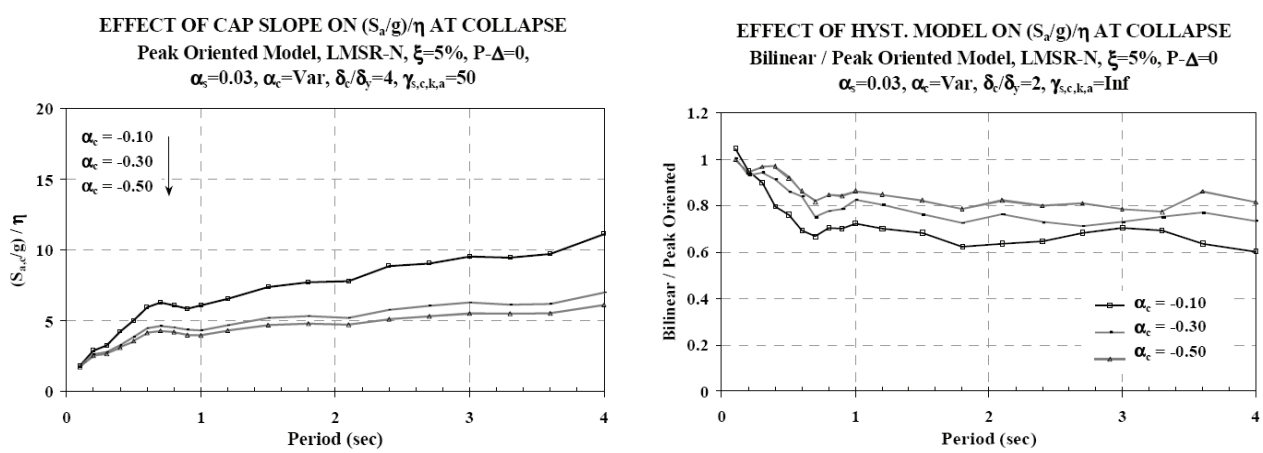

Figure A-24 (a) Effect of the post-peak stiffness to the median collapse capacity spectra for a peak-oriented model and (b) the ratio of collapse capacities for different hysteretic models.

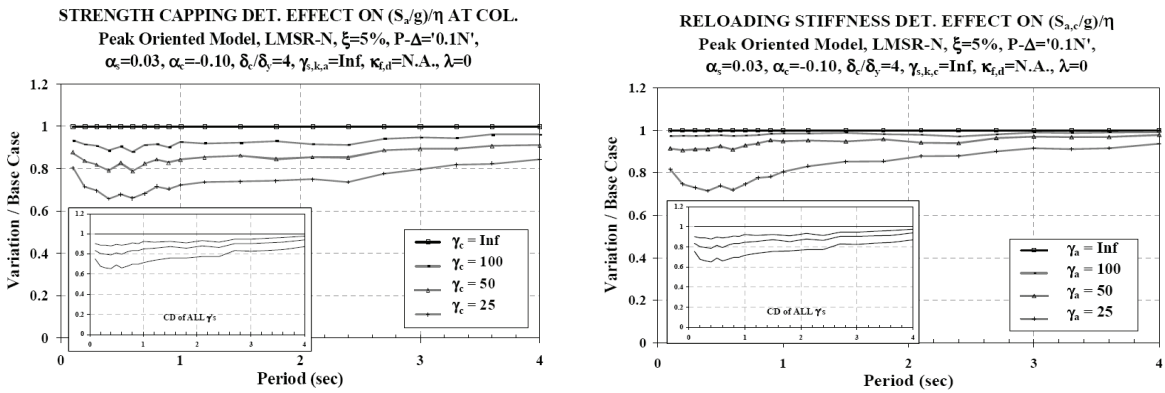

Figure A-25 Effect of (a) post-yield slope and (b) reloading stiffness cyclic deterioration on the collapse capacity.

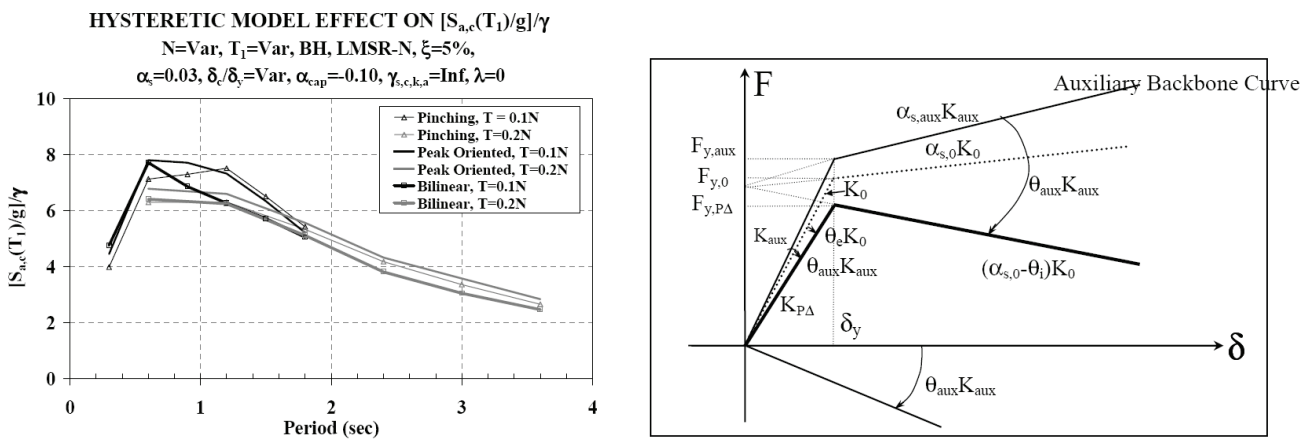

Figure A-26 (a) Effect of the beam-hinge hysteretic model on the median MDOF collapse capacity and (b) the generation of an equivalent SDOF system by using an auxiliary backbone curve to incorporate *P-Δ*.

Summary of Findings:

For the SDOF oscillator it was found that there is a complex interplay between the parameters that defines the dynamic response. Their relative values are significant. The cyclic deterioration was found to be unimportant in the pre-peak region and only mildly important post-peak. Furthermore, its influence does not depend on the type of ground motion, i.e. whether it is near or far field or long in duration. The peak-strength ductility and the post-peak slope are the most dominant parameters. Regarding the hysteresis laws, kinematic hysteresis produces lower capacities than the pinching or the peak-oriented, which are roughly similar. The residual strength becomes important only when it is large enough. Finally, the application of damping in a mass-proportional or stiffness-proportional formulation becomes an important issue after yielding, as the tangent stiffness is constantly changing.

The study of the MDOF frames concluded that these higher-mode-influenced frames fail mostly due to a lower-story mechanism. There is a large dependence of the collapse capacity on the first-mode period. In general the effects of the hinge hysteresis and backbone parameters were similar to the SDOF results. It was also observed that the inelastic instability coefficient (i.e. the difference between the post-peak slope with and without *P-Δ*) was often much larger than the elastic stability coefficient. Thus, surrogate SDOFs need a separate inclusion of the *P-Δ* effects in the pre- and post-peak regions. Such equivalent SDOFs were shown to have good accuracy in predicting the collapse capacity.

Relevant Publications:

Ibarra, L.F., and Krawinkler, H., 2005, *Global collapse of frame structures under seismic excitations*, John A. Blume Earthquake Engineering Research Center, Report No. 152, Department of Civil and Environmental Engineering, Stanford University, Stanford, California.

Rahnama, M. and Krawinkler, H., 1993, *Effect of soft soils and hysteresis models on seismic design spectra*, John A. Blume Earthquake Engineering Research Center, Report No. 108, Department of Civil Engineering, Stanford University, Stanford, California.

Medina, R., 200), *Seismic demands for nondeteriorating frame structures and their dependence on ground motions*, Ph.D.. dissertation submitted to the Department of Civil and Environmental Engineering, Stanford University, Stanford, California.

Ibarra, L., Medina, R., and Krawinkler, H., 2002, "Collapse assessment of deteriorating SDOF systems," *Proc. 12th European Conference on Earthquake Engineering*, London, UK, Paper 665, Elsevier Science Ltd.

A.2.10 Object-Oriented Development of Strength and Stiffness Degrading Models for Reinforced Concrete Structures

Author:

Kaul, R. (2004)

Abstract:

The aim of this research is to develop structural simulation models that can capture the strength and stiffness degradation of reinforced concrete frames up to collapse under earthquake-induced motions. The key modeling aspects of the element formulations include: (1) rigorous modeling of large deformation response, (2) flexural yielding and inelastic interaction between

axial force and moment (3) degradation of the element stiffness under cyclic loading and (4) axial force-moment-shear interaction for shear-critical reinforced concrete columns. Beam-column models are developed and implemented in an object-oriented analysis framework called OpenSees (Open System for Earthquake Engineering Simulation). The large deformation element formulations employ an updated Lagrangian approach. Inelastic models are based on stress-resultant plasticity to simulate inelastic hardening and softening response under combined axial loads and bending. A two-surface evolution model is proposed for combined nonuniform expansion or contraction and kinematic motion of the yield surface. The yield surface can be used to simulate inelastic section response at integration points along a beam-column element (distributed plasticity) or inelastic hinging at the ends of a beam-column element (concentrated plasticity). In the concentrated plasticity approach, the element between the hinges is quasi-elastic, in which hysteretic models are developed to model the cyclic degradation. This concentrated plasticity model is extended to simulate shear-critical column behavior, including shear strength degradation and failure, interaction between axial and shear forces, and pinched cyclic response. Implementation of the models in OpenSees is planned and structured using object-oriented programming concepts. Individual components of the inelastic modeling problem are identified and the interactions between the governing classes are established. The models are implemented in a hierarchal structure, which provides a modular and extensible software design. The accuracy and the capabilities of the proposed models are verified by comparing the analytical results with the experimental data. The models developed as part of this research provide ideal tools for conducting extensive application studies. An extensible framework is provided to facilitate tool development for nonlinear or inelastic analysis.

Summary:

The objective was the creation, and incorporation into OpenSEES, of a beam-column element with concentrated plasticity, that is appropriate for multiaxial loading of older, shear-critical RC columns. The element has been based on a yield-surface formulation and the focus was on modeling the multiaxial response of a complete RC section. The model incorporates in-cycle strength degradation, allowing for a quadrilinear backbone with a negative stiffness segment (Figure A-27). Inelastic hardening and softening were formulated according to a combined kinematic and isotropic hardening rule with either peak-oriented (for moment) or pinching (for shear) hysteretic rules (Figure A-28). There is little provision for cyclic degradation; the formulation is entirely based on the peak plastic strains and rotations, and the

direction of evolution, so depending on the details there may be no cyclic degradation.

The significant advantage of the models is their apparent extensibility and the possibilities for easy modification and incorporation into a variety of elements, an inherent feature of the object-oriented programming upon which OpenSEES has been built.

The model behavior has been calibrated and tested against a variety of RC beam-column experiments, including both shear and moment-critical columns, as well as a set of theoretical solutions for large deformation response (Figure A-29).

Representative Figures:

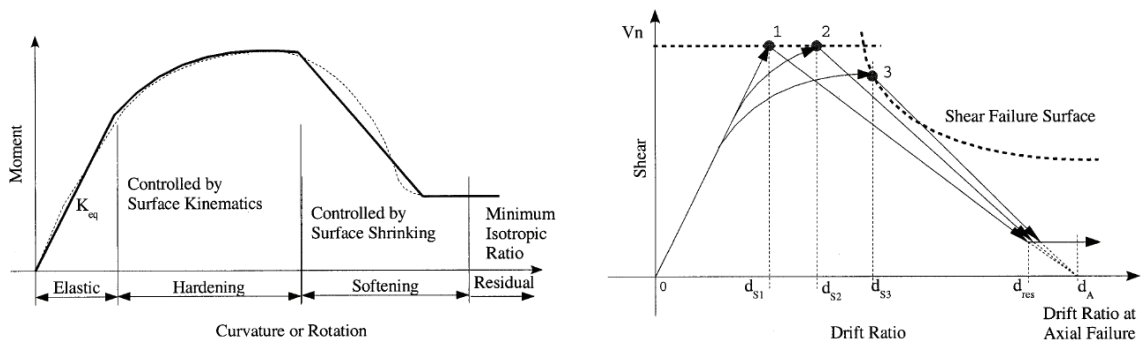

Figure A-27 Idealization of the (a) flexure spring and (b) shear spring backbones.

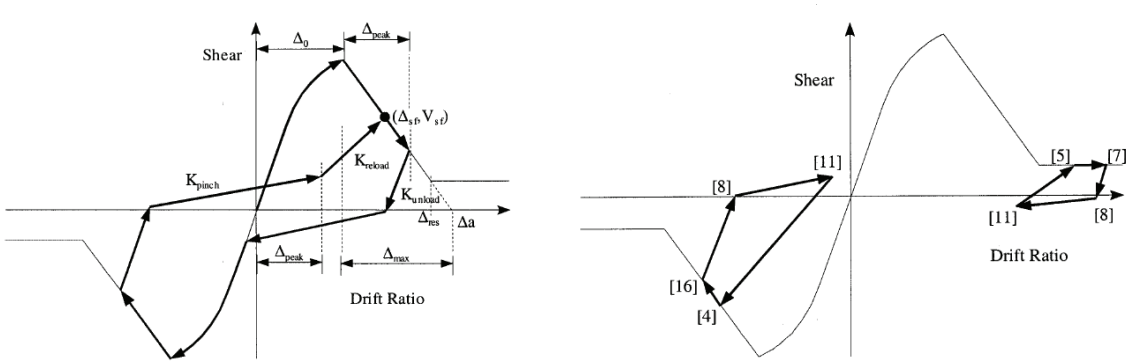

Figure A-28 (a) Full and (b) half cycle pinching hysteresis for the shear spring.

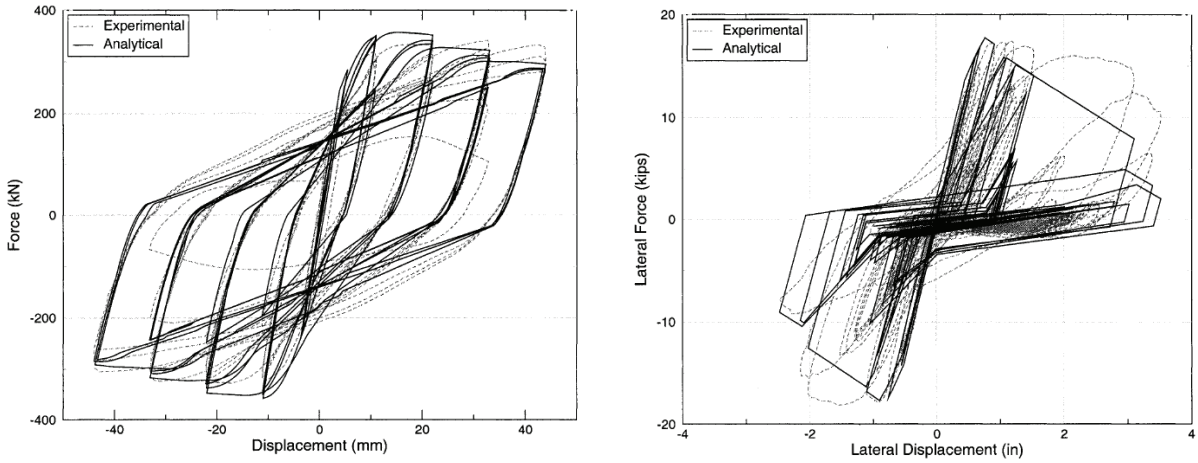

Figure A-29 Comparison of calculated versus experimental results for (a) a moment-critical column and (b) a shear-critical column.

Summary of Findings:

A reliable and extensible concentrated-plasticity beam-column element was created for RC members. Extensive testing and calibration has shown good agreement for a variety of experimental results, including shear-critical columns, large deformations, and planar moment and axial-force interaction. The only serious limitation is the limited formulation of cyclic degradation, an issue that can be potentially solved with the incorporation of damage models. The extension to 3D beam-column elements is somewhat hampered. Appropriate yield surface and evolution rules have not been incorporated, although the hysteretic material models presented are directly usable. The absence of the bond-slip effect and longitudinal reinforcement development in the element springs, are issues that still remain to be addressed.

Relevant Publications:

Kaul, R., 2004, *Object oriented development of strength and stiffness degrading models for reinforced concrete structures*, Ph.D. Thesis, Department of Civil and Environmental Engineering, Stanford University, Stanford, California.

McKenna, F.T. (1997), *Object-oriented finite element programming: framework for analysis, algorithms, parallel computing*, Ph.D. Dissertation, University of California, Berkeley, California.

Mehanny, S.S.F., and Deierlein, G.G., 2001, "Seismic collapse assessment of composite RCS moment frames," *Journal of Structural Engineering*, ASCE, Vol. 127(9).

El-Tawil, S., 1996, *Inelastic dynamic analysis of mixed steel-concrete space frames*, Ph.D. Dissertation, Cornell University, Ithaca, NY.

Elwood, K.J., 2002, *Shake table tests and analytical studies on the gravity load collapse of reinforced concrete frames*, Ph.D. Dissertation, University of California, Berkeley, California.

A.2.11 Shake Table Tests and Analytical Studies on the Gravity Load Collapse of Reinforced Concrete Frames

Author:

Elwood, K.J. (2002).

Abstract:

An empirical model, based on the evaluation of results from an experimental database, is developed to estimate the drift at shear failure of existing reinforced concrete building columns. A shear-friction model is also developed to represent the general observation from experimental tests that the drift at axial failure of a shear-damaged column is directly proportional to the amount of transverse reinforcement and is inversely proportional to the magnitude of the axial load. The two drift-capacity models are incorporated in a nonlinear uniaxial constitutive model implemented in a structural analysis platform to allow for the evaluation of the influence of shear and axial load column failures on the response of a building. Shake table tests were designed to observe the process of dynamic shear and axial load failures in reinforced concrete columns when an alternative load path is provided for load redistribution. The results from these tests provide data on the dynamic shear strength and the hysteretic behavior of columns failing in shear, the loss of axial load capacity after shear failure, the redistribution of loads in a frame after shear and axial failures of a single column, and the influence of axial load on each of the above-mentioned variables. An analytical model of the shake table specimens, incorporating the proposed drift-capacity models to capture the observed shear and axial load failures, provides a good estimate of the measured response of the specimens.

Summary:

The objective was the creation and incorporation into OpenSEES of a beam-column element with concentrated plasticity that is appropriate for multiaxial loading of older, shear-critical RC columns. The element has been based on a yield-surface formulation and the focus was on modeling the multiaxial response of a complete RC section. The model incorporates in-cycle strength

degradation, allowing for a quadrilinear backbone with a negative stiffness segment (Figure A-30). Inelastic hardening and softening were formulated according to a combined kinematic and isotropic hardening rule with either peak-oriented (for moment) or pinching (for shear) hysteretic rules (Figure A-31). There is little provision for cyclic degradation; the formulation is entirely based on the peak plastic strains and rotations, and the direction of evolution, so depending on the details there may be no cyclic degradation.

The significant advantage of the models is their apparent extensibility and the possibilities for easy modification and incorporation into a variety of elements, an inherent feature of the object-oriented programming upon which OpenSEES has been built.

Representative Figures:

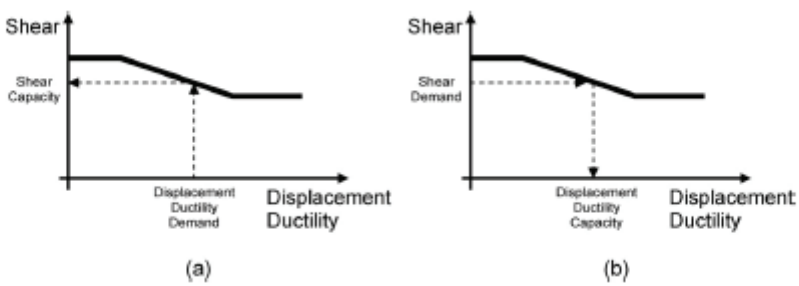

Figure A-30 Use of Sezen model to estimate (a) shear capacity and (b) displacement ductility capacity.

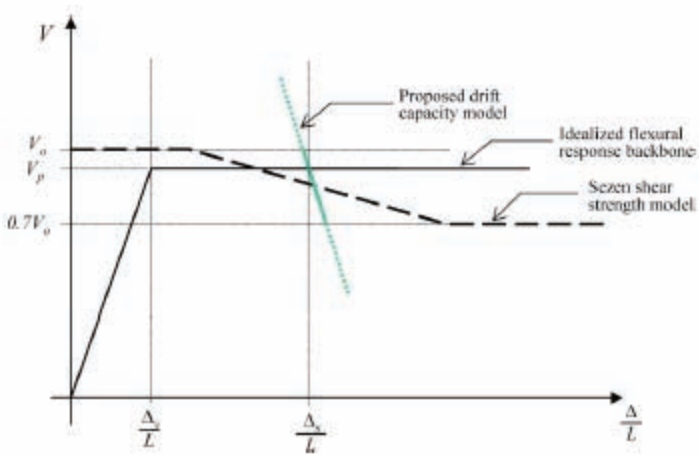

Figure A-31 Comparison of the Sezen shear strength model and the proposed drift capacity model.

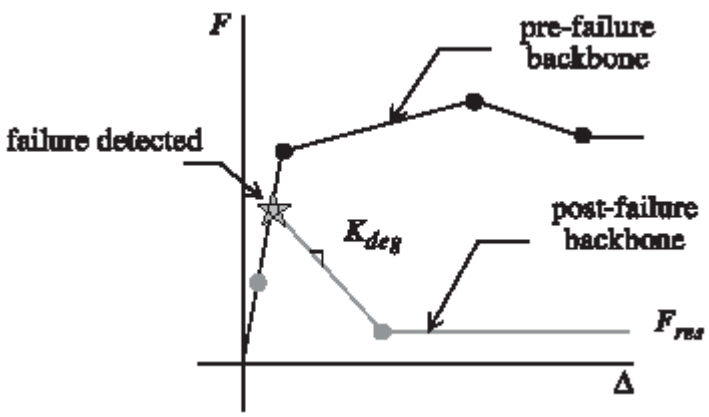

Figure A-32 Redefinition of backbone in Elwood's model after shear failure is detected.

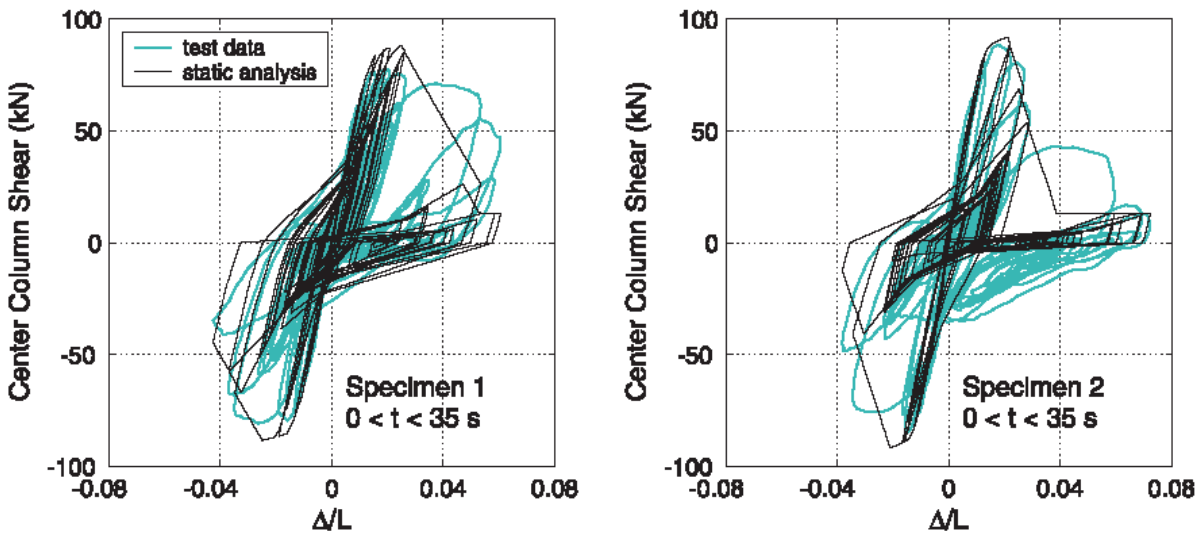

Figure A-33 Comparison of calculated versus experimental results for two shear-critical columns.

Summary of Findings:

Given the lack of agreement between existing models for the drift at shear failure and results from an experimental database of shear-critical building columns, two empirical models were developed to provide a more reliable estimate of the drift at shear failure for existing reinforced concrete columns:

$$\frac{\Delta_s}{L} = \frac{3}{100} + 4\rho'' - \frac{1}{500}\frac{v}{\sqrt{f_c'}} - \frac{1}{40}\frac{P}{A_g f_c'} \geq \frac{1}{100} \text{ (psi units)}$$

Based on shear-friction concepts and the results from 12 columns tested to axial failure, a model was also developed to estimate the drift at axial failure for a shear-damaged column:

$$\frac{\Delta_a}{L} = \frac{4}{100}\frac{1+(\tan\theta)^2}{\tan\theta + P\left(\frac{s}{A_{st}f_{yt}d_c\tan\theta}\right)} \qquad \text{where } \theta = 65°$$

The capacity models for the drift at shear and axial load failure were used to initiate the strength degradation of a uniaxial material model implemented in the OpenSees analytical platform (OpenSees, 2002). When attached in series with a beam-column element, the material model can be used to model either shear or axial failure, or both if two materials are used in series. Based on experimental evidence suggesting that an increase in lateral shear deformations may lead to an increase in axial deformations and a loss of axial load, shear-to-axial coupling was incorporated in the material model to approximate the response of a column after the onset of axial failure.

Relevant Publications:

Elwood, K.J., 2002, *Shake table tests and analytical studies on the gravity load collapse of reinforced concrete frames*, Ph.D. Dissertation, University of California, Berkeley.

Elwood, K.J., and Moehle, J.P., 2003, *Shake table tests and analytical studies on the gravity load collapse of reinforced concrete frames*. Pacific Earthquake Engineering Research Center, PEER Report 2003/01, University of California, Berkeley, Calif.

Elwood, K.J., 2004, "Modeling failures in existing reinforced concrete columns," *Can. J. Civ. Eng.*, 31: 846–859 (2004)

Elwood, K.J., and Moehle, J.P., 2005, "Drift capacity of reinforced concrete columns with light transverse reinforcement." *Earthquake Spectra*, Volume 21, No. 1, pp. 71–89,

A.2.12 Determination of Ductility Factor Considering Different Hysteretic Models

Authors:

Lee, L.H., Han, S.W., and Oh, Y.H. (2003)

Abstract:

In current seismic design procedures, base shear is calculated by the elastic strength demand divided by the strength reduction factor. This factor is well known as the response modification factor, R, which accounts for ductility, overstrength, redundancy, and damping of a structural system. In this study, the R factor accounting for ductility is called the ductility factor, R_μ. The R_μ

factor is defined as the ratio of elastic strength demand imposed on the SDOF system to inelastic strength demand for a given ductility ratio. The R_μ factor allows a system to behave inelastically within the target ductility ratio during the design level earthquake ground motion. The objective of this study is to determine the ductility factor considering different hysteretic models. It usually requires large computational efforts to determine the R_μ factor. In order to reduce the computational efforts, the R_μ factor is prepared as a functional form in this study. For this purpose, statistical studies are carried out using forty different earthquake ground motions recorded at a stiff soil site. The R_μ factor is assumed to be a function of the characteristic parameters of each hysteretic model, target ductility ratio and structural period. The effects of each hysteretic model on the R_μ factor are also discussed.

Summary:

The focus of the research was the creation of an R-μ-T relationship that would include the effect of several backbone and hysteretic characteristics. The authors' approach was to consider such effects as completely independent from each other by considering the following models: (a) kinematic hysteresis with a bilinear backbone having positive post-yield stiffness; (b) bilinear backbone and kinematic hysteresis with cyclic degradation of the reloading/unloading stiffness; (c) bilinear backbone with peak-oriented (Clough-like) hysteresis with cyclic strength degradation; and (d) bilinear backbone with pinching hysteresis (Figure A-34). Details of the models are provided by Kunnath *et al*., (1990).

Using the elastic-perfectly-plastic model with kinematic hardening as a basis, the researchers investigated the influence of each of the four parameters and provided correction factors, in a "coefficient-like" method. These can be applied to an R-μ-T relationship based on the elastic-plastic system to account for the effect of each of the parameters.

Representative Figures:

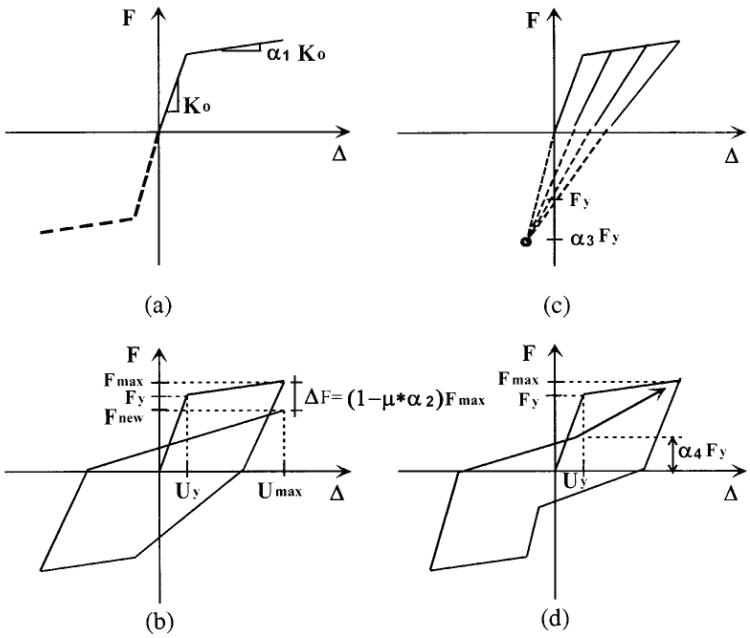

Figure A-34 The parameters investigated: (a) backbone hardening ratio; (b) unloading/reloading cyclic stiffness degradation; (c) strength degradation; and (d) degree of pinching.

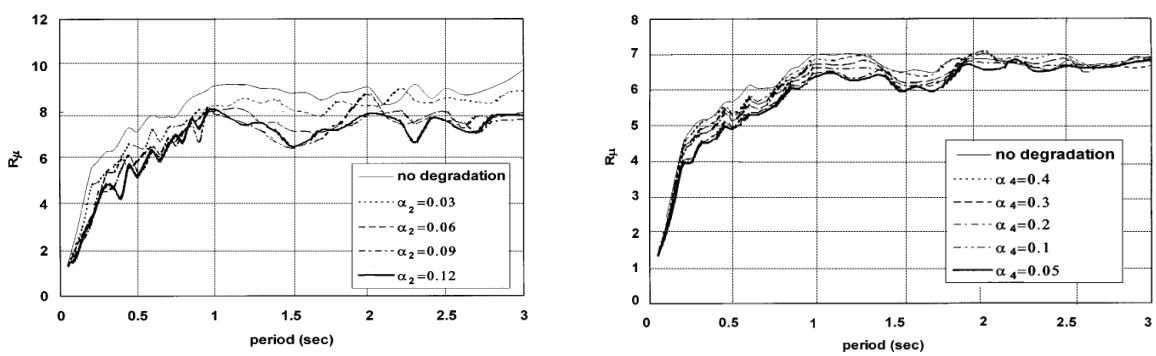

Figure A-35 The effect of (a) cyclic strength degradation and (b) degree of pinching on the mean R-factor for a given ductility.

Summary of Findings:

The results presented show the effect of the cyclic degradation of strength or of reloading and unloading stiffness, and the degree of pinching on the mean *R*-factor observed for a given ductility for SDOF systems (Figure A-35). In general the effects are relatively small. Unfortunately the influence of such parameters is evaluated separately for each parameter, only for a relatively limited range of values, and always in relation to the pure elasto-plastic system. Still, the authors do perform verifications for systems having a combination of all such characteristics, thus providing evidence that the

proposed formulas can approximate more complex systems. Perhaps the greatest limitation of this research is that it does not apply to systems with in-cycle strength degradation. Only positive post-yield stiffnesses are considered. Therefore, the influence of several investigated parameters is small, and the results cannot be applied when negative backbone slopes are present.

Relevant Publications:

Lee, L.H, Han, S.W. and Oh, Y.H., 1999, "Determination of ductility factor considering different hysteretic models," *Earthquake Engineering and Structural Dynamics*, Vol. 28, 957–977.

Kunnath, S.K., Reinhorn, A.M. and Park, Y.J., 1990, "Analytical modeling of inelastic seismic response of RC structures," *Journal of Structural Engineering*, ASCE, 116, 996–1017.

A.2.13 Effects of Hysteresis Type on the Seismic Response of Buildings

Authors:

Foutch, D.A. and Shi, S. (1998)

Abstract:

Current design procedures account for inelastic behavior in a crude manner using the *R* factor. Although different *R* values are used for different building types, the determination of a specific *R* value was not done in a very consistent or scientific manner. The hysteresis behavior of members can be different depending on the material and member type. Buildings with members that dissipate energy through full hysteresis loops (for example, steel moment frames with compact members and no joint fracture) will respond differently from buildings with members that demonstrate strength-degrading hysteresis behavior by having either non-compact steel members, concentric braces, or members with fractured joints. This paper will present results of a study that has closely examined these effects using both SDOF and MDOF systems. A procedure for developing reliability-based design methods which incorporates these effects will also be presented.

Summary:

A total of nine moment-resisting frames with three different configurations (3-story, 6-story and 9-story) were used in this study to examine the effect of the beam-hinge model on the seismic behavior of MDOF structures. Using a

suite of 12 ground motion records, all structures (numbering 3x9x8) were analyzed for several *R*-factor levels (or approximately an equivalent number of earthquake intensity levels) and the results were summarized and compared with the buildings having a basic bilinear hinge with kinematic hardening (Figure A-36).

Eight different hinge models were considered: (1) kinematic hardening with bilinear backbone (positive post-yield stiffness), (2) same as 1 but with cyclic strength degradation, (3) same as 1 but having peak-oriented (Clough-like) hysteresis, (4) same as 2 but with peak-oriented hysteresis, (5) same as 1 but with pinching hysteresis, (6) same as 2 but with pinching hysteresis, (7) fracturing connection model with pinching hysteresis and asymmetric backbones including a negative slope and a residual plateau at one direction, and (8) a purely elastic bilinear backbone that dissipates no energy (Figure A-37).

Representative Figures:

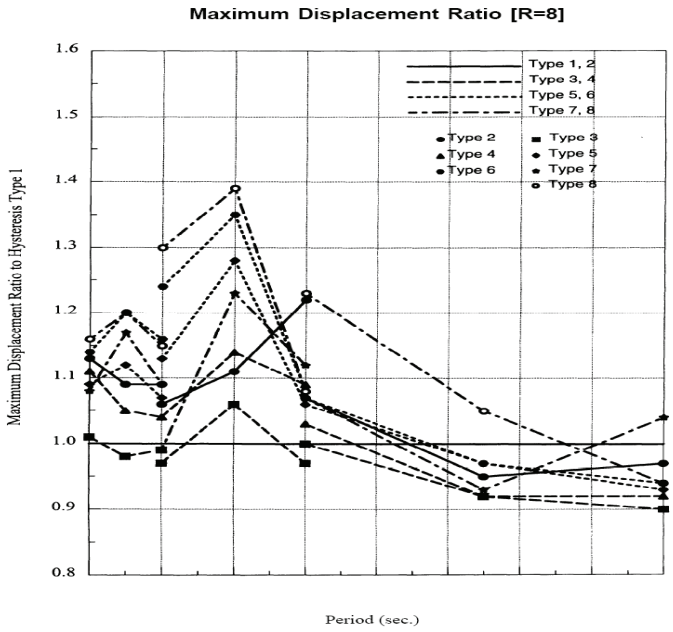

Figure A-36 Ratio of maximum displacement for all buildings and hinge types versus the hinge type 1 (kinematic hardening, no degradation).

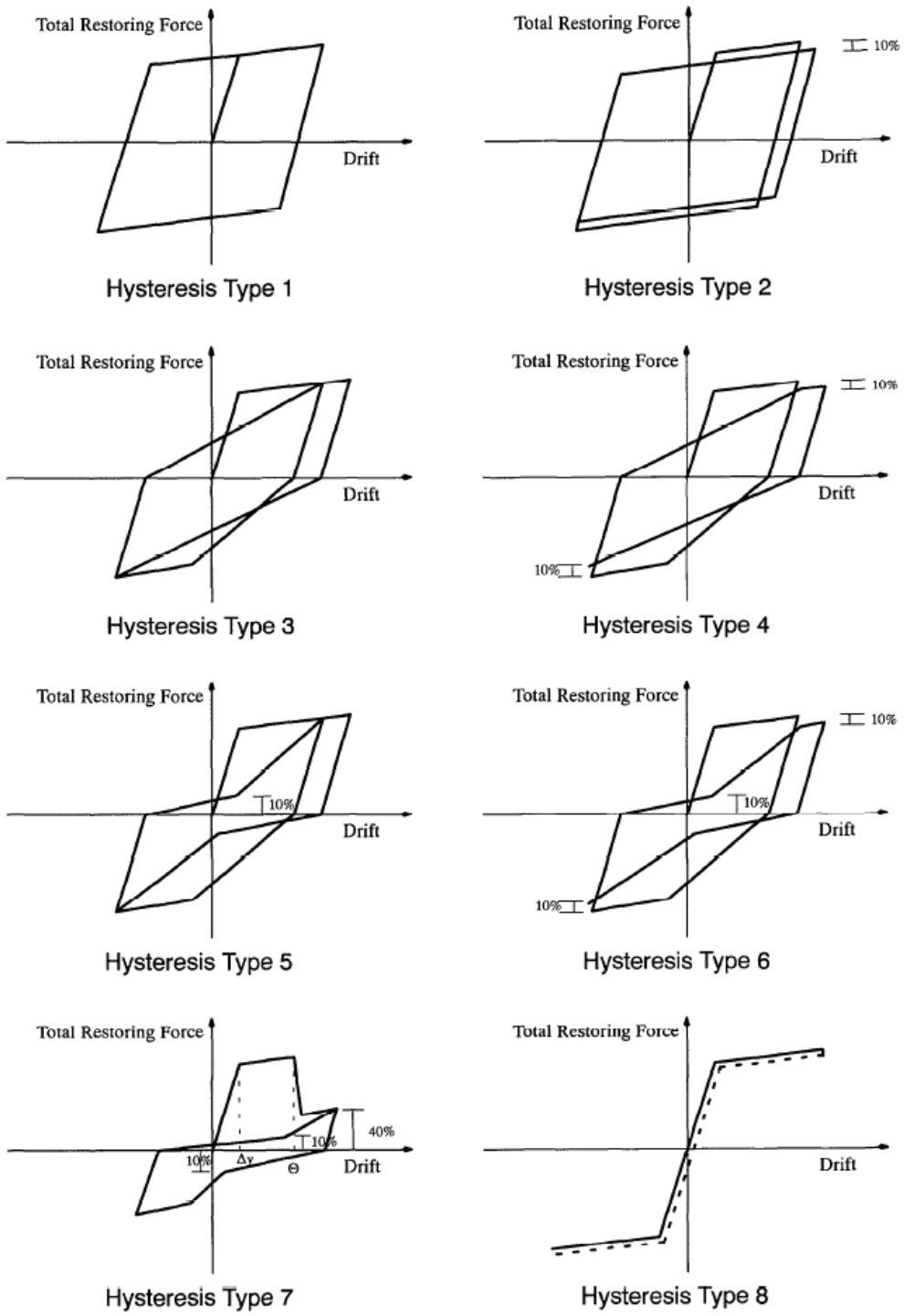

Figure A-37 The hysteresis types considered for the beam-hinges.

Summary of Findings:

The results show that the investigated plastic hinge models have a relatively similar effect on the seismic response of the structures, regardless of the structural period. Even hinge models with no energy dissipation do not produce excessive demands. At most, for an $R = 8$ reduction factor, the differences that appear are in the order of 30-40% and they only appear for a limited range of periods and models. Nevertheless, only a single backbone with in-cycle strength degradation has been considered, and even then the negative slope exists only in one direction of loading. Therefore the conclusions may be of limited use in such cases. This is an interesting exercise and one of the very few investigations that has produced data on the actual impact of local, hinge-level models on the global MDOF response.

Relevant Publications:

Foutch, D.A. and Shi, S., 1998, "Effects of hysteresis type on the seismic response of buildings," *Proc. 6th U.S. National Conference on Earthquake Engineering*, EERI, Seattle, WA.

Shi, S. and Foutch, D.A., 1997, *Evaluation of connection fracture and hysteresis type on the seismic response of steel buildings*, Report No. 617, Structural Research Series, Civil Engineering Studies, University of Illinois at Urbana-Champaign, Urbana, IL.

A.2.14 Performance-Based Assessment of Existing Structures Accounting For Residual Displacements

Authors:

Ruiz-Garcia, J. and Miranda, E. (2005)

Abstract:

The first part of this investigation describes comprehensive statistical studies to quantify residual and maximum displacement demands of inelastic SDOF systems, considering a relatively large earthquake ground motion database, and considering a large number of structural parameters. The second part of this study focuses on the evaluation of permanent (residual) and maximum (transient) drift demands of multi-story framed building models under different levels of ground motion intensity. Both parts include the formulation and implementation of simplified probabilistic approaches to estimate maximum and residual displacement demands accounting for the uncertainty in the structural response and the ground motion hazard. The study provides information towards incorporating explicitly the evaluation of

residual displacement demands for assessing the seismic performance of existing structures, or for the preliminary design phase of new structures, where structural damage control is achieved through control of lateral deformation demands.

Summary:

This study examined the effect of hysteretic behavior of maximum deformations of SDOF systems subjected to a large ensemble of 240 ground motions recorded on firm sites in California. They considered seven different types of hysteretic behavior: elastoplastic, bilinear, modified Clough, Takeda, origin-oriented, moderate degrading and severely degrading models. The modified Clough, the Takeda and origin-oriented models only exhibit stiffness degradation while the moderate degrading and severely degrading systems exhibit both stiffness and cyclic strength degradation. This study computed mean ratios of maximum deformation of degrading hysteretic models to non-degrading ones. They also studied the effect of hysteretic behavior for systems subjected to ground motions recorded in very soft soil sites and near-fault ground motions influence by forward directivity.

Representative Figures:

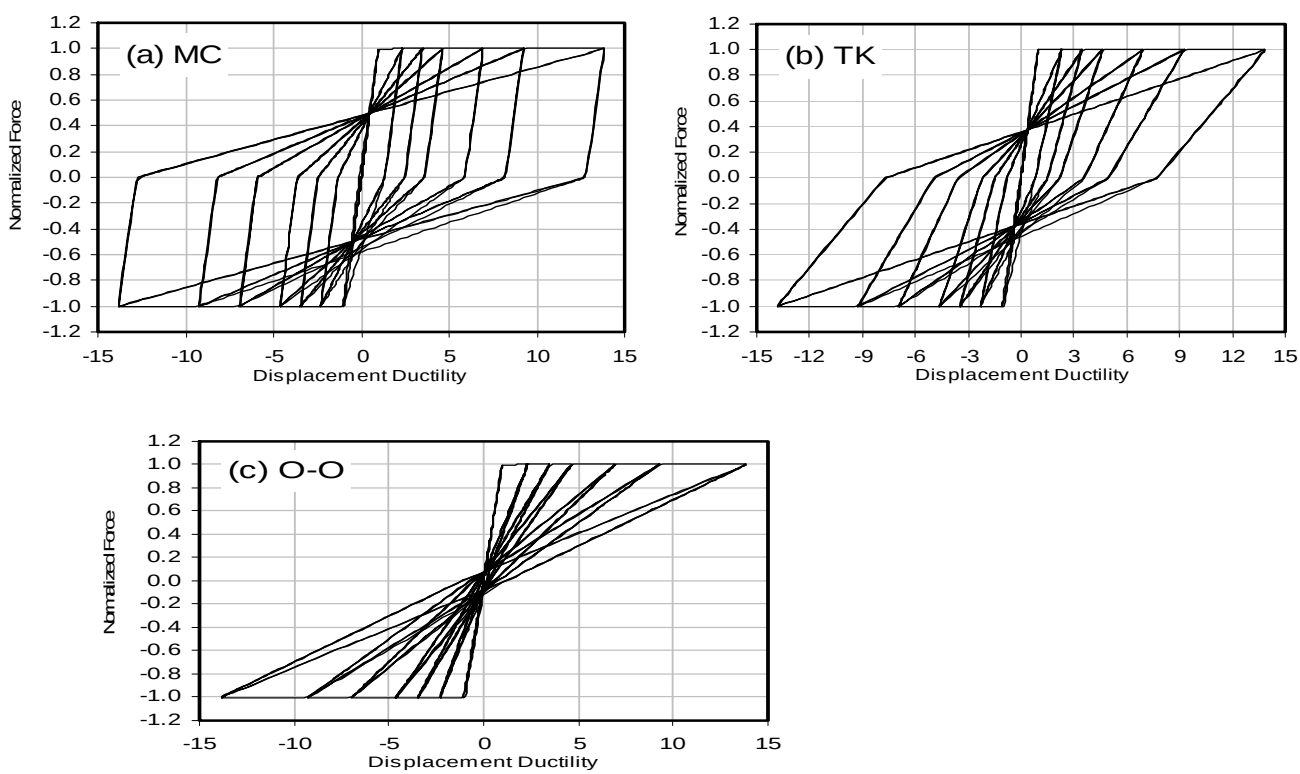

Figure A-38 Hysteretic models used in this investigation that only have stiffness degradation. (a) Modified-Clough (MC); (b) Takeda model (TK); and (c) Origin-Oriented model (O-O).

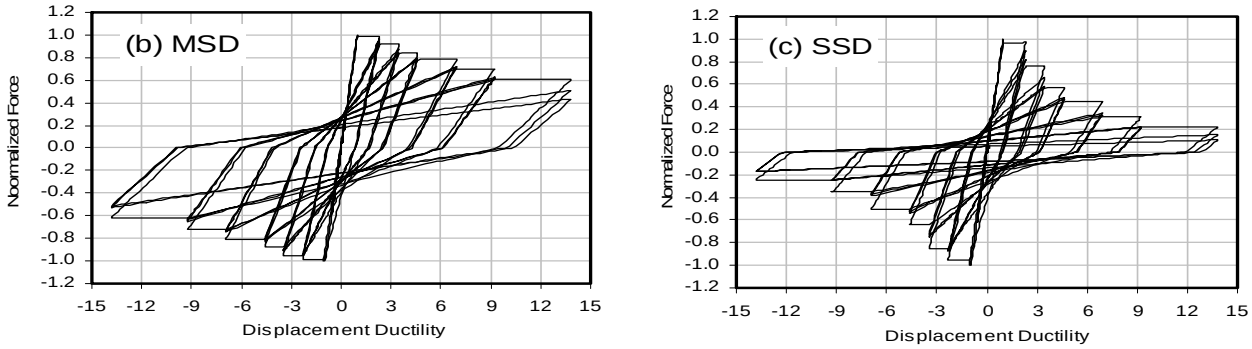

Figure A-39 Hysteretic models used in this investigation with stiffness and cyclic strength degradation. (b) Moderate Degrading (MSD); and (c) Severely Degrading (SSD).

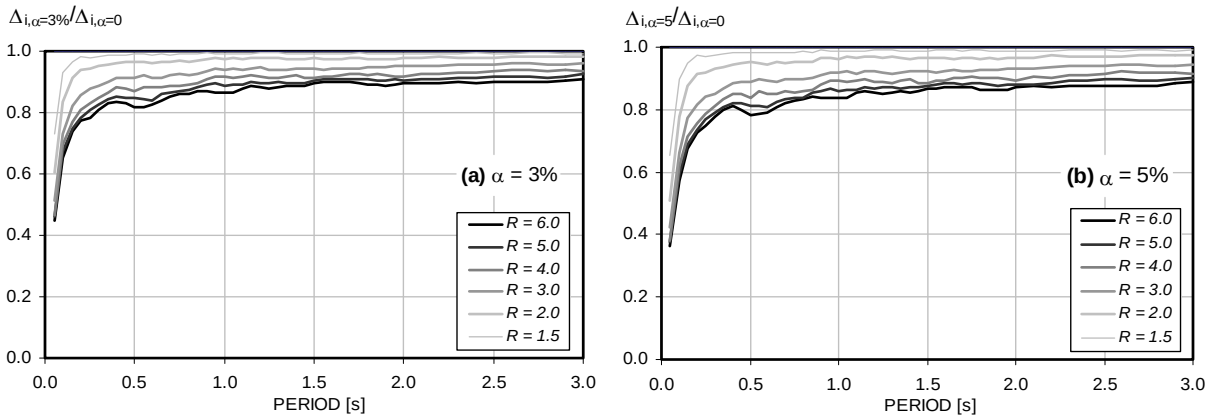

Figure A-40 Mean ratios of maximum deformation of bilinear to elastoplastic systems: (a) $\alpha = 3\%$; and (b) $\alpha = 5\%$.

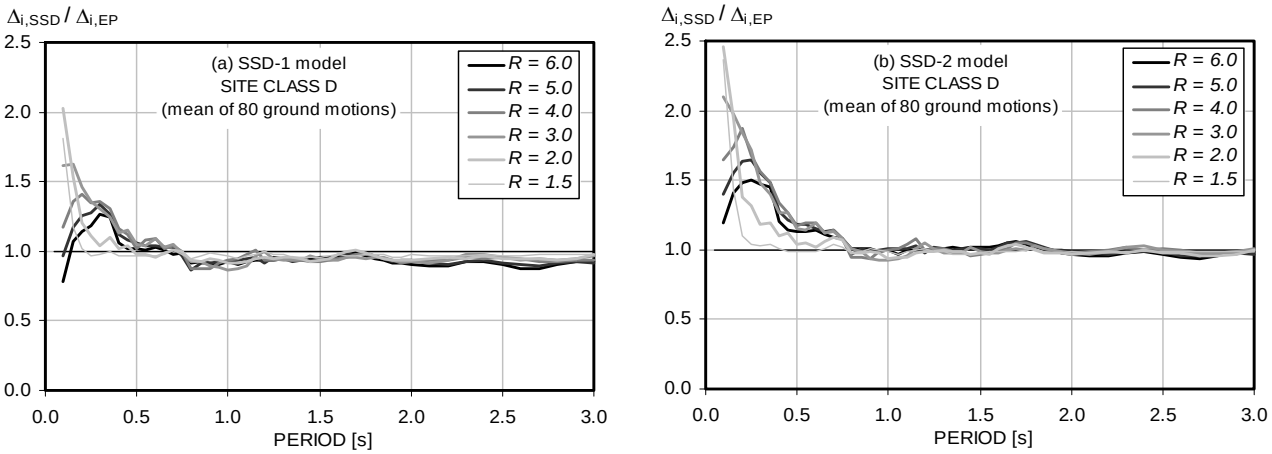

Figure A-41 Mean ratio of inelastic displacement demands in structural degrading and bilinear systems: (a) SSD-1 model; and (b) SSD-2 model.

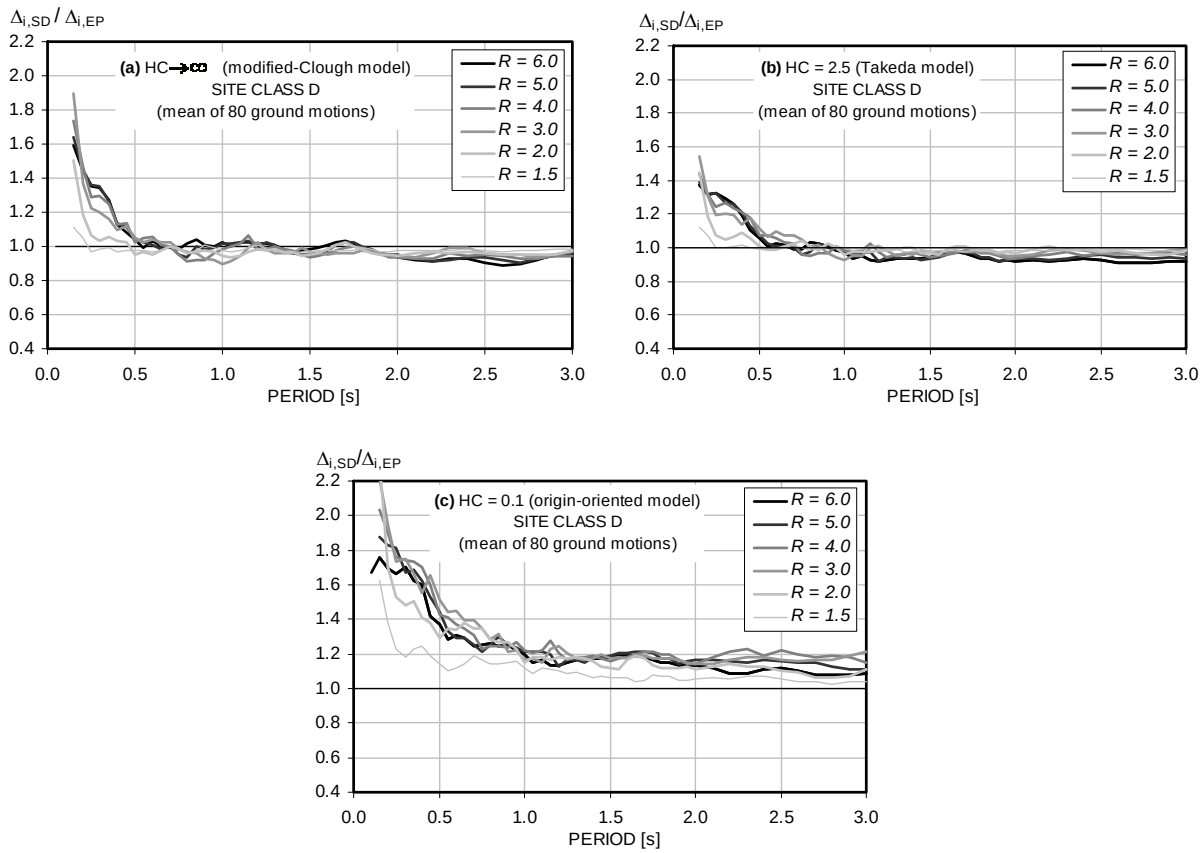

Figure A-42 Influence of hysteretic behavior on maximum deformation for three types of stiffness-degrading systems: (a) Modified-Clough model; (b) Takeda model; and (c) Origin-oriented model.

Summary of Findings:

The effect of positive post-yield stiffness was a function of period of vibration and level of lateral strength relative to the strength required to maintain the system elastic. Positive post-elastic stiffness tended to reduce maximum deformation demands but for realistic values of post-yield stiffness, with exception of systems with very short periods, reductions were small (smaller than 10%).

Maximum deformation demands of short-period degrading structures are, on average, larger than those of non-degrading systems. In general, the increment in displacement produced by degradation effects increases as the strength ratio increases (i.e., as the system becomes weaker relative to the lateral strength required to maintain the system elastic). For structures with periods longer than about 0.7 s, maximum deformation of degrading systems are on average either similar or slightly smaller than those of non-degrading systems.

The effects of stiffness degradation were larger for structures on soft soil sites than those observed for structures on firm sites. For structures with periods of vibration shorter than the predominant period of the ground motion, the lateral displacement demands in stiffness-degrading systems are on average 25% larger than those of non-degrading systems and in order to control lateral deformations to levels comparable to those in non-degrading structures, stiffness-degrading structures in this spectral region need to be designed for higher lateral forces.

Maximum inelastic displacement demands of stiffness-degrading systems are not significantly affected by the unloading stiffness provided that the reduction in unloading stiffness is small or moderate. However, for systems that unload toward the origin (that is, origin-oriented systems), or near the origin, maximum inelastic displacements are on average larger than maximum deformation demands of elastoplastic or bilinear systems and therefore the equal displacement rule should not be used for these systems. Hysteretic behaviors, in particular post-yield stiffness and unloading stiffness, have a large influence on residual displacement demands.

Relevant Publications:

Ruiz-Garcia, J. and Miranda, E., 2003, "Inelastic displacement ratio for evaluation of existing structures," *Earthquake Engineering and Structural Dynamics*. 32(8), 1237-1258.

Ruiz-Garcia, J. and Miranda, E., 2004, "Inelastic displacement ratios for structures built on soft soil sites", *Journal of Structural Engineering*, 130(12), December 2004, pp. 2051-2061

Ruiz-Garcia, J. and Miranda, E., 2005, *Performance-based assessment of existing structures accounting for residual displacements*, John A. Blume Earthquake Engineering Center, Report No. 153, Department of Civil and Environmental Engineering, Stanford University, Stanford, California, 444 p.

Ruiz-Garcia, J. and Miranda, E., 2006a, "Residual displacement ratios for the evaluation of existing structures," *Earthquake Engineering and Structural Dynamics*, Vol. 35, pp. 315-336.

Ruiz-Garcia, J. and Miranda, E., 2006b, "Inelastic displacement ratios for evaluation of structures built on soft soil sites," *Earthquake Engineering and Structural Dynamics*, in press.

A.2.15 Inelastic Spectra for Infilled Reinforced Concrete Frames

Authors:

Dolsek, M. and Fajfar, P. (2004)

Abstract:

In two companion papers a simplified nonlinear analysis procedure for infilled reinforced concrete frames is introduced. In this paper a simple relation between strength reduction factor, ductility and period (R–μ–T relation) is presented. It is intended to be used for the determination of inelastic displacement ratios and of inelastic spectra in conjunction with idealized elastic spectra. The R–μ–T relation was developed from results of an extensive parametric study employing a SDOF mathematical model composed of structural elements representing the frame and infill. The structural parameters used in the proposed R–μ–T relation, in addition to the parameters used in a usual (e.g. elasto-plastic) system, are ductility at the beginning of strength degradation, and the reduction of strength after the failure of the infills. Formulae depend also on the corner periods of the elastic spectrum. The proposed equations were validated by comparing results in terms of the reduction factors, inelastic displacement ratios, and inelastic spectra in the acceleration–displacement format, with those obtained by non-linear dynamic analyses for three sets of recorded and semi-artificial ground motions. A new approach was used for generating semi-artificial ground motions compatible with the target spectrum. This approach preserves the basic characteristics of individual ground motions, whereas the mean spectrum of the complete ground motion set fits the target spectrum excellently. In the parametric study, the R–μ–T relation was determined by assuming a constant reduction factor, while the corresponding ductility was calculated for different ground motions. The mean values proved to be noticeably different from the mean values as determined when based on a constant ductility approach, while the median values determined by the different procedures were between the two means. The approach employed in the study yields an R–μ–T relation which is conservative both for design and performance assessment (compared with a relation based on median values).

Summary:

An R-μ-T relationship was developed that is suitable for use with infilled frames having a quadrilinear elastic-positive-negative-residual backbone. The system used for the analysis contained separate springs, Takeda for the frame and shear-slip for the infill (Figure A-43). These were suitably

calibrated to generate a backbone similar to the ones observed in pushovers of infilled frames (Figure A-44). Thus, only in-cycle strength degradation was considered, while any cyclic degradation issues were not investigated.

The system was analyzed using three suites of ground motion records which were spectrum-matched to a target design spectrum. A parametric study of the quadrilinear system was then conducted by varying the period and the backbone parameters within prescribed values.

Representative Figures:

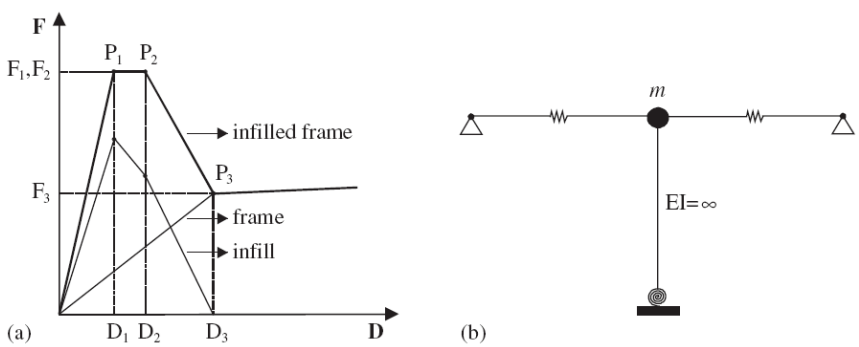

Figure A-43 The SDOF system: (a) force-displacement envelope; and (b) mathematic model.

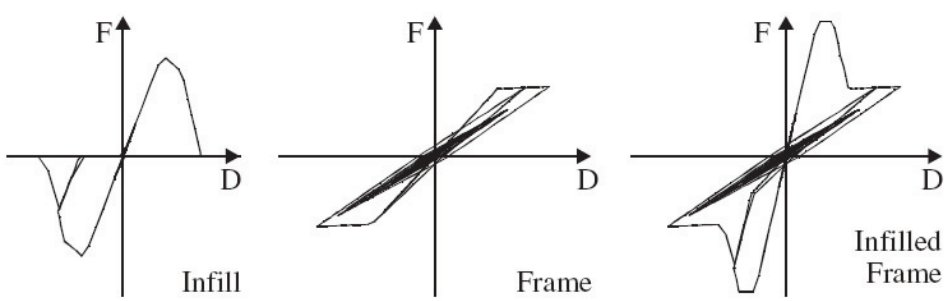

Figure A-44 The hysteretic behavior of the equivalent SDOF system.

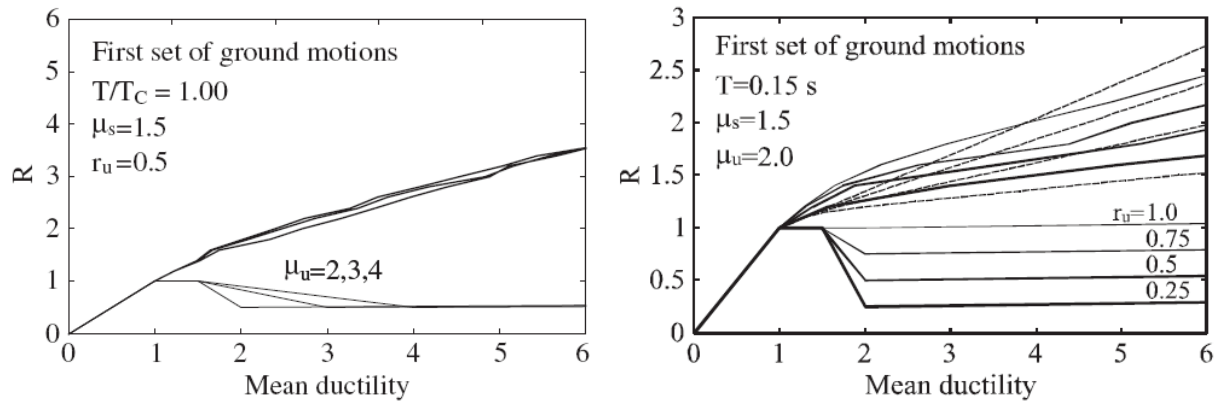

Figure A-45 The influence of negative slope and residual plateau on the mean ductility for given R-factor.

Summary of Findings:

The negative slope was found to have a very small effect on the seismic response of the system when only a short drop in strength to the residual plateau is allowed (Figure A-45a). Actually, the level of the plateau combined with a worsening negative slope were shown to be quite important, lower plateaus increase the ductility demands considerably (Figure A-45b). Approximate values were proposed for the dispersion around the mean provided by the relationship.

Relevant Publications:

Dolsek, M. and Fajfar, P., 2004, "Inelastic spectra for infilled reinforced concrete frames," *Earthquake Engineering and Structural Dynamics*, Vol. 33, 1395–1416.

Dolsek, M. and Fajfar, P., 2000, "Simplified nonlinear seismic analysis of infilled reinforced concrete frames," *Earthquake Engineering and Structural Dynamics*, Vol. 34, 49–66.

Dolsek, M., 2002, *Seismic response of infilled reinforced concrete frames*, Ph.D. thesis, University of Ljubljana, Faculty of Civil and Geodetic Engineering, Ljubljana, Slovenia [in Slovenian].